CENTER *for* MUSCULOSKELETAL RESEARCH

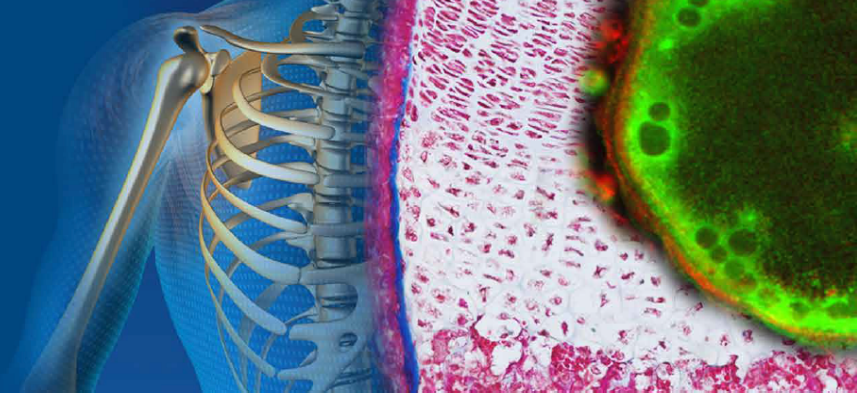

15th Annual CMSR Symposium

Thursday, October 30, 2025

Sponsored By

Department of Orthopaedics and Rehabilitation
University of Rochester Medical Center
&
National Institute of Arthritis and Musculoskeletal and Skin Diseases (NIAMS) Grant T32 AR076950-05

MEDICINE *of* THE HIGHEST ORDER

UR MEDICINE

ROCMSK Training Program

The Annual Center for Musculoskeletal Research (CMSR) Symposium is the centerpiece of the NIH/NIAMS funded T32 program entitled "Rochester Musculoskeletal (ROCMSK) Training Program" at the University of Rochester Medical Center. This program is designed to provide interdisciplinary didactic and research training in musculoskeletal science.

The overarching goal of ROCMSK Training Program is to develop future generations of interdisciplinary musculoskeletal scientists and leaders of innovations. The program is administered in the CMSR at the University of Rochester and integrates 21 highly collaborative faculty with primary appointments in seven academic and clinical departments.

The CMSR and associated training faculty represent a highly integrated group of mentors that provide research training opportunities in the following disciplines, highlighted by abstracts featured in this Symposium:

- Bone Biology and Disease
- Cartilage Mechanobiology
- Arthritis and Regenerative Therapies
- Tendon Development, Repair, and Regenerative Engineering
- Muscle Biology and Disease
- Drug Delivery
- Fracture Repair and Bone Tissue Engineering
- Musculoskeletal Infection, Stem Cells, and Musculoskeletal Development
- Skeletal Cancer Biology and Therapeutics

The education program ensures a comprehensive understanding of musculoskeletal science that is seamlessly accessible to all CMSR trainees at every academic level. ROCMSK training emphasizes basic and translational science education. The training experience aims to build competency in areas ranging from the most basic molecular and genetic studies to the design and execution of human clinical trials. This year, ROCMSK awarded two pre-doctoral and one post-doctoral training seats.

This Symposium is a celebration of the trainees' accomplishments.

15th Annual Center for MusculoSkeletal Research Symposium

Thursday, October 30, 2025

Clinical Hour Presentations

Class of '62 Auditorium (G-9425), URMC

7:00 am	*Welcome & Introduction*	***Paul Rubery, MD***
7:05 am	*Increased Rate of Distal Radius Nonunion Associated with NSAID Use Within Thirty Days of Fracture*	***Andrew Park, MD*** *Constantinos Ketonis, MD, PhD*
7:16 am	*The Effect of Lumbar Decompression on Functional Transitions in Patients with Lumbar Spinal Stenosis: Clinical and Biomechanical Evidence*	***Prasanth Romiyo, MD*** *Ram Haddas, PhD, MBA*
7:27 am	*Ulnar Nerve Transposition in Cubital Tunnel Release: Indications and Surgeon Rationale*	***Justin Wong, MPH*** *Constantinos Ketonis, MD, PhD*
7:38 am	*ACL Reconstruction Improves Patient Reported Outcomes Regardless of Social Deprivation and Socioeconomic Factors*	***Omkar Prabhavalkar, BA*** *Sandeep Mannava, MD, PhD*
7:49 am	*Racial Differences in Rates of Surgical and Non-Surgical Treatment of Complete Rotator Cuff Tears: A Propensity-Matched Database Study of 75,918 Patients*	***Nicholas Morriss, MD*** *Sandeep Mannava, MD, PhD*

Rosier Award Presentations

Class of '62 Auditorium (G-9425), URMC

	9:00 am	*Welcome & Introduction*	***Paul Rubery, MD*** ***Hani Awad, PhD***
Post-Doctoral Fellows	9:10 am	*Discovery of Telocytes within the Synovial Lymphatic System and their Role in Resolving Inflammatory Arthritis*	***Yue Peng, PhD*** *Schwarz Lab*
Post-Doctoral Fellows	9:22 am	*Integrated Imaging and Spatial Transcriptomic Analyses of Blood Vessel Coupling to Healing Tissue During Auto and Allograft Bone Transplantation*	***Xiaojie Xing, PhD*** *Zhang Lab*
Pre-Doctoral Trainees	9:34 am	*The Role of Mitochondrial Dynamics in Bone Marrow Stromal Cell Efferocytosis*	***Sandra Castillo Aguirre, MS*** *Eliseev Lab*
Pre-Doctoral Trainees	9:46 am	*Macrophage Dysfunction Enhances Bone Marrow Stromal Cell Efferocytosis and Accelerates Bone Marrow Aging*	***Zhiming (Sam) Jin, MS*** *Calvi Lab*
	9:58 am	***Break***	
Pre-Doctoral Trainees	10:20 am	*The Importance of Investing in Musculoskeletal Research from a Community Perspective*	***Francis Clement*** *MSKI Council Member*
Pre-Doctoral Trainees	10:32 am	*Taurine Transporter SLC6A6 Expression Promotes Mesenchymal Stromal Cell Function*	***Christina Kaszuba, MS*** *Bajaj Lab*
Pre-Doctoral Trainees	10:44 am	*Compartmentalized Inflammatory Landscape and Macrophage Plasticity Regulate Tet2+/- Mediated clonal hematopoiesis*	***Kevin Lee, MS*** *Yeh Lab*
Pre-Doctoral Trainees	10:56 am	*TREM1 Promotes Neutrophil Extracellular Trap Release Associated with Latent TGFβ1 Activation to Induce Age-related Osteoporosis*	***Cheng Xiang, PhD*** *Boyce Lab*
Pre-Doctoral Trainees	11:08 am	*CNN-Based Evaluation of Wrist Bone Health and Fracture Risk Using Raman Spectroscopy of the Proximal Phalanx*	***Anthony Yosick, MS*** *Awad Lab*
	11:20 am	*Three-Minute Teasers (3MT) – Finalists for Best Poster Presentations*	
	11:50 am	**Annual CMSR Group Photo**	**Class of '62 Auditorium (G-9425), URMC**
	12:00 pm	**Lunch**	**Class of '62 Auditorium (G-9425), URMC**
	12:30 pm	**Poster Session**	**Sarah Flaum Atrium (G-9500), URMC**
	2:00 pm	***Break***	

Plenary Session

Class of '62 Auditorium (G-9425), URMC

CMSR Faculty Spotlight

2:30 pm **Cherice Hill, PhD**
Biomechanical Motion Analysis in Non-Research Spaces

3:00 pm **Rebecca Irwin, PhD**
Advancing How We Study Spine Health: Intravital Imaging and Models of Age-Related Change

3:30 pm **Jeevisha Bajaj, PhD**
Osteolineage Cells Support Leukemia Progression

Keynote Presentation

4:00 pm **Robert L. Satcher, MD, PhD**
The TGFBI 'Vicious Cycle': Does it explain treatment resistance for bone metastasis?

6:00 pm ***Dinner and Rosier Awards Presentation*** — **Sarah Flaum Atrium (G-9500), URMC**

MEDICINE of THE HIGHEST ORDER

UR MEDICINE

Keynote Speaker: Robert L. Satcher, MD, PhD

Professor, Department of Orthopaedic Oncology The University of Texas MD Anderson Cancer Center

Robert Lee Satcher, Jr., MD, PhD is recognized for his varied career interests and notable successes, from his training as a chemical engineer, to his practice as an orthopaedic surgeon in oncology, and service as a mission specialist astronaut and first orthopaedic surgeon astronaut for NASA. Dr. Satcher flew on the Space Shuttle Atlantis, STS-129, in November 2009, during which he performed two spacewalks totaling over 12 hours of extravehicular activity.

Dr. Satcher has been a board member at Vorhees University (a historically Black college) where he served as board chair during which Voorhees became a University (previously Voorhees College) following a capital campaign and an expansion of graduate academic programs. Other board memberships include Harvard University Board of Overseers, Whitehead Institute of MIT, Teach For America, Space Center Houston, NASA advisory boards for human spaceflight, and National Academy of Sciences panel to assess cancer risk in Astronauts following spaceflight.

Dr. Satcher earned his BS and PhD degrees in chemical engineering from MIT and his medical degree from Harvard Medical School (Health Sciences and Technology) in 1994. His postgraduate training included postdoctoral research fellowships at the University of California (Berkeley and San Francisco); a residency in orthopaedic surgery, also at the University of California San Francisco; as well as an orthopaedic oncology fellowship at the University of Florida, Gainesville.

Dr. Satcher is currently a Professor of Orthopaedic Oncology at MD Anderson Cancer Center in Houston, Texas. Most recently, Dr. Satcher led the initiation of virtual care at MD Anderson Cancer Center and serves as the Clinical faculty lead. With over 2.5 million virtual appointments completed since inception, MD Anderson's specialized cancer expertise continued with minimal disruption throughout the pandemic. For medical care delivery in underserved countries, Dr. Satcher has participated in surgical trips to Nigeria, Burkina Faso, Gabon, Venezuela, and Nicaragua in recent years.

Dr. Satcher's research has focused on understanding how cancer spreads to the skeleton, with a focus on discovering new curative treatment options using cellular, molecular, and personalized medicine strategies. He has over 100 peer reviewed publications, and has received research grants from DOD and NIH, and serves on grant review study sections for NIH. Dr. Satcher is a member of numerous professional organizations including the Association of Space Explorers, American Academy of Orthopaedic Surgery, Musculoskeletal Tumor Society, National Comprehensive Cancer Network, to name a few. He has been involved in efforts to introduce racial equality and diversity in academia and healthcare throughout his career through committee memberships and scholarly work.

Symposium Papers

Clinical Hour Abstracts

1	Andrew Park, MD	Increased Rate of Distal Radius Nonunion Associated with NSAID Use Within Thirty Days of Fracture
2	Prasanth Romiyo, MD	The Effect of Lumbar Decompression on Functional Transitions in Patients with Lumbar Spinal Stenosis: Clinical and Biomechanical Evidence
3	Dominique Rinfret, BS	Ulnar Nerve Transposition in Cubital Tunnel Release: Indications and Surgeon Rationale
4	Patrick Castle, MD	ACL Reconstruction Improves Patient Reported Outcomes Regardless of Social Deprivation and Socioeconomic Factors
5	Nicholas Morriss, MD	Racial Differences in Rates of Surgical and Non-Surgical Treatment Of Complete Rotator Cuff Tears: A Propensity-Matched Database Study with of 75,918 Patients

Rosier Awards Post-Doctoral Trainee Presentations

6	Yue Peng, PhD	Discovery of Telocytes within the Synovial Lymphatic System and their Role in Resolving Inflammatory Arthritis
7	Xiaojie Xing, PhD	Integrated Imaging and Spatial Transcriptomic Analyses of Blood Vessel Coupling to Healing Tissue During Auto and Allograft Bone Transplantation

Rosier Awards Pre-Doctoral Trainee Presentations

8	Sandra Castillo Aguirre, MS	The Role of Mitochondrial Dynamics in Bone Marrow Stromal Cell Efferocytosis
9	Zhiming (Sam) Jin, MS	Macrophage dysfunction enhances bone marrow stromal cell efferocytosis and accelerates bone marrow aging
10	Christina Kaszuba, MS	Taurine transporter SLC6A6 expression promotes mesenchymal stromal cell function
11	Kevin Lee, MS BS	Compartmentalized inflammatory landscape and macrophage plasticity regulate Tet2+/- mediated clonal hematopoiesis
12	Cheng Xiang, PhD	TREM1 Promotes Neutrophil Extracellular Trap Release Associated With Latent TGFβ1 Activation to Induce Age-related Osteoporosis
13	Anthony Yosick, MS	CNN-Based Evaluation of Wrist Bone Health and Fracture Risk Using Raman Spectroscopy of the Proximal Phalanx

Rosier Award Best Poster Finalists

14	Ryan Adapathya, BS	Hematopoietic Stem Cell (HSC) - Macrophage Interactions Promote Preferential HSC Division in Bone Resorptive Cavities
15	Renae Duncan, MS	Role of Mitochondrial Genetics in the Response of Bone Marrow Stromal Cells to Mechanical Stimulation
16	Edgardo Franco, MS	IDH2 mutant hematopoietic stem and progenitor cells promote endothelial niche remodeling.

17	Bei Liu, MD, MS	Microfluidic-Synthesized Amorphous Calcium Phosphate Nanoparticles Enhance Osteogenesis, Suppress Osteoclastogenesis, and Promote Bone Healing in a Murine Femoral Defect Model
18	Zachary Sechrist, BS	Pancreatic Tumor-Associated IGFBP-3 Induces Dysregulated Autophagy and Mitochondrial Dysfunction in Skeletal Muscle Via TGF-β Receptor and SMAD3 Signaling
19	Eliya Tazreena Tashbib, MS	PRDM16 is required for normal nasal septal cartilage and bone development in mice
20	Adam Tyrlik, BS	Conserved disruption of human bone marrow stromal cells' transcriptional and functional heterogeneity in Myelodysplastic Syndromes

Undergraduate Posters

21	Ashleigh Barrett	Investigating the Role of Immune Checkpoint Protein TIM-3 on Macrophage Function in Bone Infection
22	Nathan Carpenter-Holmes	Translating Biomechanical Metrics into Clinical Impact: Minimum Clinically Important Differences (MCIDs) for Functional Recovery After Lumbar Spine Surgery
23	Wimeth Dissanayake	The roles of anti-resorptive vs. anabolic therapies in Hematopoietic Niche and Tet2- mediated Clonal Hematopoiesis
24	Maximilian Harkins	Multiphoton Ablation & Laser-Guided Angiogenesis for Bone Tissue Engineering
25	Kade Kaufmann	Improving Care for Spinal Deformity Patients: Utilizing Wearable Tools for Functional and Disability Assessments
26	Christina Kyriacou	Estimating Lower Extremity Joint Moments Using Alternative Approaches
27	Veena Laks	Identifying Patients Most Likely to Benefit From Shoulder Surgery: Clinical Predictors and Outcomes
28	Nidhi Patel	Tumor-Associated IGFBP-3 Regulates Macrophage Polarization and α-SMA+ Cell Migration
29	Valerie Voytsekhovskaya, BS	Galactic Cosmic Radiation Reveals Sex-Dependent Mechanisms of Bone Loss and Marrow Remodeling
30	Hannah Wang	Effects of Hydroxybisphosphonate-Conjugated Sitafloxacin on Fracture Healing and Skeletal Growth in Mice
31	Cindy Wu	Accelerated ovarian failure model of menopause increases low back pain associated behavior in mice
32	Shibo Xu	Objective Monitoring of Functional Recovery in Adult Scoliosis Using Inertial Measurement Unit (IMU)–Based Motion Recognition
33	Zhengyang Zhu	Identifying Neural Biomarkers of Chronic Low Back Pain Using Resting-State EEG and Machine Learning

Post-Graduate Posters

34	Janitri Venkatachala Babu, MS	TRPC6 Inhibition as a Potential Therapeutic for Discogenic Chronic Back Pain
35	Reshmii Bondili, BS	Preoperative Biomechanical and Patient-Reported Predictors of Surgical Recovery in Lumbar Spine Disease: Translating Motion Analysis into Precision Medicine

36	Catherine Caballero, BS	Targeted expression of Sirtuin 6 to bone marrow stromal cells reverses their age-dependent transcriptional signatures
37	Patrick Castle, MD	Patients 50 years or Older Demonstrate Similar Improvement in PROMIS Physical Function and Pain Interference Scores after ACL Reconstruction Compared to Younger Patients
38	Minhwan Chung, PhD	Defining the Piezo1 Mechanotransduction Setpoint in Articular Cartilage
39	Jeffrey Coombs, MD, BS	Improved Outcomes with Endoscopic Carpal Tunnel Release for Patients who Smoke
40	Christopher Dussik, MD	Increased Risk for Upper Extremity Amputation in Minority Patients with Necrotizing Fasciitis
41	Christopher Dussik, MD	Underutilization of Hand Corticosteroid injections and Arthroplasty for Minority Demographics in the United States
42	Eloise Fadial, MS	PRDM16 maintains cartilage homeostasis by modulating chondrocyte phenotypes
43	Rajkumar Govindan, MS	Optimizing the culture conditions of Human Hepatic Sinusoidal Endothelial Cells and iPSC-derived Hepatocytes for utilization in Liver-on-a-chip
44	Victoria Hansen, PhD	Single cell and spatial sequencing reveals cell signaling between chondrocyte types during in vivo murine chondrogenesis
45	Johannes Hasler, MS	Exploring TRPV4's Mechanosensitivity to Stiffness and Mechanical Loading in Annulus Fibrosus Mechanotransduction
46	Cih-Li Hong, DVM	Intravital Imaging of Calcium Network Topology Revealed the Immune-Modulatory Loci in the Bone Marrow
47	Atikul Islam, PhD	Over-expression of Deubiquitinase OTUD7b contributes to Age-related Osteoporosis by inhibiting bone formation
48	Sameer Jain, BS	Diabetes Mellitus is Associated with Increased Rates of Surgical Site Infection and Need for Antibiotics following Arthroscopic Rotator Cuff Repair: a Study of 73,178 Patients
49	Sameer Jain, BS	Corticosteroid Injections as Early as 12 Months Pre-Op Increases Risk of Subsequent Shoulder Surgery after Rotator Cuff Repair: A Database Study of 79,582 patients
50	Kyle Jerreld, MS	Cyclical Physiological Strain Blunts TGF-β Induced Myofibroblast Activation in a Human Tendon-on-a-Chip
51	Xingyu Jing, MS	Characterizing isolated Prx1+ mouse bone-marrow-derived stromal cells (BMSCs) in different culture methods to study skeletal aging
52	Andriy Kobryn, MD	Investigating the Role of Telocytes in Recruiting Mast Cells via Chemokine Expression
53	Chloe Kraft, BS	Dissecting TIM-3-Mediated Immunoregulation in Staphylococcus aureus Osteomyelitis
54	Gulzada Kulzhanova, MS	Transcriptomic Profiling and Human Tissue-on-Chip Modeling of Synoviocyte-Chondrocyte Crosstalk in Femoroacetabular Impingement and Hip Osteoarthritis
55	Firdavs Kurbanov, BS	Antidepressant Use and Risk of Reoperation After Wrist Fracture Fixation
56	Richard Lander, MD	Range of Motion Outcomes after Primary Flexor Tendon Repair when Evaluating for Patient, Injury, and Surgery Specific Factors

57	Richard Lander, MD	Patient, Injury, and Surgery-Specific Factors Influence Outcomes Following Flexor Tendon Repair
58	Sashank Lekkala, MS	Effect of Zinc-Coated Titanium Implants on Neutrophil Swarming and S. aureus Clearance
59	Sashank Lekkala, MS	Anti-S. aureus mAbs Against Autolysin and Pore-Forming Toxins Enhance Vital NETosis and Phagocytosis by Cytoplasts Demonstrated with Real Time Fluorescent Microscopy and Imaging Cytometry
60	Zhewen "Kevin" Li, MS	Characterizing CD8 T Cell Phenotypes in the Acute Myeloid Leukemia Bone Marrow Microenvironment
61	Haiyin Li, MD, PhD	A new mechanistic insight into the pathogenesis of Achilles tendinopathy and heterotopic ossification by study of human patient
62	Isabelle Linares, MS	Synovial Fibroblasts Exacerbate Inflammation and Peritendinous Adhesions in a Human Tendon-on-a-Chip
63	Xinying Lu, BS	Differentiation and Functional Characterization of Human iPSC-Derived Fibroblast-Like Synoviocytes
64	Alexander Mathewson, BS	Defining profibrotic spatial heterogeneity in the maturing abdominal adhesion
65	Katya McDonald, MS, BA	T cell dysfunction during Staphylococcus aureus osteomyelitis in humanized mice
66	Lucia Morales, BS	Mesenchymal Stem Cell-derived Size Separated Extracellular Vesicles for Treatment of Inflammation in a Macrophage Model
67	Nicholas Morriss, MD	Use of nonsteroidal anti-inflammatory drugs is associated with increased rates of subsequent rotator cuff repair following arthroscopic rotator cuff repair: a database study of 97,792 patients
68	Nicholas Morriss, MD	Association Between NSAID Use and Postoperative Outcomes Following ACL Reconstruction: A Retrospective Cohort Analysis
69	Samantha Muscat, MS	Achilles Tendons Maintain Homeostasis in Response to Physiological Load via Spatially-Distinct Cellular Processes
70	Dennis Nimoh, BS	Assessing the Accuracy of XSENSOR Intelligent Insoles for Motion Analysis
71	Cortney Pang, BA	Differential effect of exercise on chondrocyte viability and mechanical susceptibility in young and aged mouse knee joints
72	Amy Phan, MD	Increased Nonunion Rates for Scaphoid Fractures Treated Nonoperatively with Recent NSAID Prescription
73	Amy Phan, MD	Psychiatric Outcomes after Digital Replantation Versus Primary Digital Amputation
74	Omkar Prabhavalkar, BA	Hyperlipidemia Increases the Risk of Secondary Procedures in Patients Undergoing Arthroscopic Rotator Cuff Repair: A Database Study of 144,555 Patients
75	Omkar Prabhavalkar, BA	Application of Machine Learning Techniques to Identify Predictors of PROMIS Outcomes After ACL Reconstruction
76	Omkar Prabhavalkar, BA	ACL Reconstruction in Skiers vs Pivoting Sports Athletes: A Comparative Analysis of PROMIS Outcomes
77	Emily Schillinger, MS	Biomechanical Predictors of Injury Risk in Athletes: Translating Motion Analysis into Clinically Relevant Prevention Strategies

78	Azmeer Sharipol, MS	Bone Marrow on Chip for Advancing In Vitro Models in Preclinical Acute Myeloid Leukemia Studies
79	Ye Shu, BS	Restoring Gait Efficiency After Lumbar Decompression: Quantitative Biomarkers in Patients with Radiculopathy and Neurogenic Claudication
80	Chutamath Sittplangkoon, PhD	Targeting TRAF3 to Treat Immunosenescence and Age-Related Osteoporosis
81	Levy Sominsky, BA	Elucidating the role of S. aureus proteases in fibrin ring degradation during sitafloxacin eradication of Staphylococcal abscess communities
82	Deepak Sonker, MS	Continuous monitoring of cytokine secretion in human tendon-on-a-chip using an optical biosensor
83	Gabriella Wagner, MS	Microscope Mountable Compression Bioreactor for Real-Time Mechanosensing Studies in IVD Cells
84	Cheng Xiang, PhD	Macrophages Expressing Membrane-bound TGFβ1 in Bone Marrow Contribute to Low Bone Turnover Associated with Immunosenescence and Age-Related Osteoporosis
85	Roukaya Yaakoubi, PhD	$CD11c^{+}CD21^{-}$ Autoimmune-Associated B Cells Derived from Double-Negative $IgD^{-}CD27^{-}$ Subsets Exhibit Enhanced IFNLR1 Expression in Systemic Lupus Erythematosus
86	Anthony Yosick, MS	Metacarpal Cortical Index: An Accessible Alternative for Assessing Wrist Bone Health and Fracture Risk
87	Victor Zhang, BS	Development of a vascularized tendon fibrotic organoid in a microfluidic device

Clinical Hour Abstracts

Disclaimer

15th Annual Center for Musculoskeletal Research Symposium
October 30, 2025

Title:	Increased Rate of Distal Radius Nonunion Associated with NSAID Use Within Thirty Days of Fracture
Presenting Author:	Andrew Jae Park, MD
Co-Author(s):	Christopher M. Dussik, MD, Amy Phan, MD, Jeffrey Coombs, MD, Joseph Ferraro, MD, and Constantinos Ketonis, MD PhD
Lab PI / Mentor:	Constantinos Ketonis, MD PhD

ABSTRACT

Introduction: Nonsteroidal anti-inflammatory drugs (NSAIDs) are frequently employed in the management of distal radius fractures (DRFs) to mitigate swelling and control pain. The theoretical risk of disrupted bone healing has been previously described, but the literature is limited to single-institution studies with small sample sizes. The purpose of this study was to determine whether NSAID exposure influences nonunion rates in patients with DRFs managed operatively and nonoperatively, by leveraging a large, multicenter registry.

Methods: An analysis was conducted using the TriNetX database to compare the nonunion rate of operatively and nonoperatively treated DRFs with and without prescribed NSAIDs. The cohorts were matched based on age and known nonunion risk factors. Odds ratios were calculated to assess statistical significance.

Results: A total of 470,654 nonoperatively and 108,476 operatively treated DRFs were included. Of those, 99,488 nonoperative and 40,203 operative DRFs were prescribed NSAIDs up to one month after diagnosis. In the nonoperative cohort, the nonunion rate for the NSAIDs group was 0.40% versus 0.16% for the non-NSAIDs group, whereas in the operative cohort, the corresponding nonunion rates were 0.71% in the NSAID group compared to 0.50% for the non-NSAIDs group. The risk difference was statistically significant for both cohorts ($p < 0.05$). After matched analysis, NSAIDs were associated with an increased risk of nonunion in both operatively and nonoperatively treated DRFs, with a 1.4 (95% CI: 1.2-1.7) and 2.6 (95% CI: 2.1-3.1) odds ratio, respectively.

Discussion: NSAID administration was associated with an increased risk of nonunion in both nonoperatively and operatively treated DRFs. Limitations of this study include its retrospective, database-driven design, which depends on the accuracy of the ICD- and CPT- codes used for analysis, the inability to control for all non-union risk fractures, and the duration, dosage, and over-the-counter NSAID use. Our inability to establish a causal relationship between NSAIDs and DRF nonunion is an opportunity for further studies, particularly prospective multi-centered randomized controlled trials, to elucidate this risk fully.

15th Annual Center for Musculoskeletal Research Symposium
October 30, 2025

Title: The Effect of Lumbar Decompression on Functional Transitions in Patients with Lumbar Spinal Stenosis: Clinical and Biomechanical Evidence

Presenting Author: Prasanth Romiyo, MD

Co-Author(s): Ye Shu, BS, Tyler Schmidt, DO, Varun Puvanesarajah, MD

Lab PI / Mentor: Ram Haddas, PhD

ABSTRACT

INTRODUCTION: The prevalence of degenerative lumbar stenosis is estimated a third of the US population. Lumbar Stenosis with Neurogenic Claudication (LSNC) is defined as generalized weakness in the lower extremities exacerbated by walking and relieved with leaning forward that may be accompanied by cramping, pain, or paresthesias. The Sit to Stand (StS) task is an objective measure of functional transitional impairment with high verisimilitude to everyday movements. However, the range of motion and joint angles in LSNC patients performing functional transitions have not been firmly established. This study has two aims: (1) to identify and quantify disability and impaired movement patterns in patients with LSNC before surgery and compare them to healthy age-matched controls, and (2) to investigate the effect of lumbar decompression on these patterns in patients 3 months postoperatively.

METHODS: This study was a retrospective, single-center, concurrent cohort study comprised of patients between ages 45-68. Institutional review board (IRB) approval was obtained for this study. For Aim 1, 37 patients diagnosed with LSNC and 14 healthy age-matched controls were included. LSNC patients were tested one week before surgical intervention. For Aim 2, 36 LSNC patients completed testing both 1 week before surgery and 3 months after surgery. Before each visit, the patients completed the Oswestry Disability Index (ODI), Patient-Reported Outcomes Measurement Information System (PROMIS), and Tampa Scale of Kinesiophobia (TSK) questionnaires. All participants were fitted with a full-body external reflective marker set and performed three StS trials. The data were analyzed using a linear mixed-effects model in R (R 2025.5.1.513).

RESULTS: LSNC patients required longer StS times preoperatively (1.4 s) and postoperatively (1.6 s) versus controls (0.9 s). Preoperatively, hip flexion was reduced bilaterally (Left: 55.9° vs 66.7°, Right: 54.3° vs 66.1°), with increased hip adduction and rotation. Knee flexion was also lower compared with controls. Postoperatively, patients demonstrated reduced hip adduction and rotation, increased knee flexion (Left: 71.7° vs 66.4°), and decreased thoracic tilt (20.9° vs 27.4°) at maximum trunk lean. Patient-reported outcomes improved: ODI 23.0 vs 41.3, TSK 35.6 vs 43.5, PROMIS physical function 41.8 vs 34.8, pain 55.1 vs 65.3, and mood 35.6 vs 48.1.

DISCUSSION: Patients with LSNC required significantly longer times to complete the sit-to-stand task, reflecting impaired efficiency and functional capacity. Range-of-motion analyses revealed bilateral reductions in hip flexion, suggesting difficulty in generating forward trunk momentum. At maximum trunk lean, LSNC patients demonstrated reduced hip and knee flexion, indicative of a stiffer movement strategy. This compensatory rigidity, while protective, may increase stress on adjacent joints. At 3 months postoperatively, patients demonstrated increased knee flexion and reduced thoracic tilt at maximum forward lean, reflecting improved biomechanical efficiency, and decreased spinal loading during functional transitions. Postoperative reductions in hip adduction and rotation further suggested enhanced stability. Collectively, these findings support the role of decompression in restoring safer and more balanced movement strategies in LSNC patients. This study underscores the value of advanced motion capture technology and suggests that surgical intervention not only alleviates disability, but also facilitates restoration of safer functional mobility.

Title: Ulnar Nerve Transposition in Cubital Tunnel Release: Indications and Surgeon Rationale

Authors: Dominique Rinfret, BS; Justin Wong, BS, MPH; Constantinos Ketonis, MD, PhD

Introduction:

Ulnar nerve decompression for the symptomatic relief of cubital tunnel syndrome is an increasingly common procedure. The decision to perform an anterior ulnar nerve transposition remains largely at the discretion of the surgeon and is often indicated with ulnar nerve instability. We sought to characterize the clinical exam findings, intraoperative findings, surgeon training, and surgeon rationale on the decision to transpose. We hypothesize that surgeons in the cohort will have different rates of transposition and differing rationale in part influenced by training background and preferences.

Methods:

This was a single-center, retrospective study at a large academic center. Electronic medical records of patients aged 18 to 75 years that underwent ulnar nerve decompression and/or transposition identified via CPT code 64718, between January 2015 and December 2022, were reviewed. Exclusion criteria were traumatic mechanism of injury, revision procedures, and prior elbow surgery. Operative notes, electrodiagnostic studies (EDX), ultrasound studies, clinic notes, and patient demographics were collected and operative and clinic notes were assessed for indications for transposition.

Results:

A total of 1,019 patients that had undergone in situ releases, 282 subcutaneous transpositions, and 26 submuscular transpositions met the inclusion criteria. The EDX severity, gender, and race were similar among patients who received in situ decompression and ulnar transposition; however, patients who received a transposition had lower mean BMI (30.5 vs. 32.3; $p < 0.001$) and were younger (49.6 vs. 55.5; $p < 0.001$) compared to in situ patients. The cohort included 27 surgeons, 14 of whom performed at least 10 surgeries. Orthopedic surgeons conducted 94.1% of all cases. Although neurosurgeons accounted for 4.7% of all cases, they performed 14.2% of all transpositions. Of all surgeons, 19 performed at least one transposition, and only 9 performed at least one submuscular transposition.

Among the 309 patients who underwent transposition, 74.8% had the procedure due to some form of ulnar nerve instability, such as subluxation, perching, dislocation, or excessive mobility, which was identified pre-operatively, intra-operatively, or both. Notably, instability was documented pre-operatively in 3.1% and intra-operatively in 6.2% of patients who were ultimately left in situ.

Other reasons for transposition, including symptom severity, EDX findings, or muscle weakness, were included in 3.6% of indications. Surgeon-specific decisions, such as a history of successful contralateral transposition, accounted for 4.2% of transposed cases' rationales and were limited to a few surgeons. Importantly, in 17.5% of transpositions, the rationale was not clearly documented, though some of these cases included clinical notes

referencing features like muscle weakness that had prompted transposition in other patients.

Discussion:

Most surgeons performed at least one ulnar nerve transposition, primarily due to nerve instability identified either before or during surgery. However, 25.2% of transpositions were done for other or unclear reasons, including severe symptoms or a prior contralateral transposition. Not all cases of nerve instability led to transposition, as some unstable nerves were left in situ. Certain rationale were specific to a small number of surgeons, particularly in neurosurgery. Overall, surgeons varied in their frequency of transpositions, choice of transposition type, reasoning for the procedure, and the clarity with which they documented indications.

15th Annual Center for Musculoskeletal Research Symposium
October 30, 2025

Title:	ACL Reconstruction Improves Patient Reported Outcomes Regardless of Social Deprivation and Socioeconomic Factors
Presenting Author:	Patrick Castle, MD
Co-Author(s):	Omkar N. Prabhavalkar, BA; Melissa Holloway, MD; Hashim J Shaikh, MD; Dylan Greif, MD; Sandeep Mannava, MD PhD
Lab PI / Mentor:	Sandeep Mannava, MD, PhD

ABSTRACT

Background: Anterior cruciate ligament (ACL) reconstruction is a common procedure with generally excellent outcomes. Recently, increasing attention has been given to how social determinants of health influence recovery after orthopedic surgery. Two widely used measures of social deprivation are Area Deprivation Index (AD) and the Social Vulnerability Index (SVI). However, only a few studies have examined the relationship between ADI and patient reported outcomes following ACL reconstruction, and none have evaluated the impact of SVI. Understanding these associations is critical for promoting health equity and informing policies aimed at addressing socioeconomic barriers to recovery. Therefore, the objective of this study is to assess the influence of ADI and SVI on PROMIS scores and the likelihood of achieving a minimally clinically important difference (MCID) after ACL reconstruction. We hypothesize that greater social deprivation, as measured by ADI and SVI, will be associated with worse patient reported outcomes and lower rates of achieving MCID.

Methods: Patients who underwent arthroscopic ACL reconstruction at our institution between January 1, 2015, and December 31, 2023, were retrospectively reviewed. Inclusion criteria were age ≥13 years, diagnosis of partial or complete ACL tear, and completion of both preoperative and ≥6-month postoperative PROMIS questionnaires. Patients without a valid home address or complete survey data were excluded. Means and standard deviations were reported for continuous variables and compared between groups using one-way ANOVA tests; categorical variables were analyzed using chi-square tests. MCID was defined as one-half the standard deviation of preoperative PROMIS scores. ADI scores were calculated by geocoding patient addresses to census block groups and matching them to reference data from the Center for Health Disparities. SVI scores were matched using the patients' zip codes to the US Census SVI Data from 2022 and split into quartiles, with the highest quartile representing highest levels of social deprivation.

Results:
A total of 576 patients met inclusion criteria. The mean follow-up time was 13.0 ± 8.0 months, and the mean age was 27.9 ± 11.7 years. Baseline characteristics were similar for age, sex and ASA class across all quartiles. Patients in the highest ADI and SVI quartiles were associated with higher proportion of black patients ($p < 0.001$), higher BMI ($p = 0.0031$), and increased reliance on Medicare/Medicaid or Worker's Compensation ($p = 0.0019$). Pre-operative PROMIS Physical function (PF) and Depression (Dep) scores did not differ significantly across ADI or SVI quartiles. All ADI and SVI quartiles demonstrated significant improvement in PF, PI, and Depression at the latest follow up appointment (Table 1 and Table 2). At final follow up, the highest ADI quartile had higher PI scores (51.8 ± 9.5, $p = 0.016$) compared with lower quartiles. MCID achievement rates did not differ significantly across quartiles for PF, PI, and Dep for SVI, while Quartiles 1 and 2 had higher rates of achievement for PI than Quartiles 3 and 4 ($P = 0.043$) for ADI.

Conclusion: Higher levels of social deprivation, as measured by ADI and SVI were associated with difference in BMI, race, insurance status, and appointment adherence. Despite these disparities, there was significant post-operative improvements in PROMIS Physical Function, Pain Interference, and Depression across all quartiles, and MCID achievement rates were largely similar. These findings suggest that ACL reconstruction can provide meaningful functional and psychologic benefits to patients regardless of their socioeconomic status.

15th Annual Center for Musculoskeletal Research Symposium
October 30, 2025

Title:	Racial Differences in Rates of Surgical and Non-Surgical Treatment Of Complete Rotator Cuff Tears: A Propensity-Matched Database Study of 75,918 Patients
Presenting Author:	Nicholas Morriss, MD
Co-Author(s):	Sameer Jain BS, Omkar Prabhavalkar BA, Michaela Malin BA, Christopher Dussik MD, Brett P. Salazar MD, Patrick Castle MD, Sandeep Mannava MD, PhD
Lab PI / Mentor:	Sandeep Mannava MD, PhD

ABSTRACT

Introduction: Racial disparities in orthopedic care are documented, yet long-term comparative outcomes after complete rotator cuff (RC) tear remain incompletely characterized. We evaluated differences in surgical and nonoperative interventions between Black and White patients across multiple follow-up intervals after diagnosis. We hypothesize that Black patients will be less likely to undergo surgical repair and more likely to undergo conservative management with injection and physical therapy.

Methods: We performed a retrospective propensity score–matched cohort study using the TriNetX Research Network, a federated electronic health record database, from January 1, 2011, to December 31, 2020. Adult patients diagnosed with complete rotator cuff tear were identified using ICD-9/10 codes. Patients were categorized by race (Black or White) and matched 1:1 on age, sex, comorbidities, and relevant baseline characteristics. Outcomes assessed at 3 months, 6 months, 1 year, 3 years, and 5 years were identified by CPT codes and included rotator cuff repair (RCR), corticosteroid injection, physical therapy (PT) evaluation, other shoulder arthroscopic surgeries, and shoulder arthroplasty. Odds ratios, hazard ratios, and p-values were calculated for each outcome at each time point. Survival analyses were performed using Kaplan–Meier estimates and log-rank tests. Statistical significance was set at $p < 0.05$.

Results: Among 75,918 matched patients with complete rotator cuff tear (37,959 Black; 37,959 White), Black patients had consistently lower rates of rotator cuff repair (RCR) than White patients from 3 months (13.5% vs 15.9%, HR = 0.840; $p < 0.001$) to 5 years (19.6% vs 22.0%, HR = 0.880; $p < 0.001$). Corticosteroid injection utilization was higher in Black patients at all time points (5-year: 26.5% vs 25.6%, HR = 1.060; $p < 0.001$). Physical therapy evaluation was less frequent in Black patients (5-year: 27.0% vs 28.2%, HR = 0.947; $p = 0.007$), as was other shoulder arthroscopy (5-year: 21.2% vs 23.4%, HR = 0.896; $p = 0.012$). Shoulder arthroplasty rates were lower in Black patients at 5 years (3.6% vs 4.7%, HR = 0.757; $p = 0.005$).

Discussion: These results suggest persistent racial disparities in the management of complete rotator cuff tears, with Black patients less likely to undergo surgical interventions, physical therapy, or arthroplasty, and more likely to receive corticosteroid injections. These differences persisted over 5 years despite propensity matching. These results may implicate differences in access to care, referral patterns, patient preferences, and provider bias. Further research is needed to identify the cause of these disparities, and targeted interventions should aim to promote equitable orthopedic care.

Rosier Award Finalists Post-Doc Abstracts

Disclaimer

15th Annual Center for Musculoskeletal Research Symposium
October 30, 2025

Title:	The Function of Efhd1+ Telocytes in the Synovial Lymphatic System and Inflammatory Arthritis
Presenting Author:	Yue Peng
Co-Author(s):	H. Mark Kenney, Andriy Kobryn, Karen L de Mesy Bentley, Lianping Xing, Benjamin D. Korman, Christopher T. Ritchlin, Edward M. Schwarz
Lab PI / Mentor:	Edward M. Schwarz

ABSTRACT

Introduction: Lymphatic dysfunction is a hallmark of rheumatoid arthritis (RA) and contributes to chronic joint inflammation and damage[1]. A critical unresolved question is what signals activate mast cells that surround joint-draining lymphatic vessels to regulate lymphatic contractions? Recent scRNAseq analysis of popliteal lymphatic vessel (PLV) cells [2] identified Efhd1 as a selective marker of a previously unrecognized peri-PLV telocyte population. Telocytes are stromal cells with long telopodes that support tissue organization and cell communication. Notably, these telocytes are significantly reduced in RA synovium [3]. Transmission electron microscopy and confocal microscopy further revealed direct contacts between mast cells and telocyte networks, suggesting that these peri-PLV telocyte networks sense osmotic and mechanical stress in the joint and signal to peri-PLV mast cells that release vasoactive molecules to modulate lymphatic function.

Methods: PLVs from tamoxifen-treated Efhd1-CreERT2 x Ai9 mice were cultured ex vivo to establish co-cultures of tdT+ telocytes and tdT- fibroblasts. Osmotic stress responses were assessed using sucrose, with Fluo-4 and MitoSOX-Green dyes measuring Ca++ flux and mitochondrial ROS respectively. We also performed Matrigel invasion assays +/- TGF-β, and bulk RNAseq of FACS purified tdT^+ telocytes cultured on low, intermediate, and high stiffness-defined extracellular matrix (ECM) substrates.

Results: Telocytes exhibited significantly greater Ca++ flux in response to sucrose-induced hyperosmotic stress than fibroblasts (63.83% ± 6.86% vs 45.95% ± 5.33%, $p<0.01$), and increased mitochondrial ROS production was only observed in telocytes (10min vs baseline, $p<0.0001$). Fibroblasts displayed greater invasive capacity in Matrigel vs. telocytes (209.80 ± 17.38 μm vs 183.06 ± 28.26 μm). Bulk RNAseq showed tdT+ telocytes differentiated into myofibroblasts on stiff ECM. Consistently, scRNAseq trajectory analysis of synovial lymphatic system (SLS) cells predicted telocyte-to-fibroblast differentiation, supporting their potential contribution to pathogenic fibroblast populations.

Discussion: Our findings support a model in which Efhd1+ telocyte networks regulate joint homeostasis by sensing osmotic stress and relaying signals to mast cells, thereby promoting lymphatic clearance. Mechanistically, telocytes exhibit high cytosolic Ca++ flux and increased mitochondrial ROS (Mitoflash), coupled with low invasive capacity, consistent with Efhd1 mediated regulation of mitochondrial Ca++ uptake and inhibition of YAP/TAZ metastasis pathway [4]. In contrast, under conditions of chronic inflammation and stiff ECM, telocytes lose Efhd1 expression, acquire myofibroblast features, and activate the YAP/TAZ pathway enhancing invasiveness. Collectively, our study identifies telocytes as a critical stromal population that senses osmotic and mechanical cues to regulate SLS functions, which highlights their potential as therapeutic targets to restore joint drainage and limit damage from arthritis.

1. Bouta, E.M., et al., 2018. 14(2): p. 94-106.
2. Kenney, H.M., et al., Arthritis Res Ther, 2022. 24(1): p. 64.
3. Rosa, I., et al., J Cell Mol Med, 2021. 25(4): p. 2274-2278.
4. Meng, K., et al., Cancer Sci, 2023. 114(5): p. 2029-2040.

15th Annual Center for Musculoskeletal Research Symposium
October 30, 2025

Title:	Integrated Imaging and Spatial Transcriptomic Analyses of Blood Vessel Coupling to Healing Tissue During Auto and Allograft Bone Transplantation
Presenting Author:	Xiaojie Xing
Co-Author(s):	Tianfeng Miao, Samantha Mill
Lab PI / Mentor:	Xinping Zhang

ABSTRACT

Background: Autograft and allograft are commonly used in reconstruction of large bone defect. Utilizing a murine segmental femoral bone graft transplantation model, we previous show that autografts demonstrate enhanced endochondral bone formation and rapid bone remodeling largely due to the robust osteogenic and angiogenic activities elicited by periosteum. In contrast, the absence of periosteum in allografts leads to persistent fibrotic tissue formation, contributing to inferior healing and poor osseointegration. The goal of this study was to integrate lineage tracing and spatiatranscriptomics analyses to delineate the cellular and genetic underpinning of vessel coupling to auto and allograft bone healing.

Methods: Auto and allografting samples were harvested at weeks 1, 2, and 5 post-surgery. A Col1(2.3)GFP; AplnCreER; Ai14 (tdTomato) transgenic mouse line was used to trace the coupling of sprouting endothelial cells (EC) to osteoblasts and healing tissue. NanoString GeoMx Digital Spatial Profiling technology was used to perform spatial and temporal gene expression analyses across bone forming (BF) and non-bone forming (NBF) regions. Following quality control, ~13,000 genes from selected ROIs were retained following low-expression filtering and batch correction across three replicates. These data were used for DEG and GO enrichment analyses, GSEA and ssGSEA of pathway activity, and CellChat-based cell–cell communication analysis.

Result: Lineage tracing utilizing dual-fluorescent mouse models labeling osteoblasts and sprouting vessels revealed distinct spatial coupling of sprouting ECs with osteoblasts and fibrotic tissue in BF and NBF regions of auto- and allografts. Spatial transcriptomic profiling with GeoMx showed heightened oxidative phosphorylation in BF regions and sustained hypoxia, inflammatory signaling and glycolytic metabolism in fibrotic tissues. The GSEA showed intergroup differences mostly pronounced at week 2 with BF-associated EC expressing pro-angiogenic factors (Itgb3, Tgfbr2), suggesting enhanced vessel growth to support osteogenesis. In contrast, EC from FT regions showed upregulated anti-apoptosis markers (Col18a1, Ramp2), indicating enhanced survival in a potentially stressful or inflammatory microenvironment. Further ssGSEA analyses demonstrates EC in BF regions had higher level of OXPHOS and fatty acid metabolism, consistent with the high energy demands of bone repair, whereas hypoxia remained pronounced in FT regions despite the presence of abundant sprouting vessels, as confirmed by histological observations, likely reflecting the limited perfusion or functional immaturity of these microvessels. Intercellular communication analysis indicated preferential Slit-Robo, Wnt, and BMP pathway activation between OB and EC in BF regions, supporting coordinated osteogenesis and angiogenesis. Conversely, FT areas showed dominant Cxcl5-Ackr1, CD34-Selp, and Il22–Il22ra1 interactions, highlighting enhanced inflammatory signaling in this region.

Conclusion: This study highlights increased mitochondrial activity and metabolic reprogramming in bone-forming regions, reflecting the high energy and oxygen demands for bone repair. Conversely, persistent fibrotic regions during allograft healing show upregulation of inflammatory genes and pathways, underscoring barriers to graft integration. Further analyses are needed to validate the potential targets for therapeutic intervention aimed at reducing fibrotic tissue formation and promoting better osseointegration.

Rosier Award Finalists Pre-Doc Abstracts

Disclaimer

15th Annual Center for Musculoskeletal Research Symposium
October 30, 2025

Title:	The Role of Mitochondrial Dynamics in Bone Marrow Stromal Cell Efferocytosis
Presenting Author:	Sandra Castillo Aguirre
Co-Author(s):	Sarah Catheline, Renae Duncan, Xingyu Jing, Emily Quarato, Laura Calvi, Roman Eliseev
Lab PI / Mentor:	Roman Eliseev

ABSTRACT

Introduction: Senescence of bone marrow stromal cells (BMSCs), precursors of bone-forming osteoblasts, contribute to age-related bone loss. Despite their critical role in bone microenvironment, the mechanism underlying age-dependent BMSC dysfunction is incompletely understood. Efferocytosis, the clearance of apoptotic cells by macrophages, is a vital process that declines with age within the bone marrow due to macrophages dysfunction, leading to a reduced clearance of end-stage apoptotic neutrophils (aPMNs). A recent study done together by Calvi and Eliseev groups, has shown that excessive efferocytosis by BMSCs impairs osteogenic differentiation and promotes senescence. This suggests that efferocytosis contributes to, and could be a novel mechanism of, BMSC dysfunction. We have observed that following neutrophil efferocytosis, mitochondria in BMSCs become less functional, produce more ROS, and are more fragmented. The mechanism of efferocytosis by BMSCs is not well understood. Therefore, our objective is to understand the mechanism of both aPMN attraction to BMSC and mitochondrial dysfunction in BMSC post-efferocytosis. We hypothesize that aPMN efferocytosis promotes mitochondrial fis-sion via DRP1, leading to mitochondrial dysfunction and senescence in BMSCs

Methods: To explore the role of mitochondrial fission (fragmentation) in efferocytosis and BMSC dysfunction, BMSC-specific Prx1Cre mice were crossed with Drp1f/f mice to delete Drp1, a key protein in mitochondrial fission. In vitro assays were conducted to assess the impact of Drp1 deletion on mitochondrial morphology, cellular metabolism, oxidative phosphorylation (OXPhos), senescence, and osteogenic potential following aPMN exposure. BMSCs were isolated, cultured, and exposed to varying doses of aPMN at ratios of 3:1 and 10:1 (aPMNs : BMSCs). Flow cytometry (to measure rate of efferocytosis), Seahorse assay (to assess cellular metabolism and OXPhos), and osteogenic differentiation assays (to evaluate osteogenic potential) were performed. To investigate whether targeting mitochondrial fission could rescue MSC function, bone phenotypes were analyzed in young (3-4 months) and middle-aged (12-13 months) Drp1f/f and Prx1Cre/+ mice using DEXA.

Results: Initial findings of mitochondrial morphology confirmed inhibition of fission (higher aspect ratio, i.e. elongated mitochondria) in Prx1Cre;Drp1f/f BMSCs compared to controls. Efferocytosis rates were significantly lower in these cells at 10:1 aPMNs : BMSCs ratio suggesting efferocytosis was impaired in Cre+ cells. The Seahorse assay revealed that ATP production was initially similar between Cre- and Cre+ cells but declined significantly in Cre+ cells following aPMN treatment (3:1), with the greatest reduction observed at the 10:1 ratio. Additionally, ALP staining at day 7 showed a significant decrease across all conditions in Cre+ cells, which was corroborated by reduced Alpl expression. Furthermore, suppressed cell growth in response to efferocytosis was observed in both Cre+ and control cells. Whole-body composition analysis revealed that femoral bone mineral density (BMD) was higher in young Cre+ females compared to Cre- littermates. Bone mineral content (BMC) was also elevated in young Cre+ females. No significant differences in BMD or BMC were observed in tibias across age or sex groups, although data collection is ongoing.

Discussions: Collectively, these preliminary findings indicate that Drp1-mediated mitochondrial fission is essential for maintaining BMSC function, osteogenic potential, and efficient efferocytosis in response to apoptotic neutrophils. Notably, femoral BMD was higher in young Cre+ females compared to controls, despite reduced osteogenic potential observed in vitro. This discrepancy may reflect compensatory signaling from other cell types or microenvironmental influences. Ongoing studies aim to further manipulate mitochondrial fission to validate and extend these findings.

15th Annual Center for Musculoskeletal Research Symposium
October 30, 2025

Title:	Macrophage dysfunction enhances bone marrow stromal cell efferocytosis and accelerates bone marrow aging
Presenting Author:	Zhiming Jin
Co-Author(s):	Emily R. Quarato, Swachi H. Patel, Jane Zhang, Adam Tyrlik, Catherine Caballero, Ronald Lakony, Nataliia Vdovichenko, Chunmo Chen, Noah Salama
Lab PI / Mentor:	Laura M. Calvi

ABSTRACT

Background: Bone marrow aging is marked by dysregulation in osteogenesis and hematopoiesis, partially caused by dysfunction of bone marrow (BM) stromal cells (BMSCs) under stress. One major stress inducer is the accumulation of uncleared apoptotic cells, with potential transformation into necrosis, driving chronic inflammation. Aged BM macrophages, with the loss of key efferocytic receptor Axl, have phagocytic defects associated with increased end-stage neutrophils, inflammation, and myeloid skewing. To compensate, aged BMSCs, known as non-professional efferocytes, increase engulfment of apoptotic cells, which enhances senescence and decreases function. However, whether defects in macrophage phagocytosis drive increased BMSCs efferocytosis remains unknown. Insulin-like growth factor 1 (IGF1) was reported to decrease with aging in the BM and can inhibit non-professional efferocytes in clearing apoptotic cells. Our published datasets comparing young and aged macrophages suggested reduced IGF1 expression transcriptionally. Hence, we hypothesized that reduced macrophage efferocytosis increases BMSCs efferocytosis, via reduced IGF1 signaling, leading to their decreased function in osteogenesis and hematopoietic support in aging.

Experiments & Methods: To assess how efferocytosis defects in BM macrophages drive BMSCs efferocytosis, we used young (3-4-month-old) mice lacking Axl in macrophages (Axlf/f x LysM-Cre). The efferocytic capacity of BMSCs and BM macrophages was assessed via an in vivo efferocytic challenge, where labeled apoptotic human neutrophils were injected retro-orbitally, and validated engulfment using flow cytometry. BMSCs' function changes were evaluated by quantifying hematopoietic progenitor cell populations and osteogenic differentiation (CFU-OB assay). To examine transcriptomic alterations suggesting macrophage–stromal communication, BMSCs and macrophages from WT and transgenic mice were flow-sorted and proceeded for bulk RNA sequencing. The role of IGF1 signaling was tested by adding IGF1 to primary bone marrow cultures and by generating BMSC-specific IGF1 receptor–deficient mice (Prx-Cre+/- x Igf1rf/f), both of which were analyzed in the efferocytic challenge. The molecular mechanism by which IGF1 suppresses BMSCs efferocytosis was assessed via western blotting.

Results: In Axlf/f x LysM-Cre mice, we confirmed a decrease in efferocytosis by macrophages, while efferocytosis by BMSCs was doubled ($n=7$, $p<0.01$). In BM, we observed increased short-term hematopoietic stem cells, progenitors throughout the myeloid lineage, neutrophils, and monocytes ($n=7$, $p<0.05$), an early myeloid shift confirmed by complete blood counts ($n=22$, $p<0.05$). Colony-forming assays showed reduced osteoblastic differentiation ($n=4$, $p<0.01$). Thus, defective macrophage function increases BMSC efferocytosis, leading to their impaired differentiation and premature myeloid skewing. Transcriptional CellChat analysis revealed reduced stromal–macrophage signaling through downregulation of CCL7–CCR3, while a heatmap showed a shift of BMSCs from osteogenesis toward adipogenesis, accompanied by diminished HSC support. Mechanistically, we observed a significant decrease in BMSC efferocytosis with IGF1 treatment ($n=3$, $p<0.01$), while macrophages remained less affected. In the Prx-Cre+/- x Igf1rf/f model, we also observed an enhanced apoptotic cell clearance by Igf1r-deficient BMSCs ($n=4$, $p<0.05$). Previous lab data suggested pharmacologic inhibition of Axl, but not Mertk or Tyro3, reduced BMSC efferocytosis in vitro, highlighting Axl as the key efferocytic receptor. In ST2 cells, the western blot indicated a suppression of Axl in response to IGF1, revealing how young macrophages restrain stromal cells from performing efferocytosis.

Discussion & Conclusion: These data suggest that reciprocal changes in BM macrophage and BMSC efferocytosis, via IGF1 signaling, cooperate to regulate myeloid shifting and skeletal changes associated with aging.

15th Annual Center for Musculoskeletal Research Symposium
October 30, 2025

Title:	Taurine transporter SLC6A6 expression promotes mesenchymal stromal cell function
Presenting Author:	Christina Kaszuba
Co-Author(s):	Christina M. Kaszuba, Benjamin J. Rodems, Sonali Sharma, Cameron D. Baker, Edgardo I. Franco, Takashi Ito, Palomi Schacht, Kyle P. Jerreld, Emily A. Johnson, Bradley R. Smith, Chen Yu, Emily R. Quarato, Francisco A. Chaves, Jane L. Liesveld, Laura M. Calvi, Hani A. Awad, Roman A. Eliseev, and Jeevisha Bajaj
Lab PI / Mentor:	Jeevisha Bajaj, Hani Awad

ABSTRACT

Background & Hypothesis: Mesenchymal stromal cell (MSC) differentiation is critical for the development, maintenance, and repair of bone tissue. This occurs within the bone marrow microenvironment, which consists of various stromal populations and structural components that support skeletal homeostasis. MSCs also promote self-renewal of hematopoietic stem cells and regulate their differentiation. Analysis of our own and publicly available sc-RNA seq datasets of the murine non-immune bone and bone marrow indicates that MSCs express high levels of Slc6a6, the taurine transporter (TauT). Taurine, a non-essential amino acid has been shown to mitigate the onset of bone defects in aged mice. However, the role of taurine in regulating the differentiation fate of MSCs, especially in young populations, remains unclear. Here, we use Slc6a6-/- mice to determine the impact of loss of taurine uptake on MSC function in young, 16 week animals.

Experiments, Methods, & Results: Experiments were conducted using young TauT genetic loss-of-function murine models, with all experiments separated by sex. We find that TauT loss impacts MSC populations in vivo (n=15) and impairs MSC osteogenic differentiation in vitro (n=6). This correlates with decreased bone mineral density (n=6) and bone strength (n=10) in young TauT knockout mice. Importantly, shRNA-based knockdown of TAUT expression in primary human MSCs reduces osteogenic differentiation (n=3), indicating a key role of taurine uptake in MSC function. Consistent with this, we find that TauT null MSCs are unable to support self-renewal and expansion of co-cultured hematopoietic stem and progenitor populations (n=3). Mechanistically, TauT loss results in metabolic changes that lead to increased oxidative stress (n=5) and reduced Wnt/b-catenin signaling (n=5), which induce MSC senescence (n=4) and apoptosis (n=8). Further, we found an upregulation of gene sets related to immune response. Collectively, our data identify taurine as a key regulator of MSC maintenance and osteogenic fate determination. Quantifiable outcomes were compared using ANOVA or student's unpaired T-tests.

Discussion & Conclusion: We find that TauT loss leads to impaired Wnt pathway activation. Wnt signaling plays a critical role in regulating MSC osteogenic fate. We find that GSK3β inhibition and β-catenin stabilization, can rescue osteogenic differentiation in TauT-/- MSCs. In addition, our metabolomic analysis of TauT-/- MSCs identifies a significant downregulation of myo-inositol. Myo-inositol plays an essential role in antioxidant and metabolic regulation, and Wnt signaling. Consistent with this, we show that myo-inositol can not only restore normal ROS levels in TauT-/- MSCs but also rescue their osteogenic differentiation capacity. Loss of antioxidants like taurine and myo-inositol, and subsequent increase in ROS levels, possibly lead to impaired Wnt activation, senescence, and impaired MSC osteogenic fate. Collectively, our data shows that TauT is a key regulator of MSC function and suggests that modulating taurine uptake in these cells may be of therapeutic interest in instances of bone fracture, osteopenia and osteoporosis.

Patients with acute myeloid leukemia (AML), or those undergoing chemotherapy often develop osteopenia/osteoporosis. We recently identified a key role of taurine uptake by TauT expressing AML cells in the bone marrow in promoting AML progression. It is thus possible that expanding cancer cells deplete available taurine in the bone marrow, leading to reduced taurine availability for MSCs. This may impair bone marrow MSC function and contribute to defects in osteogenic differentiation and subsequent osteopenia. Given the dual requirement for taurine by leukemia cells as well as MSCs in the bone marrow, it may be of interest to study the dynamics of taurine uptake, and the impact of taurine inhibitors or supplemental taurine on bone health in models of these aggressive leukemias.

15th Annual Center for Musculoskeletal Research Symposium
October 30, 2025

Title: Compartmentalized inflammatory landscape and macrophage plasticity regulate Tet2+/- mediated clonal hematopoiesis

Presenting Author: Kevin Lee

Co-Author(s): Cih-Li Hong, Wimeth Dissanayake, Gulzada Kulzhanova, Alex Pfeffer, Senthil Sivakumar, Emily R. Quarato, Lauren Bennodt, Jeevisha Bajaj, Chia-Lung Wu, Laura M. Calvi

Lab PI / Mentor: Shu-Chi A. Yeh

ABSTRACT

Background: Clonal hematopoiesis (CH) is diagnosed when greater than 2% of blood cells contain mutations associated with hematological cancer. Tet2 loss-of-function in hematopoietic stem cells (HSCs) is a prevalent driver in CH and widely affects myeloid neoplasms. It is understood that both the mutation-associated mechanisms and cell-extrinsic factors, such as inflammation, lead to selective expansion of mutant cells within the bone marrow (J. Exp Med. 218:e20201544, 2021). Despite the presence of these systemic factors, our prior work showed that clonal expansion of Tet2 clones is compartmentalized by bone marrow cavities with bone resorptive activities, whereas cells remain solitary at sites predominated by bone formation. Guided by these findings, we hypothesize that the pro- and anti-CH factor(s) released by resident niche cells is impacted by the local bone remodeling process within micro marrow cavities. Elucidating the niche factors and cellular crosstalk around Tet2+/- cells will help us uncover targetable microenvironmental mechanisms that may be preserved across mutations.

Methods: We recently reported that ultralow-dose irradiation enables engraftment and intravital tracking of disease initiating niches in CH (Sci. Reports 14:20486, 2024). We further utilized bone front staining (Calcein blue and Alizarin Red, 30mg/kg) administered 2 days apart to discern between bone forming and resorbing cavities. To assess niche factors, we harvested cells from Tet2+/- growth hot spots and cold spots under image guidance for single cell transcriptomics at week 1/week 22 post transplantation (10x Genomics). Functional and mechanistic studies of the niche marrow macrophages (identified by the single cell and imaging) were performed using cytokine secretion assays in primay macrophage culture. Tet2+/- Clonal burden was evaluated in Csf1r-cre+ vs. cre-;Il10-floxed models and via macrophage polarization treatment. One-way ANOVA, Mann-Whitney or unpaired tests were used based on normality test.

Results: We showed that Tet2+/- cell expansion remained restricted within the marrow cavities undergoing bone remodeling (N=5) and revealed host Cd206+ marrow macrophages(MMs) association to Tet2+/- cells throughout disease progression (N=12). Via spatial single cell transcriptomics and functional assays, we found that within the bone resorptive cavities, immune responses were upregulated along with upregulation of Il1b. When these cultured Cd74/Cd206+ marrow macrophages were treated in calcium conditions (1.5mM [Ca2+])(Nat Comm. 13(393), 2022) and nano-particle hydroxyapatite (100ug/mL) mimicking bone resoprtion, the MMs secreted higher IL1b, a known driver of CH, when compared to the control. More interestingly, macrophages from the bone forming cavities had significantly downregulated immune response (FDR=0.044), exhibited anti-inflammatory M2 phenotypes (CD206+) and remained low MHCII positivity even when stimulated by pro-CH inteferon-y (100ug/mouse). To test whether this inflammation-resistant feature is a result of anti-inflammatory Il10 and its role in suppressing Tet2 growth, we evaluated clonal development in mice carrying macrophage-specific (Csf1r-cre) deletion of Il-10. The results showed that IL10 deletion resulted in a marked increase in total clonal burden and depletion of Tet2 growth coldspots. Treatment using M2-polarizing IL-4 or MHCII monoclonal antibody mitigated clonal development.

Discussion: This work builds upon the idea that bone remodeling shapes inflammatory landscapes and CH progression. We showed that CD206+ MMs can exhibit distinct transcriptomic profiles, antigen presentation, and cytokine secretion shaped by local bone remodeling. Our study is limited by the technical limitation to measure local cytokine levels in individual cavities. Nevertheless, the finding presents a targetable mechanism and warrants further studies on the use and precautions on bone-modulating management in clonal blood disorders.

15th Annual Center for Musculoskeletal Research Symposium
October 30, 2025

Title: TREM1 Promotes Neutrophil Extracellular Trap Release Associated With Latent TGFβ1 Activation to Induce Age-related Osteoporosis

Presenting Author: Cheng Xiang

Co-Author(s): Atikul Islam, Jun wu, Rong Duan, Zhenqiang Yao, Lianping Xing

Lab PI / Mentor: Brendan F Boyce

ABSTRACT

Background & Hypothesis: Osteoporosis is characterized by weakened bones and increased fracture risk, associated with increased numbers of immune cells in bone marrow (BM) that negatively influence bone mass. We previously reported that neutrophils secreting TGFβ1 exacerbate bone loss during aging. Neutrophil extracellular traps (NETs) are released by neutrophils in response to infections, but also in non-infectious conditions and contribute to tissue damage and inflammation, but their role in bone loss during age-related osteoporosis is unknown. Triggering receptor expressed on myeloid cells 1 (TREM1), expressed on neutrophils, modulates cell functions and amplifies Toll-like receptor 4 (TLR4)-mediated inflammatory responses. We hypothesize that TREM1 levels increase in neutrophils during aging and promote NETosis in BM to activate latent TGFβ, thus promoting age-related osteoporosis.

Experiments & Methods: ELISA and Immunofluorescence staining (IF) with NETosis markers to assess NETosis in BM from 3-mon-old young and 18-mon-old aging mice. Cytokine array, single cell and flow cytometry to characterize neutrophil NETs. A TREM1 inhibitor (LR12) or agonist Ab were used to examine their effect on NETs released in BM from young and aging mice by comparing dsDNA generation and visualizing NETs (using Sytox Green). NETs were generated following established procedures to examine their effects on osteoblast (bone marrow mesenchyme stromal cell (BMSC,) and bone-derived mesenchyme progenitor cell (BdMPC)) or osteoclast (bone marrow macrophages (BMMs)) precursor differentiation in vitro. We evaluated changes in bone volume and turnover in vivo following pharmacological intervention of NETosis using LR12, DNase I and Cl-amidine (a NETosis inhibitor) in aging mice, as well as in an aging PAD4 KO mouse model, or intraperitoneal injection (i.p.) injection of enriched NETs into 3-mon-old mice. A TGFβ1 neutralizing Ab was used to assess if TGFβ in NETs inhibits bone formation. Mass spectrometry, ELISA, IF and Western blotting were used to study the relationship between NETosis and TGFβ activation.

Results: Levels of dsDNA, DNA- myeloperoxidase (MPO) complex, and neutrophil elastase (NETosis biomarkers) were increased in the BM of aging mice. NETs colocalized with citrullinated histone 3, MPO and Ly6G in aging mouse BM, but rarely in young mice. TREM1 was increased in BM neutrophils of aging mice and was positively associated with increased ROS levels. Modulating TREM1 expression with LR12 or agonist Ab reduced and increased NETosis rates, respectively. In addition, TLR4 expression was upregulated and co-expressed with TREM1 on neutrophils in BM of aging mice, associated with upregulation of TREM1 mRNA, promotion of TREM1 multimerization on the surface of neutrophils, and activated downstream signaling. Moreover, single cell and flow cytometry data showed that TREM1-high neutrophils have increased NETosis and neutrophils with NETosis have high CXCR2 (mature neutrophils) and low CXCR4 (senile) and TGFβ1 expression. NETs promoted osteoclastogenesis and inhibited osteoblast differentiation in vitro in a dose-dependent manner, and i.p. injection of NETs induced bone loss in young mice in vivo, while targeting NETosis increased bone mass in aging mice. The inhibitory effects of NETs on bone formation in vitro were rescued by blocking TGFβ1 signaling. Mechanically, MMPs especially MMP9, were enriched in NETs and significantly increased active TGFβ1 levels, which was rescued by blockage of MMPs and DNase I.

Discussion & Conclusions: The TLR4-TREM1 axis is upregulated in the BM of aging mice, associated with increased levels of ROS that promote NETosis and of MMPs (primarily MMP9) in NETs that significantly upregulate activation of TGFβ1, thereby promoting age-related osteoporosis.

Keywords: Age-related osteoporosis, neutrophil extracellular traps, TREM1, TGFβ1

15th Annual Center for Musculoskeletal Research Symposium
October 30, 2025

Title:	CNN-Based Evaluation of Wrist Bone Health and Fracture Risk Using Raman Spectroscopy of the Proximal Phalanx
Presenting Author:	Anthony Yosick
Co-Author(s):	Mohammad Hosseini, Sadia Afrin, Sophia Turbide MD, Andrew Berger PhD, Hani Awad PhD
Lab PI / Mentor:	Hani Awad PhD

ABSTRACT

Background & Hypothesis: Dual-energy X-ray absorptiometry (DXA) is the clinical standard for assessing bone mineral density (BMD) and diagnosing osteoporosis (OP) using T-scores. Alternatively, the Fracture Risk Assessment Tool (FRAX) incorporates additional patient factors to estimate a 10-year probability of fracture. Both methods, however, neglect compositional qualities that contribute to fracture toughness. Raman spectroscopy (RS) provides a non-ionizing, non-destructive molecular fingerprint of bone. Traditional RS analysis often focuses on parametrizing select spectral components leaving much spectral information unused, limiting a comprehensive assessment of bone quality. We hypothesized that full-spectrum RS can be leveraged through convolutional neural network (CNN) analysis to improve OP diagnosis and fracture risk assessment. This study aims to evaluate the sensitivity and specificity of CNN-based analysis of the full-spectrum RS of the proximal phalanx bones to predict the wrist (1/3 radius) T-scores and wrist fracture toughness, compared to RS parameter-based regression approaches. The proximal phalanx was selected for its accessibility, minimal soft tissue coverage, and potential to reflect systemic skeletal properties at sites of fragility fractures.

Experiments & Methods: Human cadaveric specimens (n=25 female, mean age 70.2±14.8 years, BMI 26.5±7.7 kg/m^2) were obtained from Anatomy Gifts Registry. Given higher OP risk in females, only non-paired female forearms were included. DXA scans of the 1/3 radius (Hologic Horizon Ci) classified donors as normal (N; n=8), osteopenic (OPE; n=6), or OP (n=11). Biomechanical testing simulated a fall on an outstretched hand (FOOSH) using established protocols with forearms mounted in pronation with 15° radial abduction and loaded at 3.3 mm/s on an Instron ElectroPuls E10000. This consistently produced clinically relevant radial fractures, from which force-displacement data determined work to fracture. Following testing, second proximal phalanx specimens were dissected and rehydrated in 1xPBS for 2 h prior to spatially offset Raman spectroscopy (SORS). SORS was collected using an 830 nm, 100 mW laser at 0- and 3-mm offsets. Raw spectra were preprocessed and fluorescence removed using an iterative algorithm and normalized to the phosphate (v_1PO_4) peak and used to calculate phosphate to matrix ratio (PTMR; 924-986 cm^{-1}), carbonate to matrix ratio (CTMR; 1054-1098 cm^{-1}), and carbonate to phosphate ratio (CTPR), with Amide I (1596-1720 cm^{-1}) as the matrix reference. Predictive modeling included partial least squares regression (PLSR) with leave-one-out cross-validation (LOOCV) using PTMR, CTMR, CTPR, age, and BMI, and an established CNN model trained with LOOCV on the full spectrum (744-1740 cm^{-1}) with age and BMI. Donor-level results were obtained by averaging all spectral results and classified as N (T-score > -1), OPE (-2.5 < T-score ≤ -1), OP (T-score ≤ -2.5), and low (≥19 J) versus high (<19 J) fracture risk, based on FOOSH thresholds.

Results: PLSR best predicted T-scores (R^2=0.779; RMSECV=0.923), while CNN had lower accuracy (R^2=0.664; RMSECV=1.137). Both models distinguished WHO categories with high accuracy; N vs OP classification achieved AUCs of 1.000 (PLSR) and 0.989 (CNN). CNN outperformed PLSR for predicting work to fracture (R^2=0.151; RMSECV=7.926 J). For fracture risk classification, CNN outperformed PLSR (AUC=0.873 vs 0.833).

Discussion & Conclusions: Both parameter-based and full-spectrum SORS effectively predicted wrist T-scores and fracture risk. CNN offered improved fracture risk classification, achieving accuracy comparable to T-scores and superior to FRAX. Limitations include the analysis of exposed bone samples and a single FOOSH orientation. Future work will evaluate transcutaneous SORS and other major fracture sites. These findings highlight SORS as a promising tool for osteoporosis screening, longitudinal monitoring, and early fracture risk assessment.

Rosier Award Finalists 3MT Posters

Disclaimer

15th Annual Center for Musculoskeletal Research Symposium
October 30, 2025

Title: Hematopoietic Stem Cell (HSC) - Macrophage Interactions Promote Preferential HSC Division in Bone Resorptive Cavities

Presenting Author: Ryan Adapathya

Co-Author(s): Cih-Li Hong, Kevin Lee, Wimeth Dissanayake, Joseph Collins, Montgomery L. Whalen, Laura M. Calvi, Leonard I. Zon

Lab PI / Mentor: Shu-Chi A. Yeh

ABSTRACT

Background: Hematopoietic stem cells (HSCs) are responsible for producing all mature blood and immune cells in the body throughout life. Under inflammatory stress (e.g., aging), HSCs can proliferate, causing compromised stemness and skewed myeloid differentiation, ultimately resulting in increased risks of infection and myeloid malignancies. HSCs primarily reside in the bone marrow which provides cellular and molecular factors to instruct HSC fate. Recently, we showed that individual marrow cavities are characterized by distinct stages of bone remodeling. Marrow cavities can be classified as either bone forming (non-resorptive, NR) or bone resorbing (resorptive, RE), and the stressed HSCs almost exclusively expanded in the RE cavities. Notably, we found that HSCs exhibit close spatial association with marrow macrophages. Macrophages have been reported to regulate HSC clonality in a zebrafish model: Stressed HSCs express “don’t-eat-me” (MHCI) signals through the TLR3 axis, which promotes pro-inflammatory macrophages to take up HSC cytoplasmic materials (termed grooming), resulting in HSC division (Rodrigues et al. Science, 2024). Taken together, these lead to the hypotheses that (1) the grooming mechanism is conserved in murine models, and (2) macrophages in RE cavities are pro-inflammatory and facilitate this interaction, which regulates HSC division under stress and myeloid bias.

Methods: To test the hypotheses, we performed intravital imaging using two photon microscopy on murine calvarial bone marrow. For visualizing HSC-macrophage interactions, we utilized a transgenic mouse model in which GFP is restricted in the HSCs (Mds1GFP;Flt3cre). In determining whether the grooming mechanism is conserved, we retro-orbitally injected a fluorescent MHC-I antibody (Biolegend). As a positive control, we used grooming inducer DL-PPMP (drug found through prior screening). For investigating the difference in HSC behavior between NR and RE cavities, we delivered bone front staining two days before imaging to track bone resorption. HSC-macrophage interaction frequencies were calculated and processed in GraphPad Prism. Unpaired t-tests or Mann-Whitney tests are used to determine statistical significance based on data normality.

Results: Through intravital imaging, we observed HSC-interactions resembling grooming interactions, as reported in zebrafish. With the addition of DL-PPMP, the interactions increased and significantly increased the MHCI expression on the interacting HSCs. Via time-lapse tracking every 5 minutes for 8 hours, HSC division was observed at 30 minutes after the interactions with marrow macrophages. Quantifying the frequencies of grooming across marrow cavities, we showed that grooming interactions predominantly occurred in RE cavities at the steady state and notably, under acute inflammation. Anti-resorptive treatment (zoledronate, 1.2ug/mouse) significantly reduced the frequency and suppressed HSC division.

Discussion: The presence of MHCI on grooming HSCs suggests that the grooming mechanism between HSCs and macrophages may be conserved in mouse models. This is further supported by the DL-PPMP positive control, which increased both overall grooming interactions and MHCI expression. The coincidence of inflammation-induced expansion and increased grooming in RE cavities suggests a potential mechanism underlying compromised HSC stemness and skewed differentiation. Ongoing work of this project includes understanding mechanisms and roles of grooming in a mammalian context. We will use macrophage-specific knockout models (e.g., Csf1r-cre) to test the effect of pro- and anti-inflammatory cytokines and adhesion molecules involved in such interactions. In conjunction, we will conduct reconstitution assays with HSCs isolated from WT vs. knockout models to determine the functional significance. The finding will provide insight into novel therapeutic targets to mitigate HSC dysfunction under inflammatory stress.

15th Annual Center for Musculoskeletal Research Symposium
October 30, 2025

Title: Role of Mitochondrial Genetics in the Response of Bone Marrow Stromal Cells to Mechanical Stimulation

Presenting Author: Renae Duncam

Co-Author(s): Sarah Catheline, Sandra Castillo Aguirre, Chen Yu, Xingyu Jing

Lab PI / Mentor: Roman Eliseev

ABSTRACT

Background & Hypothesis: Age-related bone loss is driven not only by hormonal changes but also, according to recent research, by mitochondrial dysfunction. Emerging evidence suggests that this aging-related mitochondrial dysfunction may be reversible. Combinations of single nucleotide polymorphisms (SNPs) form mitochondrial DNA (mtDNA) haplogroups, which correlate with variation in mitochondrial oxidative phosphorylation (OxPhos) efficiency and also in bone phenotype. The oldest African mtDNA haplogroups, L and M, have a small number of SNPs, resulting in efficient OxPhos and stronger bones, while Eurasian haplogroups have less efficient OxPhos and weaker bones. Inbred C3H/HeJ (C3H) mice mimic the African population, and C57BL/6 (C57) mice mimic the Eurasian population in both mitochondrial OxPhos efficiency and bone phenotype. Our data show that mechanical stimulation of osteogenic lineage cells activates their mitochondria, thus regulating bone metabolism. This study explores the impact of mtDNA haplotype on the response of BMSCs to mechanical stimulation induced by forced exercise. We will test the hypothesis that exercise will increase mitochondrial OxPhos, osteogenicity of BMSCs, and bone-forming function in OBs and improve bone phenotype in aged trained mice; C3H mice will have a more robust response than the C57 strain.

Experiments & Methods: To study this, we used 18-month-old male and female C57 and C3H WT mice. Mice were subjected to mechanical stimulation using a treadmill. Mice were trained for two weeks, and both trained and untrained control mice were euthanized, and femurs were isolated for micro-CT. Serum samples were collected for the markers of bone formation and bone resorption. Colony-forming unit (CFU) assays were performed using BMSCs obtained from femurs. Freshly isolated BMSCs were utilized to assess mitochondrial oxidative function via flow cytometry. Data analysis was performed using GraphPad Prism. Means and standard deviations are calculated, with comparisons made using Student's t-test (for two variables) or a one-way ANOVA followed by an appropriate post hoc test (for multiple variables). A P-value of less than 0.05 was regarded as statistically significant.

Results: Exercise significantly increased BMSC colony formation, especially in C3H mice. Trained male and female mice had significantly improved mitochondrial membrane potential compared to the untrained controls. Bone turnover markers showed a significant reduction in resorption (CTX-1) in trained females, with no significant changes in males. After two weeks of exercise, micro-CT shows no difference in bone phenotype in aged C57 male and female mice. Longer-term training of 8 weeks significantly increased bone mineral density in cortical and trabecular bone.

Discussion & Conclusions: Our findings show that exercise increases BMSC colony formation, with C3H mice displaying more colonies formed compared to C57, which is consistent with C3H mice having a more robust bone phenotype. The increase in mitochondrial function in both sexes indicates that exercise enhances oxidative metabolism. Female mice exhibited shifts in bone turnover, showing reduced bone resorption, and showed sex specific responsiveness as hormonal factors may increase the benefits of exercise. While the cellular and metabolic functions were improved by the short-term training, longer-term training was needed to increase cortical and trabecular BMD, highlighting a required progression from cellular to skeletal adaptations. Overall, the bone anabolic effect of mechanical stimulation via exercise involves activation of BMSC oxidative and clonogenic function. The exact role of these BMSC changes in the effect of exercise is a subject of ongoing studies.

15th Annual Center for Musculoskeletal Research Symposium
October 30, 2025

Title: IDH2 mutant hematopoietic stem and progenitor cells promote endothelial niche remodeling

Presenting Author: Edgardo Franco

Co-Author(s): Christina M. Kaszuba, Benjamin J. Rodems, Sonali Sharma, James McGrath, and Jeevisha Bajaj

Lab PI / Mentor: Jeevisha Bajaj

ABSTRACT

Background & Hypothesis: Myelodysplastic syndromes (MDS) are a group of hematologic disorders, characterized by a block in differentiation of myeloid-lineage hematopoietic stem and progenitor cells (HSPCs), leading to abnormal hematopoiesis and progressive bone marrow failure. HSPCs can be regulated by cues from the local bone marrow niche, which includes cells such as mesenchymal stromal cells, osteoblasts, and endothelial cells. Endothelial cells (ECs) can regulate HSPC self-renewal, differentiation, and aid in bone marrow homing. Prior work suggests that hematological malignances such as acute myeloid leukemia (AML) and MDS are associated with morphological and functional changes in the bone marrow microenvironment. For instance, bone marrow biopsies of MDS patients show an increase in micro vessel density, indicating endothelial remodeling. However, it is not known if endothelial niche remodeling can precede the onset of MDS phenotype and thus promote the expansion of malignant cells. To determine this, we used murine models of MDS driven by Isocitrate Dehydrogenase 2 (IDH2) mutations, which is associated with a high risk of developing secondary AML, highlighting its role in disease progression.

Experiments & Methods: To define the impact of IDH2 mutant cells on the endothelial niche, we established an in vivo murine model by transplanting HSPCs from 8–12-week-old conditional knock-in Idh2R140Q/+; Vav-Cre+ mice in wild-type (WT) mice conditioned with ultra-low dose irradiation that minimally impacts the ECs. Complete blood count (CBC) analysis is used to determine if MDS associated symptoms, such as thrombocytopenia and anemia, are detected in the transplant model. To determine if the endothelial niche is altered before development of MDS associated symptoms, we analyzed ECs (defined as CD45-Ter119-CD31+) 2-months post-transplant (n=12 WT recipients, 10 Idh2R140Q/+ recipients). As MDS is a disease associated with aging, we used HSPCs from indigenous Idh2R140Q/+; Vav-Cre+ mice that display features of MDS, which prior work has shown starts at 20 weeks. We thus tested if HSPCs from 20-week-old Idh2R140Q/+; Vav-Cre+ mice can accelerate development of endothelial defects in WT recipients.

To test if the expanded endothelial niche is associated with defects in endothelial function, we used in vitro co-culture assays. Human umbilical vein endothelial cells (HUVECs) were cultured in either a 12-well plate or on the microdevice featuring a silicon membrane (μSiM) platform. Then, HSPCs are seeded on top of the HUVECs monolayer for 72 hours. Afterwards, HUVECs are processed in either a Matrigel-based angiogenesis tube formation assay (n=4), or in a FITC-dextran permeability assay (n=4).

Results: Chimerism of Idh2R140Q/+ HSPCs in recipient mice increased over time relative to controls engrafted with WT HSPCs, with a significant increase starting at 2-months. Our analysis identified a nearly 2-fold increase in ECs in Idh2R140Q/+ recipients compared to the WT controls, even in the absence of a frank MDS associated phenotype in the blood. We find that transplanting 20-week Idh2R140Q/+ HSPCs can lead to 2 to 4-fold higher chimerism at 2 months compared to that seen with 8-12-week-old Idh2R140Q/+ donors, suggesting accelerated disease onset ECs co-cultured with Idh2R140Q/+ HSPCs from 8–12-week-old mice formed 18% longer and 16% more tubes than those co-cultured with age and sex-matched WT cells. Our experiments using the μSiM platform indicate that ECs co-cultured with Idh2R140Q/+ HSPCs show 1.4-fold increased FITC dextran permeability.

Discussion & Conclusions: These data indicate that remodeling of the endothelial niche precedes onset of pathological parameters associated with MDS. Idh2R140Q/+ HSPCs can promote neo-angiogenesis and increase permeability. Our findings reveal that the endothelial niche permeability and neo-angiogenesis precede the onset of MDS associated cytopenia and may promote disease progression.

15th Annual Center for Musculoskeletal Research Symposium
October 30, 2025

Title: Microfluidic-Synthesized Amorphous Calcium Phosphate Nanoparticles Enhance Osteogenesis, Suppress Osteoclastogenesis, and Promote Bone Healing in a Murine Femoral Defect Model

Presenting Author: Bei Liu

Co-Author(s):

Lab PI / Mentor: Hani Awad

ABSTRACT

INTRODUCTION: Critical-sized bone defects from trauma, tumor, or osteomyelitis remain a major challenge in orthopedic reconstruction. Autografts are limited by donor site morbidity and availability, while allografts and xenografts risk immune rejection and disease transmission. Calcium phosphate scaffolds are widely used but often lack biomechanical strength and osteoinductivity. To overcome these limitations, we developed carboxymethyl chitosan/amorphous calcium phosphate nanoparticles (CMC/ACP NPs), which can be 3D-printed with polycaprolactone (PCL) to regenerate bone. We subsequently optimized NP synthesis via microfluidics, enabling precise control of particle properties and yield. Here, we tested microfluidic-synthesized NPs in 3D-printed PCL scaffolds for effects on osteogenesis, osteoclastogenesis, and bone regeneration in a mouse femoral defect.
METHODS: CMC/ACP NPs were synthesized using a microfluidic chip, purified by dialysis, and characterized by dynamic light scattering (DLS) and scanning electron microscopy (SEM). Lyophilized NP powder was incorporated into PCL (3:1 NP: PCL) and 3D-printed into cylindrical scaffolds. Cytocompatibility and osteogenesis were evaluated in murine ST2 stromal cells using CCK-8, alkaline phosphatase (ALP), Alizarin Red S (ARS), and RT-PCR. Osteoclastogenesis was assessed in bone marrow macrophages treated with M-CSF/RANKL ± NPs using TRAP staining, F-actin, NF-κB, NFATc1, and resorption pits. Angiogenesis was tested in HUVECs spheroid assays embedded in collagen ± 500 μg/mL NP. To investigate the NP osteoregenerative properties in vivo, female BALB/cJ mice (n=3/group) were used to create 3-mm femoral defects, which were reconstructed with PCL or PCL+NP scaffolds. Bone formation was assessed quantitatively using X-ray and micro-CT.
RESULTS: NPs averaged 120.9 nm (PDI 0.17, zeta potential –19.9 mV) and were stable over 6 months. SEM confirmed uniform spherical morphology. NPs were cytocompatible, with no reduction in ST2 or BMM viability. In ST2 cells, NP treatment enhanced mineralization in a dose-dependent manner, with maximal ARS staining at 500 μg/mL on days 14 and 21. ALP activity peaked at day 7 and was unchanged by NP. RT-PCR showed dose-dependent increases in RUNX2 and OCN and the highest COL1A1 expression at 500 μg/mL on day 14. Osteoclast assays demonstrated a dose-dependent reduction in TRAP+ cells, resorptive pits, with near-complete inhibition at 500 μg/mL, accompanied by dose-dependent decrease in NF-κB and NFATc1 nuclear localization. In HUVEC spheroid assays, NP at 500 μg/mL enhanced cumulative sprout length compared to controls, suggesting pro-angiogenic activity. In vivo, both scaffold groups supported bone formation; however, PCL-only scaffolds mineralized primarily at defect margins, leaving a central void, whereas PCL+NP scaffolds showed mineralization throughout the scaffold. Longitudinal analysis indicated higher incremental bone formation in the NP group, particularly at months 2–3.
DISCUSSION: Microfluidic-synthesized CMC/ACP NPs embedded in 3D-printed PCL scaffolds enhanced osteogenesis and suppressed osteoclastogenesis, yielding greater mineralization in murine femoral defects. These effects are likely mediated by ACP-derived calcium and phosphate ion release that upregulates osteogenic programs in MSCs and inhibits NF-κB/NFATc1 signaling in pre-osteoclasts. Angiogenic enhancement was observed in HUVEC spheroid assays, although validation in murine endothelial cells is needed to confirm relevance to our in vivo model. This manufacturable approach ensures uniform particle size and charge and can be scaled through arrayed microfluidics. Future work will optimize NP loading in scaffolds, incorporate biomechanical testing, and define the mechanistic contributions of ion release. Collectively, this strategy offers a clinically translatable, off-the-shelf scaffold to accelerate bone repair in critical-sized long bone defects.

15th Annual Center for Musculoskeletal Research Symposium
October 30, 2025

Title:	Pancreatic Tumor-Associated IGFBP-3 Induces Dysregulated Autophagy and Mitochondrial Dysfunction in Skeletal Muscle Via TGF-β Receptor and SMAD3 Signaling
Presenting Author:	Zachary Sechrist
Co-Author(s):	Karen de Mesy-Bentley, Edward Schwarz
Lab PI / Mentor:	Calvin Cole

ABSTRACT

INTRODUCTION: Pancreatic ductal adenocarcinoma (PDAC) is a debilitating cancer where 80-85% of patients develop skeletal muscle wasting (SMW), a crippling syndrome that reduces treatment tolerance, overall survival and is directly responsible for 30% of patient deaths due to accelerated respiratory impairment. Currently, the underlying mechanisms are poorly understood and no FDA approved therapies exist to treat cancer-related SMW and improve patient outcomes. Our lab previously identified tumor secreted Insulin-like Growth Factor Binding Protein 3 (IGFBP-3) as a potential factor of PDAC-induced SMW in two independent pre-clinical murine models of PDAC. Interestingly, recent literature and data from our laboratory show that cancer-related SMW in these models may result from non-canonical interactions between IGFBP-3 and TGF-⍰⍰ receptors in skeletal muscle previously known to induce dysregulated autophagy and mitochondrial dysfunction in skeletal muscle. Here we tested the hypothesis that PDAC promotes dysregulated autophagy and mitochondrial function downstream of IGFBP-3 activated TGF-β receptor signaling in skeletal muscle and study intramuscular lipids (IML) as a potential biomarker. METHODS: C57BL/6J female mice (6-8 weeks) were randomized to three groups (n=10): 1) no tumor control (NTC), 2) KP2-Luc parental murine tumor cells, or 3) IGFBP-3-/- KP2-Luc. Weekly dual energy X-ray absorptiometry (DEXA) scans monitored longitudinal changes in lean mass. Mice were injected orthotopically with 5x104 tumor cells. At sacrifice tibialis Anterior (TA) muscles were preserved for Oil Red O (ORO) and transmission electron microscopy (TEM). Quadriceps muscles were flash frozen for transcriptomics and western blot analysis for markers of autophagy: FOXO1, ULK1 and LC3b. Statistical analyses were performed using GraphPad Prism software. One-way ANOVA or student t-test was used to analyze changes between groups. $p<0.05$ was considered significant. RESULTS: KP2 parental animals experienced a significant decline in % change in lean mass compared to NTC animals (NTC: 10.22% +/- 7.78 vs. KP2: -6.43% +/-12.26, $p<0.01$). TEM analysis on the TA muscles identified the presence of double membrane autophagosomes in the region adjacent to myonuclei and increased accumulation of intrafibrillar lipid droplets adjacent to dysfunctional mitochondria which are absent in NTC muscle. Interestingly, ORO positive fibers are increased in wasting muscle serving as a biomarker for the IML droplets and mitochondrial dysfunction. Bulk RNA sequencing and metabolomics reveals reduced mitochondrial efficiency in muscle from KP2 parental mice. Animals inoculated with IGFBP-3-/- tumors experience attenuated loss of lean mass compared to KP2 parental animals ($p<0.05$). KP2 animals demonstrate an increase in FOXO dependent autophagy and IML compared to NTC and IGFBP-3-/- animals ($p<0.05$) indicating reduced mitochondrial dysfunction in IGFBP-3-/- animals. DISCUSSION: Our lab has shown an increase in muscle specific tgfβr1 expression and downstream signaling in PDAC dependent on IGFBP-3. This study identified direct evidence for increases in autophagy, IML accumulation, and mitochondrial dysfunction in PDAC-associated SMW via TEM that correlates with ORO staining and indicates the potential of IML as a biomarker of muscle dysfunction. Moreover, our data suggests that muscle dysfunction in PDAC is attenuated by reducing tumor secreted IGFBP-3 indicating the potential for anti-IGFBP-3 therapy in PDAC-associated SMW. Further work will validate IML accumulation through perilipin staining. Lastly, muscle from IGFBP-3-/- animals will be submitted for TEM to validate a reduction in dysregulated mitochondria and autophagy suggested by western blot data.

ACKNOWLEDGEMENTS: This research is supported by NIH grants (K01 CA240533, T32 AR076950-06, P30AR69655, and P50CA257911).

15th Annual Center for Musculoskeletal Research Symposium
October 30, 2025

Title:	PRDM16 is required for normal nasal septal cartilage and bone development in mice
Presenting Author:	Eliya Tazreena Tashbib
Co-Author(s):	Victoria Hansen, Eloise Fadial, Alexis Klee, Maeve O'Brien, Karin Pryharski
Lab PI / Mentor:	Dr. Chia-Lung Wu

ABSTRACT

INTRODUCTION: Abnormal epigenetic regulation may lead to craniofacial anomalies (~35% of birth defects). A recent GWAS study indicates that abnormal craniofacial development in humans is associated with PRDM16, a histone methyltransferase and transcription factor. Previous studies have shown that Prdm16 global knockout (gKO) mice exhibited shortened Meckel's cartilage and mandible. However, Prdm16 gKO mice are neonatal lethal, making it challenging to dissect the role of PRDM16 in a tissue-specific manner. Thus, the goal of the current work is to unravel the function of PRDM16 in craniofacial cartilage and bone development, using an osteochondral lineage-specific Prdm16 conditional knockout mouse model (Col2a1Cre; Prdm16fl/fl, cKO). We hypothesize that PRDM16 is a critical regulator of chondrogenesis and osteogenesis.

METHODS: Mouse skulls from WT and Prdm16 cKO mice were collected at P5, P15, 4-wk, and 12-wk of age (IACUC-approved protocol). Craniofacial bone and cartilage were assessed via μCT and histological analysis. IHC against hypertrophic chondrocyte/bone (RUNX2) and apoptotic marker (CASP3) was performed in the nasal septum (n≥3/group, with Student's t-test). 4-wk-old nasal cartilage was submitted for scRNA-seq (n=4/group) and Visium HD spatial transcriptomics (Spatial-seq; n=2/group). The sequencing data were analyzed for differentially expressed genes, differentiation trajectory, and gene regulatory networks (GRN).

RESULTS & DISCUSSION: Both male and female cKO mice exhibited significantly shorter nasal and cranial lengths vs. WT mice at 4- and 12-wk of age. The 4-wk-old male WT and cKO showed similar nasal BV/TV. However, 12-wk-old male cKO mice, but not female, had significantly higher nasal BV/TV than corresponding WT mice, suggesting a potential sex-dependent role of PRDM16 in nasal bone development. As female cKO and WT showed similar nasal BV/TV, we focused on male mice thereafter. Histological analysis revealed severe nasal septal deviation at both 4- and 12-wk of age, but no apparent deviation in male cKO mice at P5 and P15. Our scRNA-seq analysis identified 4 distinct conserved chondrocyte populations in WT and cKO cartilage. Importantly, cKO mice showed downregulation of septal Mgp/Vit+ chondrocytes (71% vs. 33%) and upregulation of Col10a1/Serpina3n+ hypertrophic chondrocytes (HCs; 41% vs. 3%) compared to WT. Pseudotime trajectory analysis revealed that Foxp1-high progenitors first differentiate into Mgp/Vit+ chondrocytes, which then bifurcate into cell fates of either Col10a1/Serpina3n+ HCs or Col1a1/Dio2+ fibrotic chondrocytes (FCs). Furthermore, GRN analysis suggested that the downregulation of transcription factors Creb1 and Srf, along with their associated targets (Cdkn1a, Maff, Atf3, and Nr4a1) in the cKO mice, may drive Mgp/Vit+ chondrocytes toward Col10a1/Serpina3n+ HCs. IHC analysis also showed increased expression of RUNX2 and CASP3 at the deviated cartilage of 4-wk-old cKO vs. WT. These findings indicate that PRDM16 plays a critical role in modulating chondrocyte differentiation and apoptosis. Interestingly, Spatial-seq further revealed that Mgp/Vit+ chondrocytes in nasal cartilage and Col3a1+ fibrotic cells within nasal bone were both located near the deviation site, implying that altered cell-cell interactions between these two cell populations may be responsible for the septal deviation. We are currently performing cell-cell crosstalk analysis using MultiNichenet to pinpoint the molecular mechanisms underlying nasal septal cartilage deviation.

CONCLUSION: We demonstrated that cKO of PRDM16 in the osteochondral cell lineage leads to severe nasal septal deviation in mice, potentially resulting from accelerated chondrocyte hypertrophy and apoptosis as well as increased osteogenesis. Our findings highlight the functionality of PRDM16 in craniofacial development and provide a potential therapeutic target for patients with congenital nasal bone/cartilage disorders.

15th Annual Center for Musculoskeletal Research Symposium
October 30, 2025

Title:	Conserved disruption of human bone marrow stromal cells' transcriptional and functional heterogeneity in Myelodysplastic Syndromes
Presenting Author:	Adam Tyrlik
Co-Author(s):	Adam Tyrlik, Yuko Kawano, Hiroki Kawano, Dalia Ghoneim, Thomas J. Fountaine, Daniel K Byun, Mark W. LaMere, Jason H. Mendler, Tzu-Chieh Ho, Noah A. Salama, Benjamin J. Frisch, Jason R. Myers, Siba El Hussein, John M. Ashton, Mitra Azadniv, Youmna Kfoury, David T. Scadden, Michael W. Becker, Roman Eliseev, Jane L. Liesveld
Lab PI / Mentor:	Laura Calvi

ABSTRACT

Bone Marrow Stromal Cells (BMSCs) are non-hematopoietic cells that provide a favorable microenvironment for Hematopoietic Stem Cells and progenitors, producing supportive factors and immunomodulatory cytokines. Dysfunction in BMSCs contributes to the development of Myelodysplastic Syndrome (MDS), a marrow failure syndrome characterized by a significant increase in all-cause mortality due to leukemia progression, susceptibility to infection and cardiovascular complications. Across patients, MDS is highly mutationally heterogenous with disruption in over 100 unique identified, frequently in combination posing a major therapeutic challenge. In contrast, conserved MDS-induced changes in the BMSC population would represent appealing treatment targets. In this study, we isolate Lineage- CD271 (NGFR)+ BMSCs from healthy and MDS human bone marrow aspirates and perform single-cell RNA sequencing. We use osteogenic, adipogenic, osteochondral, and fibroblastic fate-associated genes to identify three major, previously described BMSC populations. We then identify significant upregulation of hematopoietic support genes, including CXCL12, CSF1, LEPR, and VCAM1 within the mixed adipo- and osteo- genic population, indicating BMSCs that are more likely to be engaged in hematopoietic support. Based on transcriptional data we demonstrate a broad, conserved change in immunomodulatory capacity, and a loss of heterogenicity within this supportive BMSC population across multiple mutationally heterogenous MDS patients. Utilizing an extended sorting strategy that includes CD106 (VCAM1) and CD146 (MCAM) in addition to CD271, we sorted both CD271+CD146-CD106- (NLC) and CD271+CD146+CD106+ (NVML) cells. With RNA sequencing we demonstrate that this sorting strategy isolates distinct populations, and that NVML cells are transcriptionally similar to the Supportive BMSC population identified by single cell RNA seq based on fate associated gene expression and MDS associated transcriptional changes. We then show that, when functionally compared to the NLC population, sorted NVML cells have higher adipogenic and chondrogenic differentiation capacity, increased mitochondrial membrane potential and increased capacity for support of bone marrow from healthy controls, while the capacity to provide hematopoietic support is diminished in the context of MDS. Thus, we identify both transcriptionally and functionally a specific highly hematopoietically supportive human BMSC population that could further be studied in MDS clinical trials. Conserved changes in this population in the context of MDS, despite mutational heterogeneity, may represent a new therapeutic opportunity.

Undergraduate Posters

Disclaimer

15th Annual Center for Musculoskeletal Research Symposium
October 30, 2025

Title: Investigating the Role of Immune Checkpoint Protein TIM-3 on Macrophage Function in Bone Infection

Presenting Author: Ashleigh Barrett

Co-Author(s):

Lab PI / Mentor: Gowrishankar Muthukrishnan

ABSTRACT

Background: TIM-3 is an immune checkpoint protein that is expressed on multiple immune cells, such as: T cells, dendritic cells, and macrophages. It is known that TIM-3 acts as an inhibitory receptor on exhausted T cells, resulting in lack of effector function. In chronic Staphylococcus aureus bone infection, my lab has found evidence of this phenomenon. However, the role of TIM-3 on non-lymphoid cells, such as macrophages, remains to be fully characterized. Quiescent macrophages constitutively express TIM-3, but upon infection or injury they upregulate cytokines such as TNF-α and IL-10 while downregulating TIM-3. Galectin-9 (Gal-9), a TIM-3 ligand produced by myeloid cells, is well recognized for its role in driving TIM-3–mediated exhaustion in T cells. However, its function in macrophages remains poorly understood. This study aims to determine whether TIM-3 is an inhibitor of macrophage function in the context of S. aureus bacterial infection. In this study, I hypothesize that upon TIM-3 deletion, macrophages will have a more activated and pro-inflammatory response to infection.

Methods: We isolated bone marrow cells from tibias and femurs of male and female wild-type/control mice (Havcr2fl/fl, n = 4) and TIM-3 macrophage conditional knockout (cKO) mice (Havcr2fl/fl x Cx3Cr1cre, n = 3). Cells were cultured with M-CSF for six days to differentiate into macrophages. They were then infected with a GFP-expressing MRSA strain for one hour at various multiplicities of infection (MOI = 0, 0.1, 1), followed by a 30 minute treatment of gentamicin to kill extracellular bacteria. We measured 1) bacterial clearance via colony-forming unit (CFU) quantifications 6 hours post-infection, 2) performed flow cytometry 18 hours post-infection, and 3) analyzed cell supernatant via ELISAs for TNF-α and IL-10 cytokine production 24 hours post-infection.

Results: CFU quantifications revealed that bacterial burden increased in a concentration dependent manner with increasing MOI, and that TIM-3 cKO mice had trending higher burden compared to control mice. We found that IL-10 protein levels at an MOI of 1 were higher in the control condition compared to TIM-3 cKO. Conversely, we found that TIM-3 cKO cells produced higher protein levels of TNF-α compared to control macrophages at an MOI of 1. Our flow cytometry analysis confirmed TIM-3 knockout on the cKO macrophages and found a significant decrease in TIM-3 expression on control macrophages from MOI 0.1 to 1 infection conditions ($p = 0.024$). Additionally. we found higher levels of proliferation (Ki-67+) in TIM-3 cKO macrophages compared to controls, mirroring in vivo results. Finally, we found that MRSA infection promotes both control and TIM-3 cKO macrophages to express significantly higher levels of Gal-9 ($p < 0.05$) and MHC-II ($p < 0.05$), which is a surrogate for activation/antigen presentation.

Discussion: Our findings reveal that TIM-3 cKO macrophages produce significantly higher levels of Galectin-9 in a concentration-dependent manner following MRSA infection. This enhanced Gal-9 production represents a key discovery, as it may provide critical insight into the mechanisms driving T cell exhaustion during MRSA bone infection. In addition, TIM-3 cKO macrophages exhibit a more pro-inflammatory and activated phenotype, characterized by elevated TNF-α, reduced IL-10, and increased proliferative capacity. This alteration in macrophage function would likely be beneficial and may help counteract the detrimental immune suppression that characterizes chronic bone infection. Our ongoing and future studies are focused on how TIM-3 cKO macrophages regulate Gal-9 mediated T cell function.

15th Annual Center for Musculoskeletal Research Symposium
October 30, 2025

Title: Translating Biomechanical Metrics into Clinical Impact: Minimum Clinically Important Differences (MCIDs) for Functional Recovery After Lumbar Spine Surgery

Presenting Author: Nathan Carpenter-Holmes

Co-Author(s): Ram Haddas, Ye Shu

Lab PI / Mentor: Ram Haddas

ABSTRACT

Introduction: Minimum Clinically Important Differences (MCIDs) represent the smallest measurable change in a clinical outcome that patients perceive as meaningful. MCIDs are critical for guiding clinical decision-making, interpreting the effectiveness of interventions, and bridging the gap between statistical significance and meaningful patient benefit. They provide clinicians with objective benchmarks for determining whether a treatment has produced a real, functional improvement and can inform patient counseling, rehabilitation progression, and return-to-activity decisions. Despite their importance, MCIDs for gait and standing balance remain undefined in patients undergoing lumbar spine surgery, limiting the ability to assess postoperative functional recovery objectively. The present study aimed to establish MCIDs for walking and standing balance metrics in lumbar spine patients, providing reproducible thresholds for clinically meaningful improvement that can inform both surgical outcomes and rehabilitative strategies.

Methods: Fifty-six patients undergoing lumbar spine surgery were assessed at one week preoperatively and at three and six months postoperatively. Participants were instrumented with 42 reflective markers and completed five walking trials and three one-minute eyes-open standing balance trials per session. MCIDs were calculated using a distribution-based approach (0.5 × standard deviation) and validated with an anchor-based method using Oswestry Disability Index (ODI) scores and expert clinician input. Key gait metrics included walking speed, cadence, stride and stance times, stride length, mediolateral and anteroposterior foot placement, limp index, and gait deviation. Standing balance metrics included sagittal, coronal, and total head sway.

Results: MCIDs for gait metrics were: walking speed 0.123 m/s; cadence 8.26 steps/min; stride time 0.242 s; step time 0.117 s; single-limb support 0.031 s; double-limb support 0.238 s; stride length 0.125 m; anteroposterior heel distance 0.068 m; mediolateral foot distance 0.029 m; limp index 0.029; gait deviation 5.12. MCIDs for standing balance were: sagittal head sway 1.12 cm; coronal head sway 1.31 cm; total head sway 13.33 cm.

Conclusions: This study establishes the first clinically validated MCIDs for gait and standing balance in lumbar spine surgery patients, providing quantitative thresholds for meaningful functional improvement. These values can guide clinicians in evaluating postoperative recovery, tailoring rehabilitation, and making patient-centered decisions regarding activity progression and return to work. The findings highlight the importance of objective functional metrics in addition to patient-reported outcomes and emphasize that even small improvements in gait or balance can be clinically significant. Future studies should apply these methods to larger, diagnosis-specific cohorts to refine MCID estimates and enhance their applicability across diverse lumbar spine populations, ultimately advancing evidence-based postoperative care.

15th Annual Center for Musculoskeletal Research Symposium
October 30, 2025

Title: The roles of anti-resorptive vs. anabolic therapies in Hematopoietic Niche and Tet2-mediated Clonal Hematopoiesis

Presenting Author: Wimeth Dissanayake

Co-Author(s): Kevin Lee, Cih-Li Amy Hong

Lab PI / Mentor: Shu-Chi Allison Yeh

ABSTRACT

Background: Clonal Hematopoiesis (CH) is a disorder which results from the accumulation of mutations, such as TET2 and ASXL1, in the Hematopoietic Stem Cells (HSCs). Age related inflammation promotes the expansion of these mutants within the bone marrow, resulting in patients from 60-70 years old being most commonly affected. These patients are known to be at greater risk of cardiovascular disease and show increased overall mortality due to CH. As there are few effective treatments for CH, preventing mutant clone expansion is crucial. Recently, it has been shown that the local bone microenvironment plays a key role in regulating HSC expansion. However, until recently, the role of the local bone remodeling microenvironment in regulating clonal expansion has remained an enigma. This is particularly notable due to the common use of drugs that alters bone remodeling as treatments for osteoporosis, a disease which primarily effects those most at risk for CH expansion. Our preliminary results have confirmed that anti-resorptive drugs, such as zoledronic acid, can impair the clonal expansion of Tet2+/- cells through disruption of CD206+ bone marrow macrophage interactions with mutant clones and increasing anti-tumor immunity. Several prominent studies have reported the beneficial effects of bone anabolic therapies in maintaining the bone marrow niche and HSCs during homeostasis and clonal disorders. However, their roles for the pathogenesis stage of precursor diseases and for the CD206+ marrow macrophages are less clear. We previously showed that the extent of early clonal expansion fluctuates with respect to dynamic bone remodeling. Therefore, we hypothesize that anti-resorptive and anabolic treatment may change local bone remodeling at the microscopic level that result in distinct clonal dynamics during the pathogenic stage.

Methods: To evaluate the role of anabolic drugs, we assessed the effects of Parathyroid Hormone (PTH) analogs on the expansion of Tet2+/- transplanted cells in a 0.5 Gy low- dose irradiated mouse model. Intermittent PTH was given prior to or after transplantation to discern potential impact on homing and engraftment of the transplanted cells. Intravital imaging, peripheral blood analyses, and complete blood count were then evaluated at defined time points (N=3).

Results: After 10 weeks of intermittent treatment (daily, 5 days a week, 100ug/kg), mice treated with PTH showed reduced peripheral burden, with significantly increased lymphocytes and decreased neutrophils in complete blood cell counts, compared to untreated mice. However, within the first 5 weeks after secession of treatment, PTH treated mice showed significantly increased Tet2+/- peripheral engraftment. This corresponded with a decrease in the lymphoid shift observed. Extended observation of peripheral blood after end of treatment showed plateau in clone engraftment. Although intravital imaging performed at 20 weeks post transplantation revealed significantly higher clonal burden in PTH treated mice, it did not correspond to a compromised blood parameters, indicating that PTH may be able to support both the impaired and healthy bone marrow niche.

Discussion and future work: Our ongoing work includes characterizing how reprogramming of bone marrow resident cells by PTH may have impact on clonal competition between healthy and mutant cells, compared to anti-resorptive treatment. It is also critical to evaluate how PTH and bisphosphonate combination therapies interact with this bone marrow niche to regulate Tet2+/- expansion.

15th Annual Center for Musculoskeletal Research Symposium
October 30, 2025

Title: Multiphoton Ablation & Laser-Guided Angiogenesis for Bone Tissue Engineering
Presenting Author: Maximilian Harkins
Co-Author(s): Samantha Mill
Lab PI / Mentor: Xinping Zhang and Edward Brown

ABSTRACT

Introduction: Bone is a highly vascularized organ that provides structural support, mineral storage, hematopoiesis, and a dynamic interface for muscle action. However, when bone is injuried beyond a critical threshold, natural repair often fails due to poor vascularization. Poor angiogenesis is a major cause of non-healing fractures and a persistent barrier to the success of bone grafts and biomaterial implants. Because bone health depends on microvasculature supporting osteoblasts, immune cells, and matrix remodeling, recreating vascular networks is essential for both regenerative therapies and disease modeling.

Microfluidics and bioprinting have had limited success in replicating the sub–10 μm capillaries and organ-specific architectures needed for bone modeling. To overcome this, we developed a laser-guided angiogenesis (LGA) workflow based on two-photon ablation in collagen hydrogels. This technique enables machining of perfusable, biomimetic channels at cell-relevant scales while preserving the surrounding extracellular matrix. By integrating bone-specific vascular imaging into programmable ablation toolpaths, we aim to generate prevascularized constructs that advance bone tissue engineering and provide a platform for studying bone disease.

Methods: Type-I collagen gels (4–8%) were cast in a custom microfluidic chamber with two parallel channels with a pressure differential between them. A custom-built MATLAB application integrated with ScanImage drives an Arduino-controlled, motorized XY stage to convert user-defined masks (2D images, CAD-derived paths, or point clouds) into line toolpaths for in-gel ablation. To predictably control matrix removal while preserving surrounding collagen, we validated a dose metric $D=(P/A)^2 t$ by varying laser power P and pixel dwell time t at fixed beam area A. Collagen integrity and ablation efficacy were quantified by changes in SHG signal (ΔSHG) and signal-signal ratios (S/S). Patency and cell-scale transport were assessed by perfusing 10 μm fluorescent microspheres through ablated connections between parallel channels.

Results: ΔSHG exhibited the expected log–log linearity with dosage across 4–8% gels (slope ≈ 1 in the non-saturated regime), consistent with the quadratic intensity dependence embedded in D. When dosage was held constant, neither P nor t alone correlated with ΔSHG (p = 0.79 for both), supporting D as the controlling variable. A reproducible transition to saturation was observed at high D, as it was at low D. Bead perfusion confirmed patency and demonstrated transport at single-cell length scales (≈10 μm). Practical engineering improvements—PEI/GA chamber conditioning to secure gels and a casting approach that mitigates incubation bubbles—stabilized constructs for flow experiments. Flow was confirmed via transmitted light microscopy and two-photon microscopy alike. The system also produced fine, complex geometries in collagen, illustrating spatial control for future bone-mimetic networks.

Discussion: This work established a effective two-photon dose that allows us ablate channels for cell-scale flow while safeguarding surrounding collagen. This creates a tractable path toward endothelial seeding and co-culture with osteogenic cells in collagen (i.e., prevascularized bone-like tissue modules) without overexposing the matrix. Present limitations are primarily mechanical (stage repeatability affects complex multi-branch reconnections); nevertheless, the platform already supports (i) perfusion at cell scale, (ii) collagen-preserving ablation windows, and (iii) import of bone-derived masks for organ-specific patterns. The next steps are endothelialization of ablated channels, osteoblast/MSC seeding in the bulk gel, and flow-conditioned co-culture to probe how microvascular geometry and shear influence osteogenic function and matrix remodeling.

15th Annual Center for Musculoskeletal Research Symposium
October 30, 2025

Title:	Improving Care for Spinal Deformity Patients: Utilizing Wearable Tools for Functional and Disability Assessments
Presenting Author:	Kade Kaufmann
Co-Author(s):	Ye Shu, William Lavelle, Yair Barzilay, Prasanth Romiyo, Tyler Schmidt, Alan Daniel, Bassel Diebo, Addisu Mesfin, Varun Puvanesarajah, Ram Haddas
Lab PI / Mentor:	Ram Haddas

ABSTRACT

INTRODUCTION: Disability and functional assessments of spinal deformity are notoriously inaccurate for diagnosis and prognosis. Although high quality, motion lab data's higher cost prohibits adoption as a standard of care (SOC). In contrast, wearables are both cost-effective, broadly available and have been incorporated into telehealth SOC for various populations. Although wearable sensors are widely used to monitor general health metrics, few devices have been validated explicitly for assessing outcomes directly related to spinal impairments. Understanding patients' real-world movement patterns can help clinicians understand symptoms and recovery. Therefore, the aims of this study are: 1. Validate the accuracy of spine-specific wearable sensor measurements against a Gold standard motion capture system; and 2. Recognize at-home activities in deformity patients and perform a retrospective analysis to calculate clinically relevant variables.

METHODS: Forty-two adults with scoliosis and matched controls were recruited and fitted with an inertial measurement unit (IMU; Vicon) sensor positioned at T1 in addition to the standard full-body marker configuration. Participants completed a standardized battery of functional assessments and daily activities (walking, standing, lifting, sitting) recorded simultaneously by both systems. For the at-home component, only the T1-mounted IMU was worn, with activities performed twice daily over two days. Machine learning–identified activity segments were retrospectively analyzed with clinic MATLAB pipelines to calculate gait, sway, and Cone of Economy (CoE) for further analysis. The spine angles collected by both methods were aligned and the similarity quantified via Intraclass Correlation Coefficient (ICC).

RESULTS: Validation analyses demonstrated excellent agreement between IMU- and motion capture–derived spine angles for maximal ranges of motion during static balance and gait tasks (Romberg flexion/extension ICC = 0.98; walking flexion/extension ICC = 0.97). Good agreement was observed for ranges of motion across several activities (ICC = 0.75–0.88), with moderate agreement in dynamic lifting tasks (ICC = 0.65–0.74). Transitional and multiplanar movements, including sit-to-stand, showed weaker reliability (ICC < 0.65), indicating the need for refinement in complex activity detection. Clinically relevant measures during walking and balance tasks demonstrated strong consistency across systems. Retrospective analysis of at-home recordings yielded clinical metrics within acceptable limits compared with marker-based motion capture, with cone of economy and maximal sway in both coronal and sagittal planes demonstrating the strongest concordance.

DISCUSSION: This study demonstrates that wearable inertial measurement units (IMUs) combined with a segment-level recurrent neural network pipeline can reliably capture key functional activities in adult scoliosis patients, including standing, walking, and lifting. The model achieved high precision and recall for these core movements, while transitional activities such as the timed-up-and-go remain more challenging, highlighting areas for refinement. This approach addresses a key clinical gap: traditional static imaging cannot capture dynamic compensatory strategies that influence pain, disability, and long-term outcomes. Wearables enable objective, continuous monitoring of spinal function in patients' natural environments, providing actionable insights for surgical planning, postoperative rehabilitation, and individualized treatment. Preliminary validation supports feasibility for longitudinal monitoring, offering a scalable method to track recovery and identify subtle impairments that may otherwise go undetected. Wearable sensors provide a clinically actionable, objective method to monitor dynamic spinal function in real-world settings, guiding surgical and rehabilitation decisions and supporting personalized care for adult spinal deformity patients.

15th Annual Center for Musculoskeletal Research Symposium
October 30, 2025

Title: Estimating Lower Extremity Joint Moments Using Alternative Approaches
Presenting Author: Christina Kyriacou
Co-Author(s):
Lab PI / Mentor: Dr. Cherice Hill

ABSTRACT

Introduction: Lower extremity joint moments are crucial to consider when characterizing normative and pathologic gait. Estimation of joint kinetics is typically done using 3D marker-based motion capture and 3D force plates, but these modalities are expensive and often only available in motion analysis labs, thereby preventing community-based joint kinetic assessment. Data collection alternatives such as marker-less motion capture and in-shoe pressure or force insoles are portable and more cost-effective than traditional data collection approaches, but the feasibility of estimating joint moments using these combined data inputs has not been previously demonstrated. The purpose of this study was to evaluate the feasibility of estimating lower extremity sagittal moments using alternative modalities including marker-less motion capture and pressure insoles.

Methods: 14 participants completed walking, jogging, and drop-vertical jump landing tasks. Kinematic data was collected using 3D marker-based and marker-less (Theia3D) motion capture, and kinetic data was collected using 3D force plates and XSENSOR in-shoe pressure insoles; all data was collected simultaneously. Sagittal joint moments were estimated using 4 methods: (1) 3D marker-based motion capture and 3D force plates (3D, gold standard), (2) Theia3D marker-less motion capture and 3D force plates (T+FP), (3) Theia3D marker-less motion capture and XSENSOR pressure insoles with the insoles estimating center of pressure and load (T+XS_C,L), and (4) Theia3D marker-less motion capture and XSENSOR pressure insoles with the insoles estimating only center of pressure (T+XS_C). Sagittal ankle, knee, and hip moment peaks were compared between the gold standard (3D) method and each alternative method using linear correlations, intraclass correlation coefficients (ICCs), and Bland-Altman analyses (alpha=0.05) to assess consistency and alignment between approaches.

Results: Consistency between peaks calculated using the gold standard and alternative methods was highly variable. The methods using marker-less motion capture and in-shoe pressure insoles typically underestimated joint moments. Even moments estimated using marker-less motion capture and force plates showed notable offsets from the gold standard data. In some cases, the alternative methods underestimated moments consistently compared to the gold standard, which provides the ability to develop predictive models to combat systemic biases. In other cases, however, moments computed through alternative methods were inconsistent in their relationship with the gold standard data. The T+FP method showed better consistency with the gold standard than either of the methods using XSENSOR data; this trend was fairly consistent across tasks (walk, jog, DVJ). Both methods involving XSENSOR data showed particularly poor consistency at the hip during jogging. Overall, walking showed the worst results of the three tasks when using XSENSOR force data.

Discussion: These results demonstrate feasibility to estimate some sagittal plane joint moments using 3D marker-less motion capture and pressure insoles but indicate that further optimization is needed. Limitations regarding the spatial alignment and time synchronization between the XSENSOR insoles and motion capture system likely contributed to variability within results; future work will refine this process. These findings support the possibility of joint moment estimations outside of a lab environment, driving broader representation in biomechanical research. Additionally, this work suggests that even when optimally collected, data from these alternative approaches should not be directly compared to gold standard data. Instead, it is likely necessary that new normative values are defined using these methodologies. Future work will develop algorithms to predict full continuous joint kinetics from data collected outside of a lab using marker-less motion capture and pressure insoles.

15th Annual Center for Musculoskeletal Research Symposium
October 30, 2025

Title:	Identifying Patients Most Likely to Benefit From Shoulder Surgery: Clinical Predictors and Outcomes
Presenting Author:	Veena Laks
Co-Author(s):	Patrick Castle, MD; Dylan N. Greif, M.D; Nicholas Morriss, MD; Ye Shu, BS; Ilya Voloshin, M.D; Sandeep Mannava, M.D, Ph.D
Lab PI / Mentor:	Ram Haddas, PhD, MBA

ABSTRACT

Introduction: Shoulder arthroplasty, including both anatomic and reverse procedures, is among the most common and effective interventions for patients with debilitating shoulder pain and loss of mobility. However, postoperative recovery is highly variable, with some patients achieving substantial functional restoration while others experience limited improvement. Currently, surgeons lack validated tools to predict which patients are most likely to benefit, limiting the ability to personalize surgical decision-making, guide rehabilitation strategies, and manage patient expectations. This represents a critical knowledge gap with direct implications for clinical outcomes, health system efficiency, and patient quality of life. To address this unmet need, this study aims to identify preoperative kinematic and patient-reported outcome measurement information system (PROMIS) factors associated with clinically meaningful recovery after shoulder surgery, using a responder analysis framework. By integrating objective biomechanical assessments with patient-reported metrics, the proposed work has the potential to establish clinically actionable predictors of surgical success.

Methods: This retrospective cohort study was conducted at the University of Rochester Medical Center (2024–2025) and included 40 patients undergoing shoulder arthroplasty (25 anatomic, 15 reverse). Patients were fitted with a full-body reflective marker set and performed standardized hygiene trials (hand-to-lap, reach-behind-back) one week preoperatively and at 3- and 6-month follow-up. Kinematic data and joint range of motion were extracted across timepoints. Treatment response was defined as achieving the minimal clinically important difference (MCID ≥13) in PROMIS Function and Pain Interference scores. Patients exceeding this threshold were labeled as responders. Predictive modeling was performed using LASSO regression and Extreme Gradient Boosting (XGBoost), with feature importance derived from standardized coefficients and SHAP values. Model performance was evaluated with 5-fold cross-validated AUC to determine the most influential preoperative kinematic and patient-reported predictors of clinically meaningful recovery.

Results: The final XGBoost model achieved a mean cross-validated AUC of approximately 0.78 (3-month) and 0.80 (6-month), indicating good discrimination between responders and nonresponders. At the 3-month mark, the strongest predictors were minimum shoulder and spine rotation and other thoracic and cervical movements. These features indicate that early recovery is characterized by a mix of global trunk compensations and targeted neck mobility improvements. At the 6-month mark, the top predictors were spine rotation range of motion and neck oblique range of motion, followed by other neck mobility measures. Higher values in these metrics were generally associated with greater likelihood of being a responder, which suggests that better preoperative cervical and thoracic rotational capacity supports long-term functional gains.

Discussion: Preoperative kinematic patterns of the shoulder, cervical spine, and trunk were strongly predictive of postoperative recovery following shoulder arthroplasty. At three months, functional improvement was associated with broader compensatory strategies, particularly trunk and cervical mobility, suggesting that early recovery relies on global movement adaptations. By six months, however, successful outcomes were more dependent on refined cervical and spinal control, reflecting a transition from compensatory to more localized joint-specific function. These findings underscore the importance of preoperative kinematic assessment as a potential prognostic tool, allowing surgeons to better stratify patients by recovery potential, set realistic expectations, and guide targeted rehabilitation strategies that evolve across the postoperative timeline.

15th Annual Center for Musculoskeletal Research Symposium
October 30, 2025

Title: Tumor-Associated IGFBP-3 Regulates Macrophage Polarization and α-SMA+ Cell Migration

Presenting Author: Nidhi R. Patel

Co-Author(s): Zachary R. Sechrist, Isabel Porterfield

Lab PI / Mentor: Calvin L. Cole

ABSTRACT

Introduction : Pancreatic ductal adenocarcinoma (PDAC) is a leading cause of cancer-related deaths, with mortality and incidence rates continuing to rise. Findings from our lab identified Insulin-Like Growth Factor Binding Protein-3 (IGFBP-3) as a key regulator of tumor cell proliferation, as its ablation from non-metastatic KCKO and metastatic KP2 orthotopic tumor models significantly induces tumor necrosis. However, there are no significant differences in tumor size at end of life between parental and IGFBP-3-/- groups, nor are there significant reductions of IGFBP-3 expression in solid tumors. PDAC tumor mass is largely constituted by fibroblasts and macrophages, which have been shown to express IGFBP-3. Here we test the hypothesis that tumor-associated IGFBP-3 regulates the quantity, polarization, and IGFBP-3 expression levels of fibroblasts and macrophages.

Methods: NIH 3T3 fibroblasts and RAW 264.7 macrophages were plated into 6-well plates at a density of 50,000 cells/well for 24 hours before treatment. Cells were treated with parental or IGFBP-3-/- KP2 conditioned media (CM) and compared to untreated controls (n=3/group). Macrophages received additional treatments of rmIFN-γ (50ng/mL), rmIL-4 (20ng/mL), and rmIGFBP-3 (5μg/mL). 72 hours after treatment, cells were lysed for RNA collection and analyzed for transcriptional changes in igfbp3, markers of M1 polarization (nos2), and M2 polarization (arg1). Additionally, parental and IGFBP-3-/- tumors were analyzed using immunofluorescence (IF) staining to observe in-vivo colocalization of IGFBP-3 with CK19+ tumor cells, α-SMA+ fibroblasts/endothelial cells, or CD68+ macrophages. The IF signals were quantified using ImageJ software. Single cell RNA sequencing for IGFBP-3 expression was performed on KP2 murine tumors. One-way ANOVA was performed using GraphPad Prism software to analyze fold-changes in transcription of applicable targets between different treatment groups and differences in IF stain intensities between KP2 parental and IGFBP-3-/-tumors.

Results: Macrophages cultured in KP2 CM and rmIL-4 exhibit significantly increased arg1 expression compared to untreated cells, with parental CM treated cells exhibiting significantly higher arg1 expression than IGFBP-3-/- CM treated cells ($p<0.0001$). rmIFN-λ treated macrophages exhibited a significant increase in nos2 expression. Macrophages treated with parental CM, IGFBP-3-/- CM, rmIGFBP-3, rmIFN-λ, or rmIL-4 did not exhibit any significant changes in IGFBP-3 transcription. IGFBP-3 transcription is significantly reduced in both parental and IGFBP-3-/- CM treated fibroblasts ($p=0.0003$), with no differential expression being observed between the parental and IGFBP-3-/- CM treatments. IF images of the murine tumors show that IGFBP-3 localizes with CK19+ tumor cells in KP2 parental tumors, and that α-SMA+ cells increase in quantity and colocalize with IGFBP-3 in IGFBP-3-/- tumors. Single cell RNA sequencing on solid KP2 tumors revealed that IGFBP-3 is primarily expressed by tumor cells and endothelial cells.

Discussion : This study demonstrated that fibroblasts and macrophages are not responsible for the non-significant reduction of IGFBP-3 expression observed in murine IGFBP-3-/- tumors. However, macrophages were revealed to exhibit reduced M2-like polarization when cultured in the absence of tumor-associated IGFBP-3, minimizing the presence of characteristic pro-tumorigenic phenotypes. Histology of murine tumors indicates that α-SMA+ cells, alluding to fibroblasts or endothelial cells, secrete IGFBP-3, which is supported by previous data identifying elevated angiogenesis and endothelial cell recruitment in IGFBP-3-/- tumors, alongside single cell RNA sequencing data identifying tumor and endothelial cells as the primary secretors of IGFBP-3. Future work will focus on repeating CM cultures with endothelial cells and quantifying macrophage polarization under the specified treatment conditions using flow cytometry.

15th Annual Center for Musculoskeletal Research Symposium
October 30, 2025

Title:	Galactic Cosmic Radiation Reveals Sex-Dependent Mechanisms of Bone Loss and Marrow Remodeling
Presenting Author:	Valerie Voytsekhovskaya
Co-Author(s):	Catherine Caballero, Yuko Kawano MD/PhD, Hiroki Kawano MD/PhD, Emily R. Quarato PhD, Nataliia Vdovichenko MS
Lab PI / Mentor:	Laura Calvi

ABSTRACT

Radiation accelerates aging-like changes in the bone marrow microenvironment (BMME), a specialized niche of stromal and hematopoietic cells essential for sustaining blood and skeletal health. Galactic cosmic radiation (GCR), relevant to both spaceflight and therapeutic exposures, induces clustered DNA damage, oxidative stress, and inflammation that compromise BMME function. While radiation effects on hematopoiesis and bone are well documented, the role of sex as a biological variable remains poorly defined. We hypothesized that GCR exposure elicits sex-specific alterations in hematopoietic output and skeletal remodeling.

Six-month-old male and female C57BL/6 mice were exposed to either sham or continuous 100 cGy GCR. Longitudinal analyses were performed six months post-irradiation. Flow cytometry quantified hematopoietic and stromal populations, while dual-energy X-ray absorptiometry (DXA) assessed bone mineral density. Experiments were replicated across three independent cohorts conducted over three years. Statistical comparisons were performed using unpaired two-tailed t-tests (GraphPad Prism).

Female mice exhibited reduced hematopoietic output accompanied by cortical and trabecular bone loss, whereas male mice demonstrated pronounced myeloid skewing without measurable bone loss. These divergent outcomes reveal sex-dependent mechanisms of BMME injury and skeletal remodeling following low-dose GCR exposure.

Our findings establish sex as a critical determinant of hematopoietic and skeletal resilience after GCR. This work advances understanding of astronaut health risks and offers translational insights for cancer survivors and occupationally exposed populations. By defining sex-specific skeletal and hematopoietic responses to radiation injury, these results provide a foundation for future mechanistic studies aimed at preserving bone integrity and mitigating long-term hematopoietic and skeletal fragility.

15th Annual Center for Musculoskeletal Research Symposium
October 30, 2025

Title: Effects of Hydroxybisphosphonate-Conjugated Sitafloxacin on Fracture Healing and Skeletal Growth in Mice

Presenting Author: Hannah Wang

Co-Author(s): Sashank Lekkala, Youliang Ren, Allie Jia Hui Tay, Jeffrey D. Neighbors, Frank H. Ebetino, Shuting Sun, Noah M. Joseph, Edward M. Schwarz, Chao Xie

Lab PI / Mentor: Edward Schwarz/Chao Xie

ABSTRACT

Introduction: Chronic bone infection is considered incurable due to bacterial colonization of the osteocyte-lacuno canalicular network (OLCN). The pharmacokinetic limitations of drug delivery to this compartment of bone render the infection resistant to antibiotics. Bone-targeted bisphosphonate-conjugated antibiotics have been developed to overcome this issue. These target-and-release compounds are cleaved by acidic and/or enzymatic conditions at the bone-bacteria interface, releasing the active antibiotic and killing bacteria. Hydroxybisphosphonate-conjugated sitafloxacin (HBCS) has emerged as a leading candidate based on safety and efficacy results in mice and sheep. However, due to the bisphosphonate component in HBCS, potential concerns about adverse effects on skeletal growth and bone healing remain. To this end, we tested the hypotheses that: 1) HBCS has similar effects to its parental bisphosphonate component, HPHBP, on bone growth and fracture healing; and 2) HBCS has non-inferior adverse effects on fracture healing compared to the most potent bisphosphonate used in patients, zoledronic acid (ZA).

Methods: All in vivo experiments were approved via IACUC. We utilized a closed, stabilized, mid-diaphyseal femur fracture model with 12-week-old female C57BL/6 mice. Briefly, a stainless steel 25-gauge spinal needle was inserted into the intramedullary space of the femur, followed by three-point bending. The animals were injected i.p. with either: 1) PBS, or 2) ZA 0.1mg/kg (single dose), or 3) HPHBP 3.0mg/kg/48hr, or 4) HBCS 3.0mg/kg/48hr. The fractures were radiographically assessed on day 0 and every 7 days post-fracture. At 2- and 3-week timepoints, the mice were euthanized via heart perfusion using lead chromate-based Microfil to assess angiogenesis. The femurs were harvested and processed for μ-CT (n=5) and histological analysis (n=5). Femurs from the 4-week groups underwent biomechanical torsion testing (n=12). $p<0.05$ by one-way ANOVA.

Results: The μ-CT analyses of the fracture callus and vasculature at 2- and 3-weeks post-fracture revealed no drug effects on angiogenesis and minimal effects on callus that were limited to ZA and HBCS increased bone volume/total volume (BV/TV) vs. PBS at 3 weeks. Alcian blue staining confirmed similar amounts of soft callus in the fracture at 2 weeks, which was completely remodeled into bone by 3 weeks in all groups. TRAP staining confirmed the predicted increase in osteoclasts in the ZA group at 2 weeks, with no HBCS effects at this time point and decreases in TRAP+ area in all drug treatment groups at 3 weeks. Dynamic histomorphometry confirmed that no drug treatments altered the mineral apposition rate and bone formation rate. At 4 weeks, ZA increased the polar moment of inertia concomitant with increased maximum torque. To assess the effects of HBCS on normal long bone growth, we extended the same studies to the unfractured mice. ZA increased tibial growth plate length from unresorbed primary spongiosa, growth plate bone volume and BV/TV, and osteoclasts vs. PBS, consistent with prior reports. In contrast, HBCS had no remarkable effects on growth plate appearance, osteoclasts, and bone volume but did increase BV/TV vs. PBS.

Discussion: HBCS is a promising bone-targeted antibiotic with unprecedented in vivo bactericidal effects within bone marrow staphylococcus abscess communities (SACs) and the OLCN. Based on this efficacy profile, we proposed a Phase 1 clinical trial in patients being treated with external fixation frames for tibia fractures, as 30% of the pins are expected to become infected and could be harvested for analysis during conversion to internal fixation. While regulators favorably reviewed this trial design, potential concerns about HBCS inhibition of fracture healing were expressed. Through our findings, this concern about HBCS is further abated on top of the pre-clinical and clinical evidence that bisphosphonates do not inhibit fracture healing.

15th Annual Center for Musculoskeletal Research Symposium
October 30, 2025

Title: Accelerated ovarian failure model of menopause increases low back pain associated behavior in mice

Presenting Author: Cindy Wu

Co-Author(s): Lianne Trigiani, Laura Berkowitz, Nozomi Nishimura, Chris B. Schaffer, Rebecca M. Irwin

Lab PI / Mentor: Rebecca M. Irwin

ABSTRACT

BACKGROUND: Injury or degeneration of the intervertebral disc (IVD) can lead to chronic low back pain and current IVD treatments fail to halt degeneration or promote tissue regeneration, highlighting a pressing clinical need. Clinical data show age related sexual dimorphisms where menopausal women develop more severe IVD degeneration and pain sensitization compared to age-matched men, but the mechanisms driving this difference are unclear. Recently, a chemically induced model of accelerated ovarian failure has been developed in mice that models temporal hormonal changes that occur during menopause in humans. This inducible menopause model shows accelerated articular cartilage degeneration compared to age-matched controls, but IVD health and pain has not been evaluated in this model. Therefore, the objective of this study was to evaluate low back pain using a spontaneous behavioral assessment in a murine model of accelerated ovarian failure compared to age-matched controls.

METHODS: Accelerated ovarian failure model (VCD): WT female mice ages 8-9 months received 20 intraperitoneal injections over a period of 26 days of either VCD (160 mg/kg) in sesame oil or sesame oil alone (vehicle control, n=5/group). Only female mice were used to evaluate the effect of menopause on pain compared to age-matched female mice. Vaginal cytology: Vaginal lavages were performed for estrus cycle characterization where saline lavages were analyzed using a Hemacolor Stain Set® to determine estrus cycle state at days 42-79 post-injection. Spontaneous pain assessment (open field): Open field behavior testing was performed as a spontaneous assessment of low back pain in mice that is consistent across models and corresponds to low back pain in humans. Briefly, mice were placed in an open field box (40 cm x 40 cm) with low light (30 lux) for 5 minutes. Recordings of mouse movement were assessed using the DeepLabCutTM software package to characterize mouse velocity, stationary time, field coverage. Ovarian histology: Mice were euthanized on day 79 and ovaries were collected, fixed, paraffin-embedded, sectioned and stained with H&E.

RESULTS: VCD mice showed cycle irregularity by day 66 by a loss of estrus stage and prolonged diestrus phase, indicative of late perimenopause/early menopause. Further, VCD mice had smaller ovaries compared to vehicle controls. Open field behavior assessments across a habituation period of 3 days showed VCD mice moved slower (↓velocity) and showed different stationary time responses compared to vehicle controls; VCD mice had significantly higher stationary time on the first day (day 52), and this metric remained consistent throughout the habituation period. There was no difference in field covered proportion between groups during the habituation tests.

DISCUSSION & CONCLUSIONS: The VCD mice demonstrated accelerated ovarian failure through estrus cycle irregularity and ovary size reduction by day 79 post-injections. Spontaneous pain assessments using the open field test began during the late perimenopause stage for mouse habituation and showed significant differences between VCD and control mice. While both groups equally explored the open field area during the habituation period, the VCD mice did so with more stops and at slower speeds, suggesting pain-driven rather than anxiety-driven behavior. These pain driven behavioral responses are consistent with our hypothesis that menopause increases susceptibility to IVD degeneration. Ongoing work includes evaluating ovary follicles, lumbar spines, and knee joints from these mice.

15th Annual Center for Musculoskeletal Research Symposium
October 30, 2025

Title:	Objective Monitoring of Functional Recovery in Adult Scoliosis Using Inertial Measurement Unit (IMU)–Based Motion Recognition
Presenting Author:	Shibo Xu
Co-Author(s):	Kade Kaufmann, Ye Shu, William Lavelle, Yair Barzilay, Prasanth Romiyo, Tyler Schmidt, Alan Daniel, Bassel Diebo, Addisu Mesfin, Varun Puvanesarajah, Ram Haddas
Lab PI / Mentor:	Ram Haddas

ABSTRACT

INTRODUCTION: Spine deformities, such as adult scoliosis, involve abnormal spine curvature and rotation that can impair posture, balance, and everyday movement. Understanding patients' real-world movement patterns can help clinicians understand symptoms and recovery. Wearable inertial measurement units (IMUs) offer a low-burden way to monitor movement continuously. The study aims to develop and rigorously evaluate a segment-level motion recognition pipeline featuring broad adaptability across patients with spine deformities.

METHODS:Four adult scoliosis patients and six healthy controls were fitted with triaxial IMUs (BLUE TRIDENT, 1125 Hz) positioned below the C7 spinous process. Participants performed standardized functional activities—walking for 2 minutes, lifting a small bag three times, standing with eyes open and closed for 1 minute each, repeated sit-to-stand and lying-to-standing transitions, and the timed-up-and-go (TUG) test—twice daily over two days, logging activity times. Raw acceleration and angular-velocity signals were segmented (1.5 s windows, 1.0 s step) and features extracted in time and frequency domains. A walking identifier RNN layer, followed by an LSTM-based RNN, was trained using a 70/30 split with 5-fold cross-validation. Continuous segments were reconstructed from window-level probabilities >0.60. Performance metrics included time-weighted accuracy, segment coverage, segment precision, and mean intersection-over-union (IoU). Cohort comparisons used post-estimation analyses with $p < 0.05$.

RESULTS: The motion recognition pipeline demonstrated a robust overall accuracy of 0.75 with the RandomForest model excelling in recognizing common activities such as standing, achieving a precision of 0.74, a recall of 1.00, and an F1-score of 0.85, and Walking, with a precision of 0.79, a recall of 0.99, and an F1-score of 0.88, reflecting strong performance across these prevalent movements. Bed and Lifting activities also showed solid results, with precision, recall, and F1-scores ranging from 0.55 to 0.73, indicating reliable detection in diverse contexts, while transitional phases like TUG presented some challenges that are being addressed through ongoing refinements.

DISCUSSION: This model demonstrates that IMU-based segment-level motion recognition can provide accurate, longitudinal monitoring of functional activities in spine deformity patients. High-fidelity detection of walking and standing suggests potential for objective tracking of daily mobility and postural stability outside clinical settings. Limitations in transitional activity detection, such as TUG, highlight areas for refinement, which may improve with expanded patient datasets. Clinically, this approach enables continuous assessment of functional recovery, identification of activity-related limitations, and evaluation of rehabilitation progress. Comparing patterns between patients and healthy controls can guide personalized interventions, optimize therapy, and enhance post-surgical recovery strategies. Ultimately, this pipeline supports translation of objective movement data into actionable insights for improving spine patient care and daily function.

15th Annual Center for Musculoskeletal Research Symposium
October 30, 2025

Title:	Identifying Neural Biomarkers of Chronic Low Back Pain Using Resting-State EEG and Machine Learning
Presenting Author:	Zhengyang Zhu
Co-Author(s):	Paul Rubery, MD; Ashely Rogerson, MD; Varun Puvanesarajah, MD; Prasanth Romiyo, MD; Ye Shu, BS
Lab PI / Mentor:	Ram Haddas, PhD, MBA

ABSTRACT

Introduction: Chronic low back pain (cLBP) is the leading cause of disability and a major driver of spine care, yet objective neural biomarkers remain lacking. Current practice relies heavily on patient-reported outcomes, which are variable and often insufficient to guide treatment decisions. Resting-state electroencephalography (EEG) provides a noninvasive method to assess pain-related brain activity. Prior work has linked CLBP to increased theta and high-beta power, slowed alpha peak frequency, and abnormal cross-frequency coupling. These patterns suggest that quantitative EEG (qEEG) may serve as an objective marker of pain states. This study aimed to determine whether qEEG features can distinguish between spine patients with active pain, pain-free spine patients, and healthy controls during a Romberg task. By evaluating the discriminatory value of qEEG in a clinical cohort, we sought to establish its potential as a biomarker to support diagnosis, monitoring, and personalized management of cLBP.

Methods: Forty-eight participants completed three one-minute, eyes-open standing balance trials to assess postural control. EEG data were recorded using a Zeto WR-19 wireless headset (10–20 system, dry electrodes). PROMIS pain interference scores were collected on the same day. Participants were stratified into three groups: active pain (n = 30; PROMIS ≥55), pain-free with spine history (n = 13; PROMIS <55), and healthy controls (n = 5). EEG signals were preprocessed for artifact rejection and segmentation. Spectral bandpower ratios (delta, theta, alpha, beta, gamma) and phase–amplitude coupling (PAC) metrics were extracted. Feature selection was performed using SelectKBest, and multinomial logistic regression with cross-validation classified participants while optimizing regularization. Model performance was evaluated using macro F1-score, accuracy, ROC–AUC, and confusion matrices. This approach integrates objective cortical markers with patient-reported outcomes, enabling identification of neural signatures associated with chronic spine pain. Findings provide a framework for non-invasive biomarkers to inform clinical decision-making, monitor treatment response, and improve risk stratification in patients with spine disorders.

Results:
The multi-class model demonstrated strong group separation, achieving cross-validated macro F1-scores above 0.70 and macro ROC–AUC exceeding 0.50. The most discriminative qEEG features included elevated beta2 power ratios (25–35 Hz) in temporal–occipital and frontal–parietal regions, increased slow-wave ratios (theta/delta) in frontal areas, altered alpha1 ratios in temporal sites, and heightened theta–gamma phase–amplitude coupling. Healthy controls showed stable alpha dominance with lower theta and high-beta activity. Pain-free spine patients exhibited mild increases in slow-wave ratios compared with controls. In-pain patients displayed pronounced alpha enhancement, high-beta (beta2) dominance, and stronger theta–gamma coupling — patterns consistent with established chronic pain findings in the literature.

Discussion:
These results demonstrate that resting-state EEG can objectively differentiate patients with cLBP from pain-free patients and healthy controls, using spectral power and phase–amplitude coupling metrics. Elevated alpha and beta2 activity in the cLBP group aligns with prior chronic pain findings, supporting their potential as non-invasive neural biomarkers. The machine learning framework identified clinically relevant EEG signatures and may enable longitudinal monitoring of pain states. Resting-state EEG could provide an actionable tool for objective assessment, guiding individualized interventions and surgical decision-making in patients with chronic spinal pain.

Post-Graduate Posters

Disclaimer

15th Annual Center for Musculoskeletal Research Symposium
October 30, 2025

Title:	TRPC6 Inhibition as a Potential Therapeutic for Discogenic Chronic Back Pain
Presenting Author:	Janitri Venkatachala Babu
Co-Author(s):	Addisu Mesfin, Varun Puvanesarajah, Karin Wuertz-Kozak
Lab PI / Mentor:	Karin Wuertz-Kozak

ABSTRACT

INTRODUCTION: Low back pain is the leading cause of global disability, with discogenic etiology accounting upto 42% of cases. Intervertebral disc (IVD) degeneration is characterized by elevated pro-inflammatory cytokines, catabolic enzyme activity with nerve and blood vessel ingrowth, all of which exacerbate pain. The degenerated microenvironment is further compromised by extracellular matrix breakdown, reduced load-bearing capacity, and accumulation of metabolites such as diaclyglycerol (DAG) and lysophosphatidylcholine (LysoPC), which accelerate disease progression. Despite the marked prevalence of discogenic chronic back pain (DCBP), no pharmacological therapy directly targets these underlying mechanisms.

Transient receptor potential channels are cation-permeable transmembrane proteins that have emerged as promising therapeutic targets in various diseases. The canonical subtype TRPC6, known to regulate inflammation and pain in multiple tissues, has not yet been investigated in the context of DCBP. TRPC6 is upregulated in painful, degenerated discs and can be activated by hypo-osmotic stimuli, mechanical loading, and DAG. We hypothesize that in degenerated IVDs, elevated DAG (likely in combination with mechanical loading and osmotic pressures) activates TRPC6, driving inflammation and catabolism, hallmarks of DCBP. Conversely,pharmacological inhibtion of TRPC6 could mitigate these pathological processes, positioning TRPC6 as a novel non-opioid therapeutic target for DCBP.

METHODS: Human IVD tissue was obtained from patients undergoing surgery for disc herniation or degenerative disc disease under institutional ethical approval. TRPC6 mRNA expression was quantified in degenerated (n=22) and non-degenerated (n=12) IVD samples using RT-qPCR. DAG levels were assessed in isolated human IVD cells (n=2) using a fluorometric assay (Cellbiolabs). TRPC6 channel activity was measured by calcium influx assays (Flexstation-3, Fura-2 QBT) in human IVD cells treated with TRPC6 activators (OAG - a DAG analog, Hyp9; n=3) or inhibitor (larixyl acetate [LA]; n=1). For gene expression studies, IVD cells were treated with Hyp9 (1μM, 18 h; n=7) or pretreated with Hyp9 (1μM, 2 h) followed by LA (10μM, 18 h; n=4). Untreated and vehicle controls were included. mRNA expression was analyzed by RT-qPCR, protein secretion quantified by ELISA (normalized to DNA), and pathway activation (hyp9 1μM for 15 or 30 minutes) examined by western blot (phospho/total ratios). Statistical analyses (normality test, t-test, ANOVA) were performed using GraphPad Prism 10.0.2.

RESULTS: TRPC6 mRNA and protein levels were significantly elevated in painful, degenerated human IVDs. Isolated human IVD cells produced DAG and TRPC6 activation by OAG or Hyp9 induced a dose-dependent increase in intracellular calcium, whereas inhibition with LA attenuated this response. Hyp9 stimulation significantly upregulated inflammatory and catabolic genes, as well as neurotrophic and angiogenic factors. At the protein level, Hyp9 increased IL-8 secretion across 18 to 48 hours, with additional cytokines like IL-6 and VEGF also being elevated. Hyp9 further activated the ERK pathway. Importantly, LA treatment following Hyp9 pre-activation significantly reduced inflammatory and catabolic gene expression and neutrophic and angiogenic factors.

DISCUSSION: Our study highlight TRPC6 as a key mediator of inflammatory and catabolic signaling in the degenerated intervertebral disc. Consistent with its upregulation in painful human IVDs, Hyp9 activation of TRPC6 elevated intracellular calcium, induced pro-inflammatory cytokine release, and activated MAPK/ERK signaling, linking TRPC6 activity directly to hallmarks of DCBP. Importantly, inhibition of TRPC6 with LA reversed these pathological effects, underscoring its therapeutic potential. These findings align with the emerging role of TRP channels as modulators of pain and inflammation in other tissues and extend this paradigm to the IVD.

15th Annual Center for Musculoskeletal Research Symposium
October 30, 2025

Title:	Preoperative Biomechanical and Patient-Reported Predictors of Surgical Recovery in Lumbar Spine Disease: Translating Motion Analysis into Precision Medicine
Presenting Author:	Reshmii Bondili, BS
Co-Author(s):	Ye Shu BS, Varun Puvanesarajah MD, Prasanth Romiyo MD, Paul Rubery MD
Lab PI / Mentor:	Ram Haddas PhD MBA

ABSTRACT

Introduction: Lumbar spine surgery is among the most frequently performed procedures for degenerative spinal disorders, yet clinical outcomes remain highly variable, with many patients experiencing persistent disability or limited functional recovery. This variability underscores a critical clinical and translational gap: the absence of validated preoperative predictors capable of identifying which patients are most likely to achieve meaningful improvement. Traditional predictors such as age, comorbidities, and imaging findings explain only part of the variability in outcomes. Innovative approaches that integrate biomechanical and patient-reported metrics may enhance precision in surgical decision-making. This study leverages a responder analysis framework to identify preoperative clinical, functional, and biomechanical features associated with treatment response following lumbar spine surgery.

Methods: An observational cohort study was conducted at the University of Rochester Medical Center Motion Lab between 2024–2025. Fifty-nine patients undergoing lumbar spine surgery with complete three-month follow-up were included. Treatment response was defined as achieving the minimal clinically important difference (MCID) in both Oswestry Disability Index (ODI) and gait speed. Twenty-two preoperative variables were assessed, including demographics, patient-reported outcomes (PROs), spatiotemporal gait metrics, and postural sway measures. Gait was evaluated via embedded force plates, while postural sway was quantified during quiet standing using 95% confidence ellipse displacement. Features were standardized and analyzed using Least Absolute Shrinkage and Selection Operator (LASSO) regression, followed by logistic regression and Extreme Gradient Boosting (XGBoost). Feature importance was assessed using standardized coefficients and SHAP values.

Results: At 3 months, 59.3% of patients achieved a clinically meaningful improvement in ODI and 37.3% in gait speed. Baseline ODI and sagittal head sway emerged as strong predictors of disability improvement, while total sway, step length, and double support time predicted gait recovery. Greater preoperative disability was paradoxically associated with larger clinical gains, suggesting a higher capacity for measurable improvement. Conversely, impaired balance control (greater sway) consistently predicted limited recovery. Predictive models demonstrated robust performance (XGBoost AUCs: 0.67 [ODI], 0.88 [gait]; logistic regression AUCs: 0.75 [ODI], 0.79 [gait]).

Conclusions: This study highlights the innovation of integrating objective biomechanical measures with patient-reported outcomes to identify surgical responders, addressing a major clinical gap in spine surgery. The findings suggest that gait and balance metrics—routinely feasible in a clinical motion analysis setting—provide meaningful predictive value for early postoperative recovery. Clinically, these measures may improve preoperative counseling by setting realistic expectations, guide individualized rehabilitation strategies, and identify patients who could benefit from prehabilitation or intensified postoperative care. Translationally, this work advances precision spine care by demonstrating a scalable, multimodal framework that can be embedded into routine surgical evaluation. Prospective validation may establish these metrics as novel clinical biomarkers for risk stratification, ultimately improving patient outcomes and reducing long-term disability after lumbar spine surgery.

15th Annual Center for Musculoskeletal Research Symposium
October 30, 2025

Title:	Targeted expression of Sirtuin 6 to bone marrow stromal cells reverses their age-dependent transcriptional signatures
Presenting Author:	Catherine Caballero
Co-Author(s):	Adam Tyrlik, Zhiming Jin, Jane Zhang, Nataliia Vdovichenko, Ronald Lakony, Jane L. Liesveld, Andrei Seluanov, Vera Gorbunova, Laura M. Calvi
Lab PI / Mentor:	Laura M. Calvi

ABSTRACT

Bone marrow stromal cells (BMSCs) are a critical cell population within the bone marrow microenvironment (BMME) that plays a crucial role in hematopoietic support and immunomodulation. Dysregulation of the BMME is a conserved driver of skeletal aging and contributes to the pathogenesis and progression of myeloid neoplasms. Thus, targeting the BMME may represent a promising strategy to restore skeletal health and maintain hematopoietic homeostasis. Aging is associated with inflammatory changes and impaired hematopoietic support in the BMME, but the underlying molecular and epigenetic mechanisms remain poorly defined. Sirtuin 6 (SIRT6), a chromatin-associated enzyme that regulates DNA repair, transcription, and transposable element repression, has emerged as a key determinant of aging, with global deficiency accelerating aging phenotypes and overexpression extending lifespan. We hypothesized that targeted overexpression of SIRT6 in BMSCs would reverse age-associated BMSC dysfunction and improve microenvironment-driven hematopoietic aging. To test this, we generated a genetic model of BMSC-specific human SIRT6 overexpression (Prx1-Cre × hSIRT6 OE). Transcriptional analysis confirmed BMSC-restricted overexpression of SIRT6. Our data revealed that aged BMSCs exhibit a pro-inflammatory transcriptional program that is significantly attenuated by SIRT6 overexpression. Notably, aged SIRT6-overexpressing BMSCs clustered transcriptionally with young control BMSCs, indicating partial rejuvenation of the aged stromal compartment. At the hematopoietic level, preliminary findings demonstrate improvement in age-associated hematopoietic stem cell expansion and attenuation of myeloid skewing in Prx1-SIRT6 OE mice, suggesting restoration of BMSC hematopoietic support function. These findings establish a novel model to dissect the contribution of BMSCs to the aging of the hematopoietic system and provide evidence that epigenetic rejuvenation of the BMME can mitigate hematopoietic decline. Reversing BMSC dysfunction may ultimately restore healthy hematopoiesis and reduce susceptibility to age-associated pathologies, including myeloid neoplasms.

15th Annual Center for Musculoskeletal Research Symposium
October 30, 2025

Title:	Patients 50 years or Older Demonstrate Similar Improvement in PROMIS Physical Function and Pain Interference Scores after ACL Reconstruction Compared to Younger Patients
Presenting Author:	Patrick Castle, MD
Co-Author(s):	Omkar N. Prabhavalkar, BA; Melissa Holloway, MD; Hashim J.F. Shaikh, MD; Sandeep Mannava, MD, PhD
Lab PI / Mentor:	Sandeep Mannava, MD, PhD

ABSTRACT

Background: Anterior cruciate ligament (ACL) reconstruction is the gold standard for treating knee instability from an ACL tear, with success rates of up to 95% in young, active patients. Historically, patients over 50 were treated non-operatively with activity modification, bracing, and therapy, but increasing activity levels in older adults have made reconstruction a viable option. This study evaluates whether patients over 50 achieve significant improvements in PROMIS scores and meet minimally clinically important difference (MCID) thresholds after ACL reconstruction. We hypothesize that outcomes in this group will be comparable to those reported in younger cohorts.

Methods: Patients who underwent arthroscopic ACL reconstruction at our institution between January 1, 2015, and December 31, 2023, were retrospectively reviewed. Inclusion criteria were age ≥13 years, diagnosis of partial or complete ACL tear, and completion of both preoperative and ≥6-month postoperative PROMIS questionnaires. MCID was defined as one-half the standard deviation of preoperative PROMIS scores. Patients over the age of 50 were propensity matched to a cohort of patients under the age of 50 in a 1:2 ratio on the basis of gender, insurance status, race, and BMI. The mean and standard deviation for continuous demographic and outcome measures were calculated and compared between groups using 2-tailed t-tests while categorical variables were compared using Chi-square analysis. Post-operative complications were examined through chart review.

Results: A total of 43 patients over the age of 50 met inclusion criteria with minimum 6-month follow-up. The mean follow-up time was 20.6 ± 14.3 months. After propensity matching, 42 patients over 50 were matched with 84 patients under the age of 50. There were no significant differences with regards to sex (p=0.70), race (p=0.88), smoking history (p=0.10), BMI (p=0.92), and insurance status (p=0.90). Patients over 50 were found to have significantly higher proportion of elevated ASA Status (p=0.0020), and Charleson Comorbidity Index (CCI) scores ($p < 0.001$). The Over 50 group showed significant improvement in PF ($P < 0.001$), PI ($P < 0.001$), but not in Depression scores ($P = 0.54$) when compared to preoperative assessments. The Over 50 patients had significantly higher preoperative ($P = 0.042$) and postoperative ($P = 0.019$) PI scores compared to the Under 50 group, but no other outcome differences were observed between the groups (Table 1). Following surgery, the two groups had similar rates of achieving of MCID. There were no postoperative complications including graft failures, infections, arthrofibrosis, patellar tendon ruptures, or cyclops lesions in the Over 50 group.

Conclusions: In this age-matched cohort study, patients over 50 demonstrated significant improvements in PROMIS Pain Interference and Physical Function scores after ACL reconstruction, with similar rates of achieving MCID compared to younger patients. These findings suggest ACL reconstruction is a safe and effective option in patients over 50, yielding outcomes comparable to younger cohorts. To our knowledge, this is the first study using PROMIS to compare age-stratified outcomes after ACL reconstruction and provides valuable guidance for counseling older patients on expected recovery and function.

15th Annual Center for Musculoskeletal Research Symposium
October 30, 2025

Title: Defining the Piezo1 Mechanotransduction Setpoint in Articular Cartilage

Presenting Author: Minhwan Chung, Ph.D.

Co-Author(s):

Lab PI / Mentor: Whasil Lee, Ph.D.

ABSTRACT

Introduction

Mechanical forces are essential for cartilage homeostasis, especially in load-bearing knee joints. Articular chondrocytes, the resident cells of cartilage, maintain the extracellular matrix (ECM) by balancing anabolism and catabolism. Physiologic exercise promotes ECM remodeling and joint health via mechanotransduction, whereas dysregulated mechanotransduction contributes to degeneration, a hallmark of osteoarthritis (OA). The mechanisms distinguishing beneficial from harmful stimuli remain poorly defined. A deeper understanding of chondrocyte mechanotransduction and metabolism will provide insights into OA therapeutics. We and others have shown that Piezo1 contributes to chondrocyte death under supraphysiologic loading and to inflammation-driven hyper-mechanosensation in OA. Yet, Piezo1 regulation under physiologic loading and the downstream pathways remain unexplored. We hypothesize that exercise or physiologic loading induces Piezo1-dependent anabolic signaling, leading to cartilage remodeling. To test this, we examined Piezo1 regulation in knee cartilage of C57BL/6 mice after voluntary wheel running and developed an ex vivo platform applying physiologic cyclic compression to porcine cartilage plugs for mechanistic studies of load-dependent signaling.

Materials and Methods

In vivo voluntary wheel running (VWR): C57BL/6 female mice (8 weeks old, N=6/group) were housed with low-resistance running wheels; controls were housed with locked wheels. Wheel activity was recorded continuously. After 1 and 2 weeks, knee cartilage was collected for mechano-death assay and immunohistochemistry.
Ex vivo cartilage model: Porcine cartilage plugs (2 mm) were harvested and cultured for 24 h. Cyclic compression (0.2 Hz; 1 h loading/1 h rest ×2) was applied using a custom Arduino-controlled syringe pump; static plugs served as controls. Viability was assessed with Calcein AM/Propidium Iodide staining. Plugs were processed for RNA (qPCR, RNA-seq), protein (Western blot), or OCT-embedded frozen sections for IHC.

Results and Discussion

In mice, sedentary (Sed, locked wheels), 1-week exercise (Exer_1w), and 2-week exercise (Exer_2w) groups ran 0, ~55, and ~152 km, respectively. PIEZO1 and TRPV4 expression were quantified by IHC. Exercise gradually increased PIEZO1 compared to sedentary controls (1.8-fold), but not TRPV4, revealing exercise-driven Piezo1 augmentation and mechano-adaptation of chondrocytes. In porcine explants, viability remained high after cyclic loading, confirming the regimen was tolerable. RT-qPCR and IHC showed increased PIEZO1 expression in loaded vs. unloaded cartilage at RNA and protein levels. RNA-seq revealed upregulation of NF-κB–related genes in loaded plugs. qPCR showed a trend toward increased Piezo1 and decreased IL-1β, with variable MMP-13 expression. Western blot confirmed enhanced NF-κB phosphorylation after loading. Together, these results suggest cyclic compression promotes a shift toward an anabolic or protective profile, positioning cartilage at the threshold between homeostasis and catabolism.

Conclusion

Voluntary exercise and physiologic loading increased Piezo1 levels in load-bearing knee cartilage both in vivo and ex vivo. RNA-seq revealed suppression of catabolic markers such as MMP13 and IL-1β, despite Piezo1 upregulation. This contrasts with Piezo1's established catabolic role, suggesting a distinct function under physiologic loading. Future studies will employ Piezo1-knockout models to define Piezo1-dependent anabolism in cartilage.

Improved Outcomes with Endoscopic Carpal Tunnel Release for Patients who Smoke

Purpose: While both endoscopic and open carpal tunnel release are effective treatments for carpal tunnel syndrome, with prior studies suggesting similar long-term outcomes, data on perioperative complication rates in high-risk populations, such as smokers, remain limited. Given the potential for impaired wound healing and increased infection risk in smokers, a better understanding of complication profiles between techniques in this subgroup is warranted. This study aimed to compare the perioperative complication rates of endoscopic vs open carpal tunnel release in patients who smoke.

Methods: We conducted a retrospective cohort study using the TriNetX database, identifying 22,435 open and 4,947 endoscopic carpal tunnel release procedures performed in patients who smoke. We assessed 90-day postoperative complication rates in both cohorts, including hospital admissions, emergency department (ED) visits, infections, nerve injuries, renal injuries, and thrombotic events. Propensity score matching was performed to reduce confounding and ensure comparability between groups.

Results: Rates of median nerve injury, postoperative admissions, ED visits, superficial infections, and acute kidney injury (AKI) were significantly higher in patients undergoing open carpal tunnel release compared to those undergoing endoscopic carpal tunnel release, with odds ratios ranging from 1.3 to 3.4. After adjusting for demographic and comorbidity variables, increased odds of median nerve injury, postoperative admissions, ED visits, and superficial surgical site infections (SSIs) remained significant.

Conclusions: Among patients who smoke, those undergoing open carpal tunnel release experienced higher 90-day perioperative complication rates compared to those treated with endoscopic release. This difference remained significant in both unmatched and propensity score–matched analyses, suggesting that endoscopic techniques may offer improved short-term outcomes for patients with nicotine dependence.

15th Annual Center for Musculoskeletal Research Symposium
October 30, 2025

Title:	Increased Risk for Upper Extremity Amputation in Minority Patients with Necrotizing Fasciitis
Presenting Author:	Christopher Dussik, MD
Co-Author(s):	Amy Phan MD, Jeffrey Coombs MD, Thomas Carroll MD, Andrew Jae-Min Park MD, Bilal Mahmood MD
Lab PI / Mentor:	Danielle Wilbur MD

ABSTRACT

Introduction: Necrotizing fasciitis of the upper extremity is often life-altering and life-threatening. Outcomes are multifactorial and depend on factors such as the delay in presentation, medical comorbidities, speed of diagnosis, and initiation of care. Healthcare disparities among underrepresented populations have been increasingly highlighted across various surgical specialties. We hypothesized that race and ethnicity would influence outcomes for necrotizing fasciitis of the upper extremity.

Methods: We queried the TriNetX database for all patients diagnosed with necrotizing fasciitis who received upper extremity surgical management between January 1, 2010, and December 31, 2023, using a combination of International Classification of Diseases (ICD) and Current Procedural Terminology (CPT) codes. We then evaluated the incidence of formal irrigation and debridement, amputation across upper extremity levels, and mortality within six months of diagnosis. Outcomes were stratified based on racial and ethnic categories as reported by the database. Chi-squared and odds ratio analyses were used to evaluate the statistical significance of trends observed across demographic groups.

Results: We evaluated outcomes for 1,253 patients undergoing upper extremity procedures in the setting of necrotizing fasciitis. Among this cohort, 519 patients underwent upper extremity amputation. Unmatched analyses comparing amputation rates after necrotizing fasciitis revealed increased rates of amputation across all minority demographics compared to non-Hispanic, white patients. Regarding procedures involving the shoulder to elbow, no variation was observed in the rates of either formal irrigation and debridement or amputation between non-Hispanic, white patients and those in the minority cohorts. However, statistically significant increased rates of amputation in the forearm/wrist and hand/fingers were observed in the minority cohorts, alongside decreases in the rate of formal irrigation and debridement of the forearm/wrist. Matched analyses showed continued increased rates of amputation across underrepresented populations as a whole, as well as among Hispanic patients and Asian/Pacific Islanders. Minority patients were at an increased risk for upper extremity amputation, with an odds ratio of 1.83. After comorbidity matching, this effect was preserved with an odds ratio of 1.63.

Discussion: Underrepresented patients with necrotizing fasciiitis undergo amputations 60% more frequently than non-Hispanic, white patients. Further investigation into social determinants of health is warranted to achieve parity in outcomes and ensure objectivity in decision-making for these at-risk groups.

15th Annual Center for Musculoskeletal Research Symposium
October 30, 2025

Title: Underutilization of Hand Corticosteroid injections and Arthroplasty for Minority Demographics in the United States

Presenting Author: Christopher Dussik, MD

Co-Author(s): Amy Phan MD, Akhil Dondapati MD, Andrew Jae-Min Park MD, Jeffrey Coombs MD, Danielle Wilbur MD, Ronald Gonzalez DO

Lab PI / Mentor: Constantinos Ketonis MD PhD

ABSTRACT

Introduction: The management of hand osteoarthritis is a cornerstone of hand surgery practice. For patients whose symptoms are refractory to less-invasive measures, corticosteroid injections and surgical interventions remain the primary treatment options. In recent years, healthcare disparities have been increasingly recognized, particularly regarding variations in pain management. This study aimed to evaluate whether such disparities exist among racial and ethnic groups in the treatment of hand osteoarthritis.

METHODS: We utilized the TriNetX database to evaluate patients diagnosed with hand osteoarthritis between January 1, 2010 and December 31, 2024. Diagnostic and billing codes were used to identify patients, gauge healthcare exposure, and assess the use of corticosteroid injections and surgical intervention across different demographics. Outcomes were stratified based on racial and ethnic identification and matching was performed to mitigate risk for confounding. Odds ratios were calculated to evaluate statistical significance.

RESULTS: A total of 816,412 patients diagnosed with hand osteoarthritis were identified. Non-Hispanic, white patients had nearly twice the odds of undergoing corticosteroid injections and demonstrated consistently higher rates of operative treatment compared to minority populations across unmatched analyses (Table 2). After matching for demographic and comorbidity variables, these disparities largely persisted despite similar overall exposure to the healthcare system.

DISCUSSION: Minority demographics have lower odds of receiving corticosteroid injections for the treatment of hand osteoarthritis. Similarly, these groups undergo operative management at considerably lower rates compared to non-Hispanic, white patients. These findings highlight the persistent disparities in treatment faced by underrepresented groups and underscore the critical importance of considering social determinants of health in the management.

15th Annual Center for Musculoskeletal Research Symposium
October 30, 2025

Title: PRDM16 maintains cartilage homeostasis by modulating chondrocyte phenotypes

Presenting Author: Eloise Fadial

Co-Author(s): Victoria Hansen, Eliya Tazreena Tashbib, Gulzada Kulzhanova, Alexis Klee, Deeksha Chinta

Lab PI / Mentor: Chia-Lung Wu

ABSTRACT

INTRODUCTION: Cartilage development is a complex process regulated by tightly coordinated transcription and epigenetic networks. Previously, we showed that PRDM16, a histone methyltransferase and zinc finger transcriptional factor, is upregulated during chondrogenesis of human induced pluripotent stem cells (hiPSCs). PRDM16 is also downregulated in the cartilage and subchondral bone of patients with osteoarthritis (OA). Global knockout of Prdm16 in mice results in abnormal osteogenic and chondrogenic differentiation, and neonatal lethality. However, the detailed molecular mechanisms by which PRDM16 regulates chondrogenesis and joint homeostasis in a cartilage-specific manner remain largely unknown. Here, we hypothesize that PRDM16 is a positive regulator of chondrocyte phenotypes and postnatal cartilage homeostasis. We aim to elucidate the regulatory mechanisms of PRDM16 by using cartilage-specific, Prdm16 conditional knockout (Col2a1-Cre;Prdm16fl/fl, cKO) mice, hiPSCs models, single-cell RNA sequencing (scRNA-seq), and CUT&RUN-seq.

METHODS: All animal procedures were approved by IACUC. Surgery to destabilize the medial meniscus (DMM) was performed to induced OA on the left knees of 16-wk-old WT and cKO mice. Right knees were used as non-surgery control. Both sexes were investigated. Joints were harvested 12wk-post surgery for μCT and histological analysis. hiPSCs with inducible PRDM16 knockdown (KD) or overexpression (OE) were generated, differentiated into chondrocytes, and submitted for scRNA/CUT&Run-seq. Gene ontology functional analysis was used to identify and annotate cell subsets. Monocle3 and iRegulon were used to construct gene regulatory networks (GRNs) and to identify transcription factors (TFs) governing chondrocyte differentiation. Data were analyzed with one- or two-way ANOVA as appropriate.

RESULTS&DISCUSSION: Significantly increased OA severity and osteophyte formation were observed in the DMM vs non-surgery joints in the WT male but not WT female mice, in line with previous findings that male mice are prone to DMM-induced OA. DMM joints also exhibited a decreasing trend in bone mineralization density vs non-surgery control. Interestingly, while Prdm16 cKO and WT mice had similar OA severity in the DMM joints, Prdm16 cKO mice also exhibited comparable OA severity between non-injury and DMM joints. These results indicate that PRDM16 is required for knee cartilage homeostasis postnatally. PRDM16 KD hiPSC-derived chondrogenic pellets exhibited severe loss of Saf-O staining, while OE of PRDM16 maintained high staining intensity. scRNA-seq unsupervised clustering of OE, KD, and WT chondrocytes revealed 5 distinct chondrocyte subpopulations. In WT, SOX5high chondroprogenitors differentiate into ANGPTL4high mature chondrocytes. Interestingly, KD cells fail to exit the chondroprogenitor stage, likely leading to poor chondrogenesis. Pseudotime and GRN analyses predicted that PRDM16 OE cells fail to transition into mature chondrocytes, and rather remain in the IGFBP5high chondrocyte population. Additionally, iRegulon analysis predicted that differentiation from SOX5high to IGFBP5high chondrocytes could be driven by TF ZBTB33. CUT&RUN-seq analysis further indicates that PRDM16 regulates ZBTB33 expression by modulating H3K4me3 status (gene activation) at its promoter region. Most importantly, these results provide essential evidence that PRDM16 modulates chondrocyte phenotypes by regulating TFs governing differentiation.

CONCLUSION/CLINICAL SIGNIFICANCE: OA is the one of the most prevalent degenerative joint disorders and has been diagnosed in approximately a quarter billion patients worldwide. Currently, there are no disease modifying drugs for OA. Our findings show that loss of Prdm16 leads to increased OA susceptibility and that PRDM16 regulates chondrocyte phenotypes by modulating H3K4me3 of several critical TFs. These findings will facilitate the development of future therapeutic applications for OA patients.

15th Annual Center for Musculoskeletal Research Symposium
October 30, 2025

Title: Optimizing the culture conditions of Human Hepatic Sinusoidal Endothelial Cells and iPSC-derived Hepatocytes for utilization in Liver-on-a-chip

Presenting Author: Rajkumar Govindan

Co-Author(s):

Lab PI / Mentor: Prof. Hani Awad

ABSTRACT

Background: Over 30% of therapeutic drug candidates fail phase I-III clinical trials due to unmanageable toxicity, and drug-induced liver injury (DILI) majorly contributes to the late-stage withdrawals, including some musculoskeletal disease lead compounds such as NSAIDs and DMARDs. To address these concerns and to evaluate the safety of new leads, there is an inherent need to integrate functional human liver with other tissue chips, such as human tendon-on-a-chip (hTOC). Liver is a major scavenging organ, and Hepatic Sinusoidal Endothelial Cells (HHSECs) are specialized endothelial cells equipped with specialized receptors aiding the liver in small molecule clearance. While highly regenerative in vivo, they lose morphology and functional characteristics in vitro and are subject to dedifferentiation with respect to changes in media. Primary hepatocytes, on the other hand, are terminally differentiated and often have a limited lifespan in vitro (~5 days). Our aim is to develop a functional healthy liver-on-a-chip (hLOC) using a modular µSIM platform to screen and evaluate the hepatotoxicity of musculoskeletal lead compounds. To establish a successful drug screening platform/liver chip, it is important to have a reproducible source of hepatocytes with preserved functional characteristics of HHSECs. This study aims to optimize the culture conditions that could support the culture of hepatocytes and HHSECs, where their functional capacity is optimum.
Methods: HHSECs were plated onto fibronectin-coated µSIM devices (with Nanoporous Si3N4 membranes) at a density of 20,000 cells/cm2 in varying ratio of Hepatic Maintenance medium (HMM) to Sinusoidal Endothelial Media (SM) (1:1, 1:3, and 3:1). Cells were fixed with 4% Paraformaldehyde (PFA) and stained with antibodies for scavenging receptors (CD32B, STAB2 and LYVE1). Human iPSC cell line (SCTi003a) was cultured on Matrigel-coated plates. Upon reaching confluence, cells were differentiated into Hepatocyte-like Cells (HLCs) using STEMdiff™ Hepatocyte Kit. The media was changed daily, and the supernatant was collected for Albumin (ALB) and Urea analysis through ELISA. On Day 10 or Day 16, cells were lifted and replated onto either Col-I or Laminin-coated µSIM devices at a density of 325,000 cells per cm2 and differentiated until Day 21, and undisturbed Day 21 HLCs were used as a control. The cells were fixed and stained with antibodies for mature hepatic markers (ALB, Alpha-1-Antitrypsin (AAT), and CYP3A4). All images were acquired using Dragonfly Spinning Disk Confocal System, and the images were analyzed through ImageJ. All experiments were carried out in triplicate, and the results were analyzed through Student's t-test in GraphPad Prism.
Results: HHSECs express CD32B and STAB2 and express fenestrations significantly higher than HUVEC in earlier passages. HHSECs tend to express these markers at a similar level in mixed media, compared to SM higher STAB2 expression was shown in 3:1 HMM to SM. HLCs derived from iPSCs show polygonal morphology characteristic of hepatocytes and express hepatic markers such as HNF4A, EpCAM, CYP3A4, and AAT and secrete ALB and Urea. When replated on Day 10, the hepatic progenitors don't attach to dishes or µSIM devices. When replated on Day 16, the HLCs attach and show characteristic morphology and stain positive for hepatic markers, with AAT and HNF4A expression levels being 67.2±13 % and 75±18.32% relative to control HLCs. We also observed ALB secretion was 59±7.8% of controls.
Discussion: Using these conditions, we will establish a multicell culture composed of major liver cells. Establishing hLOC with a sinusoidal barrier will help us develop a drug screening tool in which the biochemical analysis, combined with liver functions (AST, ALT), will help to profile the drugs as low risk, moderate risk, and high risk. By integrating this chip with other tissue chips, such as hTOC, we will potentially develop a tissue specific preclinical drug screening tool.

15th Annual Center for Musculoskeletal Research Symposium
October 30, 2025

Title: Single cell and spatial sequencing reveals cell signaling between chondrocyte types during in vivo murine chondrogenesis.

Presenting Author: Victoria L. Hansen

Co-Author(s): Gulzada Kulzhanova, Yanshi Chen, Eloise M. Fadial, Lauren Benoodt, and Chia-Lung Wu

Lab PI / Mentor: Chia-Lung Wu

ABSTRACT

The developing embryonic knee joint is a site of natural chondrogenesis and endochondral ossification. Gaining a deeper understanding of the cell-cell communication between different chondrocyte types can illuminate novel gene targets for refined in vitro chondrogenesis. The mouse model is ideal for its ease of use and availability of tools. We employed 10x Genomics multiome including both single cells RNA (scRNA-seq) and chromatin accessibility (scATAC-seq) in murine embryonic hind limbs from embryonic days (E) spanning chondrogenesis E13.5, E15.5, and E18.5 (n=8-14 hind limbs per timepoint). Furthermore, we also performed spatial transcriptomics (Spatial-seq) on tissue sections from the same timepoints (n=1 per timepoint) and localized single cells to spatial positions based on transcriptional similarity using the Seurat R package. Single cell clusters were annotated using established gene markers from literature and location they mapped to on Spatial-seq sections. Cell-cell communication between adjacent chondrocyte cell types and signal pathway analysis were assessed using additional R packages CellChat, NicheNet, and clusterProfiler. After performing cell quality control, we identified 28,919 single cells and 16 cell clusters across three timepoints including cell types such as myocytes, osteocytes, neurons, and chondrocytes. Across all timepoints there were 3010 chondrocytes total re-clustered into five subtypes: epiphyseal (n = 848 cells), interzonal (95), perichondrial (1203), pre-hypertrophic (838), and hypertrophic (26) chondrocytes. The proportion of perichondrial and interzonal chondrocytes increased over the course of embryogenesis. Differentially expressed genes (DEGs) were detected between different timepoints within the same chondrocyte subtype. Among the upregulated DEGs, we identified 78 and 16 DEGs in epiphyseal chondrocytes at E15.5 and E18.5, respectively, exhibiting differentially accessible (DA) chromatin peaks. Our results suggest that epigenetic regulation of the accessibility of chromatin regions of these genes is essential in embryonic cartilage development. Though perichondrial, interzonal, and pre-hypertrophic chondrocytes were all adjacent to epiphyseal chondrocytes, the cell-cell communication between them changed over time. Based on NicheNet prioritization analysis, at E15.5 pre-hypertrophic chondrocytes are the predominant cells signaling to epiphyseal chondrocytes. In particular, multiple collagen ligands in pre-hypertrophic chondrocytes signaling to integrin receptors in epiphyseal chondrocytes were in the top 10 ligand-receptor pairs at this timepoint, such as between collagen 9 alpha 2 (Col9a2) and integrin beta 1 (Itgb1). By E18.5, signaling to epiphyseal chondrocytes was relatively equal between perichondrial, interzonal, and pre-hypertrophic chondrocytes. At this later timepoint cell signaling through the syndencan-4 (Sdc4) receptor by ligands such as tenascin X (Tnxb) and pleiotrophin (Ptn) were among the highest priority ligand-receptor pairs. Despite the differences in prioritized ligand-receptor pairs between timepoints, there was overlap in predicted downstream gene targets such as transforming growth factor beta 2 (Tgfb2) and inhibin subunit beta A (Inhba). These targets also had DA peaks in E18.5 epiphyseal chondrocytes confirming their significance in late gestation chondrocyte development. The overlap in downstream signaling targets suggests redundancy in cell-cell communication from different chondrocyte types to epiphyseal ones. Interestingly some genes that seem to be important in natural chondrocyte development like Inhba, have also been implicated in association with osteoarthritis (OA) pathogenesis. Understanding the intricacies of molecular mechanisms behind in vivo chondrogenesis has the potential to illuminate novel targets for chondrogenesis in vitro and cartilage disease therapies.

15th Annual Center for Musculoskeletal Research Symposium
October 30, 2025

Title:	Exploring TRPV4's Mechanosensitivity to Stiffness and Mechanical Loading in Annulus Fibrosus Mechanotransduction
Presenting Author:	Johannes Hasler
Co-Author(s):	Mikkael Lamoca, Gabbie Wagner, Kory Schimmelpfennig, Shuhuan Zhang, Wolfgang Hitzl, Sami Farajollahi, Vinay V. Abhyankar, Christopher L. Lewis, Rui Liu, Karin Wuertz-Kozak
Lab PI / Mentor:	Karin Wuertz-Kozak

ABSTRACT

Low back pain (LBP), the leading cause of disability, is driven by intervertebral disc (IVD) degeneration. The annulus fibrosus (AF) provides structural support to the load bearing IVD and is highly sensitive to mechanical loading. Excessive loading disrupts matrix homeostasis, promotes inflammation, and accelerates degeneration, ultimately leading to stiffening and structural failure. Mechanosensitive transient receptor potential (TRP) channels, particularly TRPV4, sense and respond to stiffening and loading and are implicated in inflammation and pain, yet its role in IVD degeneration remains underexplored. We hypothesize that TRPV4 mediates AF cell responses to substrate stiffness and cyclic loading via Ca^{2+} signaling, thereby driving degeneration related pathways. This study aims (1) to create a stiffness adjustable polydimethylsiloxane (PDMS) based static and dynamic in vitro system, (2) to determine the effect of pharmacological TRPV4 modulation in relation to substrate stiffness, and (3) mechanical loading.

TRPV4 responses to stiffness were studied using (1) PDMS substrates by varying the Sylgard 184 and 527 ratios (0, 14, and 24 wt%), cured (24h, 65°C) and molded into well plates and cell stretching chambers. Young's modulus was obtained using a tensile tester (n=3), and surface strain of the stretching chambers were verified using digital image correlation (n=3). All cell experiments used bovine AF cells. (2) RNA seq was performed after 18-hour TRPV4 activation (2.5 µM GSK101) on each stiffness condition (DESeq2 with adj p-values, n=5). TRPV4 mediated Ca2+ flux was measured using Fura-2 QBT assay with 1 µM GSK101 on different substrate stiffnesses (n=5). (3) Mechanically induced TRPV4 activation was assessed by cyclic stretching in custom stretching chambers (8-12%, 1Hz, 14h, n=3) and was analyzed via RT-qPCR. Shapiro-Wilk test was used for normality assessment and one-way ANOVA was performed in GraphPad Prism.

(1) PDMS substrates were successfully fabricated and integrated into stretching chambers with resulting stiffness of 9, 63, and 240 kPa. Surface strain confirmed effective transmission, with magnitude depending on the stiffness. (2) TRPV4 stimulation, differentially regulated 637 genes, including genes linked to IVD degeneration, inflammation and matrix regulation. Calcium flux showed stiffness dependent intracellular Ca2+ levels, lowest at 9kPa. On the gene expression level, RNA seq revealed some stiffness dependent candidates for further investigations to study mechanical loading and substrate stiffness. However, the broad transcriptional change to stiffness was modest. (3) We demonstrated that cyclic strain activates AF cell gene expression; yet whether these responses are TRPV4 mediated remains to be investigated.

Our in vitro biocompatible PDMS substrate model successfully replicates the increased stiffness during degeneration and allows us to study mechanical loading in combination with substrate stiffness. As hypothesized, the increased stiffness resulted in increased TRPV4 activation, evidenced by enhanced Ca2+ flux, indicating a possible correlation between TRPV4 activation and stiffness-associated AF degeneration. The RNA seq results suggest that intracellular Ca2+ changes due to TRPV4 activation modulate cell behavior, promote catabolism and upregulates inflammatory genes, suggesting a central role of TRPV4 in IVD homeostasis. Although TRPV4 treatment initiated stiffness-dependent Ca2+ responses, downstream analysis at the gene expression level did not confirm a clear response, thereby suggesting that the treatment dominates stiffness effects. Finally, mechanical stretching regulated several genes that have been modulated by pharmacological TRPV4 activation. Ongoing experiments are focusing on the inhibitory effect of GSK219 to support the specificity of mechanical TRPV4 activation. Next, experiments are planned to investigate the combined impact of mechanical loading and substrate stiffness.

15th Annual Center for Musculoskeletal Research Symposium
October 30, 2025

Title: Intravital Imaging of Calcium Network Topology Revealed the Immune-Modulatory Loci in the Bone Marrow

Presenting Author: Cih-Li (Amy) Hong

Co-Author(s): Montgomery L. Whalen, Adam Tyrlik, Laura M. Calvi, Charles P. Lin, Shu-Chi Allison Yeh

Lab PI / Mentor: Dr. Shu-Chi Allison Yeh

ABSTRACT

Introduction: Intercellular communications through calcium signaling orchestrates coordinated cell functions across diverse tissues. Therefore, real time imaging of calcium flux has been a powerful tool to probe highly cooperated cellular activities such as neuronal signal transduction [Kuga, N. et. al., The Journal of Neuroscience, 2011] and endocrine secretion [Beekers, I. et. al., Ultrasound Med Biol, 2020]. Bone marrow stromal cells (BMSCs) form a pervasive 3D network in the marrow and secrete cytokines essential for regulating blood and immune cells formation. Yet, the degree of coordination among the BMSCs in the interconnected network remains poorly understood both in the setting of normal hematopoiesis and in malignancy. We hypothesize that BMSCs utilize calcium waves to achieve coordinated cytokine secretion critical for maintenance of healthy or pathological blood stem cells.

Methods: To address this knowledge gap, we developed an intravital calcium imaging platform using LepR-cre; Salsa6f mice [Zhou, B. O. et. al., Cell Stem Cell, 2014] in which tdTomato and a calcium flux indicator (GCaMP6f) are expressed in BMSCs. The calcium transients (frequency) and amplitude are analyzed per image pixel over time, and packaged into an image processing app to extract the spatiotemporal dynamics of intercellular calcium waves (ICWs), including wave frequency, wave spatial spread, and wave duration. Furthermore, to understand the functional significance of these ICWs in BMSCs, we analyzed transcriptomic profiles of the BMSC subset with upregulated cellular responses to calcium ions. Longitudinal imaging was performed to track chemotaxis behaviors with respect to the calcium network to verify transcriptomic findings. Fluorescently labeled immune cells were segmented automatically based on morphology (3–5 μm, circular) followed by quantifications of cell displacement and directionality via TrackMate in FIJI. Mann-Whitney U test and Spearman's correlation were utilized to determine statistical significance due to the non-parametric data distribution.

Results: Leveraging the imaging platform, we identified a subset of BMSCs that communicate via ICWs and respond to acute inflammation. Notably, their network activities can be disrupted by optically ablating the hub cells that initiate the waves (N =2 mice, n = 3-5 cells) or via pharmaceutical inhibition of gap junctions that transmit calcium ions (Carbenoxolone) (N = 3 mice, n = 15 cavities, p-value = 0.0078). Single cell RNA sequencing suggests that the BMSC subset expresses high level of leukocyte chemoattractant CCL2, a ligand critical for recruitment of CCR2+ leukocytes to the bone marrow. The imaging tracking results revealed that CCR2+ immune cells migrated preferentially toward areas where ICWs had occurred (N = 3 mice, n = 13 cavities of interest, Pearson correlation coefficients, r = 0.6766, p-value = 0.0222).

Discussion: CCL2 has previously been shown to attract malignant cells that suppress normal hematopoiesis and promote tumor growth [Yamazaki, S. et.al., Stem Cell Reports, 2024]. Ongoing work involves transplanting normal and leukemic blood stem cells to determine whether ICW-induced CCR2+ cell recruitment favors selection of cancerous clones. To further obtain mechanistic insight, we plan to perform these experiments in LepRcreER; Cx43 floxed mice in which gap junctions are deleted from the BMSC lineages. Additionally, given that CCL2/CCR2 antagonists have been used in clinical trials for autoimmune and cancer applications [Pozzi, S. & Satchi-Fainaro, R. Adv Drug Deliv Rev, 2024]], we also aim to evaluate how such treatments affect blood regeneration and malignancies. Overall, although the localized inflammation-modulatory cytokines are technically challenged to measure, our intravital imaging toolbox uncovered previously unrecognized hot spots of inflammation defined by a subset of BMSCs with ICW activity and potential ways of intervention.

Over-expression of Deubiquitinase OTUD7b contributes to Age-related Osteoporosis by inhibiting bone formation

Background and Hypothesis: Osteoporosis, one of the leading age-related diseases, is characterized by reduced bone mass and strength as well as an increased risk of fractures. Age-related osteoporosis (AROP) is characterized by low bone turnover, with both formation and resorption being suppressed. Antiresorptives are standard therapy for AROP. However, bone resorption is naturally reduced in AROP, which may interpret why anti-resorptive therapy remains unsatisfactory in reducing fracture rate in AROP. Anabolic drug provide transient benefits that can only be maintained by antiresorptives. So, it is essential to further investigate novel mechanisms causing bone loss in order to develop new classes of drugs for long-term treatment of AROP. Deubiquitinases (DUBs) remove ubiquitin from substrate proteins, thereby preventing their degradation by ubiquitination. OTUD7b, a DUB, binds and deubiquitinates TRAF3 to prevent its degradation and subsequent aberrant non-canonical NF-κB activation in B lymphocytes. However, it remains unclear whether OTUD7b is involved in the development of AROP. We found that OTUD7b protein levels were significantly increased in the cortical bone of aged mice and therefore hypothesize that OTUD7b inhibits bone formation and thus contributes to AROP.
Experiments & Methods: Western blotting was performed to measure protein levels. OTUD7B activity was analyzed using a DUB fluorometry assay kit. To investigate the OTUD7b function on bone formation and AROP, we generated mice with OTUD7b-loxP knockin in Rosa26 gene, which were crossed with osteocalcin-Cre (OCN-Cre) to generate OTUD7b-over-expression mice specifically in osteoblasts. Identify small molecular compound that inhibit OTUD7b activity for the treatment of osteoporosis in vivo. Bone mass was analyzed by micro-CT using a vivaCT 40 device focusing on a 1 mm section of trabecular bone in both tibia and vertebrae. H&E staining were performed blindly to measure the trabecular osteoblast differentiation. Statistical analyzes were performed using a one-way ANOVA, with $p < 0.05$ considered significant.
Results: We found that the activity and protein levels of OTUD7b were significantly increased in cortical bone samples from aged (22-months) mice compared to young (3-months) controls. Micro-CT analysis indicated that conditional knock-in of OTUD7b in osteoblast lineage cells ($OTUD7b^{Tg\text{-}OB}$) resulted in significantly reduced trabecular bone mass in vertebrae at 14-months-old but not at 6-month-old compared to their WT littermate mice. Consistent with this, osteoblast surface on the trabecular surface was reduced in OTUD7b overexpression mice, osteoblast differentiation potential of the bone marrow stromal cells and pure mesenchymal progenitor cells from OTUD7b-expressing mice were significantly reduced compared to that from littermate control mice. In contrast, TRAP-positive osteoclasts on the trabecular surface from vertebral bone of OTUD7b knock-in mice was not changed compared to that from littermate mice. Mechanistically, OTUD7B is regulated in a dual manner by ubiquitination and phosphorylation. Tumor necrosis factor-alpha (TNF-α), a multifunctional cytokine, increases OTUD7b expression. 4H-isoquinoline-1,3-dione (IQD) was originally identified as a NIK inhibitor. However, it showed no inhibitory effect on NIK activity in our experiments. In contrast, IQD reduced OTUD7b activity and OTUD7b levels through the ubiquitin-proteasomal system (UPS). Interestingly, IQD stimulated osteoblast differentiation from bone marrow stromal cells and pure MSCs. In vivo results showed that IQD

treatment at 1 and 3 mg/kg increased trabecular bone mass in both the tibia and vertebrae in the ovariectomy osteoporosis model.
Discussion and conclusions: Accumulation of OTUD7b in bone inhibits bone formation during aging and thus contributes to AROP. We conclude that pharmacologic inhibition of OTUD7b would be a promising therapeutic strategy to restore bone formation and combat AROP.

15th Annual Center for Musculoskeletal Research Symposium
October 30, 2025

Title: Diabetes Mellitus is Associated with Increased Rates of Surgical Site Infection and Need for Antibiotics following Arthroscopic Rotator Cuff Repair: a Study of 73,178 Patients

Presenting Author: Sameer Jain, BS

Co-Author(s): Nicholas Morriss, MD; Michaela Malin, BA; Omkar Prabhavalkar, BA; Christopher Dussik, MD; Brett Salazar, MD; Patrick Castle, MD; Sandeep Mannava, MD PhD

Lab PI / Mentor: Sandeep Mannava, MD PhD

ABSTRACT

Intro

Arthroscopic rotator cuff repair (aRCR) is a surgery with high rates of satisfaction and functional improvement. As aRCR utilization rises, it is essential to identify modifiable factors that impact patient outcomes. Diabetes mellitus (DM) is a known risk for post-operative infection, particularly at higher hemoglobin A1c (HbA1c) levels. This study aims to identify the impact of DM and elevated HbA1c on post-operative infection following aRCR. We hypothesized that DM would increase the risk of operative debridement (OD) and surgical site infection (SSI) and elevated HbA1c levels would also correlate with increased risk.

Methods

The TriNetX Research Network was used to identify patients who underwent aRCR between August 2005 and August 2025 using the CPT code 29827. Patients were filtered into Type 1 DM (T1DM) and Type 2 DM (T2DM) cohorts using ICD-10 codes E10 and E11 respectively. Separately, all diabetic patients were stratified into cohorts based on peri-operative HbA1c levels: <5.5%, 5.5-6.9%, 7-8%, > 8%. Patients were included if HbA1c was measured within 6 months prior to surgery. Control cohorts of non-diabetic patients were generated through 1:1 propensity score matching (caliper 0.1) to adjust for demographics and comorbidities. OD and SSI incidence were measured as primary outcomes at 60 days, 1, 2, and 5 years after aRCR. Risk analysis with odds ratio and 95% confidence intervals was performed. Significance level was set to $\alpha = 0.05$.

Results

Both T1DM and T2DM patients had a significantly higher risk of SSI within 60 days of aRCR than non-diabetics (T1DM $p = 0.0043$; T2DM $p = 0.0038$).

Compared to non-diabetics, T1DM patients were more likely to undergo OD ($p \leq 0.004$) and had increased risk of SSI ($p < 0.0001$) within 1, 2, and 5 years of aRCR.

T2DM patients were more likely to undergo OD within 5 years of aRCR ($p = 0.0069$) compared to non-diabetics. They also had an increased risk of SSI within 1, 2, and 5 years of aRCR ($p < 0.0001$).

DM patients with an A1c of 5.5–6.9% had a higher risk of OD within 60 days of aRCR compared to non-diabetics ($p = 0.0223$).

DM patients with A1c < 5.5% had a higher risk of SSI at 1, 2, and 5 years ($p \leq 0.02$) compared to non-diabetics. Those with A1c 5.5–6.9% had increased risk of OD ($p \leq 0.0265$) at all time points and SSI ($p \leq 0.0122$) at 1, 2, and 5 years. Patients with A1c 7–8% had increased SSI risk at 5 years ($p = 0.0005$). Those with A1c > 8% had a higher OD risk at 1 and 5 years ($p \leq 0.0223$) and higher SSI risk at 1, 2, and 5 years ($p \leq 0.0015$).

Discussion

In this study, DM was associated with increased rates of both SSI and OD. The effect was most pronounced in T1DM with increased risk of SSI at all time points and higher OD risk as early as 1 year postoperatively. T2DM was also linked to increased SSI risk at all time points with a modestly significant association with OD in the long term. Higher glycemic levels were correlated with greater complication rates. Patients with HbA1c >8% demonstrated the highest odds ratios for SSI and OD, with effects lasting up to 5 years. Even patients with well-controlled diabetes (HbA1c <5.5%) showed increased risk of certain outcomes which suggests that DM-related factors beyond glycemic control, such as microvascular compromise or impaired host immune response, may contribute to poor wound healing and tendon integrity.

These findings underscore the importance of optimizing perioperative metabolic control in DM patients following aRCR. While aggressive glycemic control may mitigate some risk, residual elevated complication rates suggest that preoperative counseling, vigilant postoperative surveillance, and potentially tailored rehab protocols are warranted for this population. Future prospective work should clarify whether intensive perioperative glucose management, targeted infection prophylaxis, or biologic augmentation strategies can meaningfully reduce these complications in diabetic patients undergoing RCR.

15th Annual Center for Musculoskeletal Research Symposium
October 30, 2025

Title: Corticosteroid Injections as Early as 12 Months Pre-Op Increases Risk of Subsequent Shoulder Surgery after Rotator Cuff Repair: A Database Study of 79,582 patients.

Presenting Author: Sameer Jain

Co-Author(s): Sameer Jain, BS; Nicholas Morriss, MD; Michaela Malin, BA; Omkar Prabhavalkar, BA; Christopher Dussik, MD; Brett Salazar, MD; Patrick Castle, MD; Sandeep Mannava, MD PhD

Lab PI / Mentor: Sandeep Mannava MD PhD

ABSTRACT

Introduction: Rotator cuff tears (RCT) are a highly prevalent injury with nonoperative and operative treatment options. Intra-articular corticosteroid injections (CI) are useful for symptom management in RCT. Surgically, rotator cuff repair (RCR) is largely successful, but concerns exist regarding the impact of CI on postoperative healing and failure rates. This study evaluates the impact of pre-operative CI on the risk of repeat shoulder surgery in patients undergoing RCR patients. We hypothesize that preoperative CI will increase the likelihood of subsequent shoulder surgery as well as arthroplasty.

Methods: This retrospective cohort study used the TriNetX database. Adult patients who underwent RCR between August 2006 and August 2020 were identified using CPT codes 23412, 29827, 23420, and 23410. CI was identified using CPT codes 20610 and 20611 in patients with an existing rotator cuff tear diagnosis (ICD M75.1) at the time of injection. Two treatment cohorts were defined: (1) CI < 6 months prior to RCR, and (2) CI 6-12 months prior to RCR. These were matched with cohorts who did not receive CI within 6 months and 12 months respectively. Propensity score matching (1:1, caliper 0.1) was performed to control for confounding demographic and medical comorbidities. After matching, 79,582 patients were included in the study. The 6-month treatment and control cohorts had 35,428 patients each and the 6-12 treatment and 12-month control cohorts had 4,363 each. The primary outcome was subsequent shoulder surgery – revision RCR, total shoulder arthroplasty (TSA), debridement, biceps tenodesis (BT), labrum repair, subacromial decompression (SD), lysis of adhesions (LOA), or manipulation under anesthesia (MUA) – at 6 months, 1 year, 3 years, and 5 years. Risk analysis with odds ratio and 95% confidence intervals was performed with a significance level set to $\alpha = 0.05$.

Results: Patients who received at least 1 CI within 6 months prior to index RCR surgery had a significantly higher likelihood of subsequent RCR ($p < 0.0001$), debridement ($p < 0.0001$), BT ($p < 0.0001$), SD ($p < 0.0001$), and LOA ($p = 0.009$, $p < 0.0001$) within 6 months, 1 year, 3 years, and 5 years when compared to control. They also had a significantly higher likelihood of TSA within 1, 3, and 5 yrs ($p = 0.005$, $p < 0.0001$, $p < 0.0001$) and increased likelihood of Labrum Repair within 3 and 5 yrs ($p = 0.001$, $p < 0.0001$).

Patients who received at least 1 CI between 6-12 months prior to index RCR surgery had a significantly higher likelihood of subsequent debridement ($p = 0.001$, $p = 0.001$, $p = 0.002$, $p < 0.0001$), BT ($p < 0.0001$, $p = 0.012$, $p = 0.028$, 0.015), and SD ($p < 0.0001$, $p = 0.005$, $p = 0.002$, 0.001) within 6 months, 1 yr, 3 yrs, and 5 yrs when compared control. 6–12-month CI patients had an increased likelihood of subsequent RCR within 6 months ($p = 0.045$) and 5 years ($p = 0.027$).

Discussion: This study demonstrates a significant association between pre-operative corticosteroid injections (CIs) and increased risk of subsequent shoulder surgeries following RCR. Patients who received CIs within 6 months prior to surgery exhibited significantly higher rates of arthroscopic shoulder surgery and shoulder arthroplasty. Though more limited, patients who received CIs as early as between 6-12 months preoperatively also had increased rates of revision RCR, debridement, BT, and SD. These results may indicate that corticosteroids have a subtle but significant effect on tendon healing in RCR. Corticosteroids are known to impair collagen synthesis, reduce tenocyte proliferation, and contribute to local tissue atrophy, all of which may compromise tendon integrity and repair durability. The present study suggests that these effects may be present in RCR patients in broader preoperative windows than previously recognized. Future work should explore the exact time dependent relationship, effect of CI frequency, type of corticosteroid, and details of RC pathology and repair most at risk.

15th Annual Center for Musculoskeletal Research Symposium
October 30, 2025

Title:	Cyclical Physiological Strain Blunts TGF-β Induced Myofibroblast Activation in a Human Tendon-on-a-Chip
Presenting Author:	Kyle Jerreld
Co-Author(s):	Hayley Miller
Lab PI / Mentor:	Hani Awad

ABSTRACT

Introduction: We previously engineered a human tendon-on-a-chip (hToC) featuring fibroblast-laden collagen hydrogels and a vascular flow channel separated by an ultrathin nanomembrane. While this system recapitulated aspects of tendon fibrosis driven by TGF-β, the rigid architecture did not allow cyclic loading, a critical limitation since passive-controlled motion therapy is widely regarded as the most effective intervention to mitigate peritendinous adhesions after flexor tendon repair, with mechanisms that remain debated. TGF-β is known to be a key regulator of the transitioning of fibroblasts to a diseased myofibroblast state. These myofibroblasts are the primary mediators of fibrotic scarring and are known to secrete excessive amounts of collagen and other ECM components that lead to abnormal tissue stiffness and function. To elucidate the mechanobiology of fibrosis in tendon, we developed a stretchable hToC (stretchToC) that can be leveraged to directly interrogate the changes in the diseased phenotypes of fibroblast laden collagen hydrogels. We hypothesize that physiological strain (4%) will ameliorate fibrosis by blunting TGF-β induced myofibroblast activation and adhesion-like remodeling within the construct.

Methods: stretchToC devices were fabricated from PDMS as a monolith consisting of 6 arrayed wells, each containing two pillars between which fibroblast-laden hydrogels are tethered. Flanking the wells on either end are continuous vacuum chambers that connect via tubing to a vacuum pump, allowing the PDMS to be actuated. A calibration curve relating the vacuum pressure applied and the resultant axial strain was established by tracking the pillar deflections in videos using MATLAB . Collagen hydrogels (~3mg/mL) were seeded with 500,000 cells/mL of tenocytes, derived from tenolysis surgical tissue waste. The hydrogels are then cultured for 7 days with or without TGF-β (10 ng/mL) and with or without daily cyclical physiological strain (4% strain, T = 10 sec, 1 hour duration). Contraction percentages were determined by tracing the outline of the well and the hydrogels in FIJI. After 7 days the hydrogels were fixed and stained for nuclei, F-actin, and alpha-smooth muscle actin (α-SMA). Immunofluorescent images were captured on a spinning-disc confocal microscope and the number of, and intensity of α-SMA+ cells was determined using Imaris.

Results: A univariate regression model established the relationship between the applied negative pressure and hydrogel axial strain, yielding a linear calibration between 0 and –400 mbar, corresponding to 0–4% strain. Contraction of the hydrogels was significantly increased by TGF-β treatment but attenuated by strain. Static hydrogels contracted by 28.9% (-TGF-β) and 40.7% (+TGF-β), whereas strained hydrogels by 11.0% (-TGF-β) and 26.5% (+TGF-β). The proportion and fluorescence intensity of cells expressing α-SMA was increased by TGF-β, but the application of cyclic 4% strain reduced the α-SMA staining intensity.

Discussion: Our findings support the hypothesis that cyclical mechanical strain exerts a protective effect against tissue fibrosis. The current model does not yet incorporate all the cellular and molecular components of the myofibroblast microenvironment (MME), including resident and infiltrating macrophages and the pathologic vasculature linked to fibrotic and inflammatory states. Future versions of the stretchToC will incorporate the crosstalk between these cellular components to enable a more comprehensive investigation of the impact of mechanical strain on the MME. Ultimately, these studies could provide a mechanistic understanding of the well-documented clinical benefits of physical therapy after tendon injury.

15th Annual Center for Musculoskeletal Research Symposium
October 30, 2025

Title: Characterizing isolated Prx1+ mouse bone-marrow-derived stromal cells (BMSCs) in different culture methods to study skeletal aging

Presenting Author: Xingyu Jing

Co-Author(s):

Lab PI / Mentor: Roman Eliseev

ABSTRACT

Background & Hypothesis: Skeletal abnormalities and bone fracture are prevalent in the aged population. Impaired functions of bone marrow stromal/stem cells (BMSCs) are closely associated with age-related loss of regenerative capacity. BMSCs are multipotent cells that can differentiate into bone-forming osteoblasts (OB), marrow adipocytes, or chondrocytes. Asymmetric division of somatic stem cells is important for maintaining their pool and at the same time supplying new mature cells for tissue maintenance. This process is disrupted in aging. In addition, OB dysfunction caused by metabolic changes and oxidative stgress in aged bone lead to decreased bone formation. Prior to the investigation of the above research questions, a standardized in vitro culture system should be consistently employed to ensure reliable results. Despite decades of previously published research, such in vitro system is still not optimal. Therefore, two different culture conditions are compared to establish a universal methodology for expanding BMSCs in vitro.

Experiments & Methods: The BMSC-specific paired-related homeobox protein 1 (Prx1) Cre-driven Ai9 (tdTomato fluorescent lineage tracer) mouse model was used to compare two different culture systems. Males at the age of 3-6 months were euthanized to isolate BMSCs. Isolated cells were either subjected to magnetic depletion of hematopoietic stem cells (HSCs) (CD45+) and endothelial cells (CD31+), and cultured on collagen I-coated plates (Modified) or directly cultured on the regular plates (Regular). Flow cytometry was performed to characterize the cell populations. Cells were incubated with EdU for 24h to asess the proliferation rate. Qualitative method such as histological staining and quantative analysis such as qPCR were conducted to visualize the outcome of differentiation and to evaluate the regulation of the genes related to multilineage differentiation respectively. Data was analyzed with either t-test or two-way ANOVA using GraphPad.

Results: We found that BMSCs are Prx1 positive and these Prx1+ BMSCs are capable of differentiating and proliferating in vitro. Cells cultured with modified method presented greater osteogenic and adipogenic but not chondrogenic potential, compared to those cultured via regular method. In addition, the modified method resulted in a greater proliferation rate and lower contamination with non-mesenchymal cell populations.

Discussion & Conclusion: Our study verified the Prx1+ cells in the isolated BMSCs from the mouse bone marrow. Two different culture systems were examined to determine a way to culture the BMSCs in vitro, in which the cells can better maintain their characteristic as that functioning in vivo. We found that the cells cultured on the Collagen I reserved a higher potency in adipogenesis and osteogenesis, but not chondrogenesis. Conversely, the cells cultured on the regular plastic dish tended to undergo robust chondrogenesis. Considering our research interest on the energy metabolism of BMSCs during aging, especially the pentose phosphate pathway in osteoblasts, the modified method is more beneficial for us.

15th Annual Center for Musculoskeletal Research Symposium
October 30, 2025

Title: Investigating the Role of Telocytes in Recruiting Mast Cells via Chemokine Expression

Presenting Author: Andriy Kobryn, MD

Co-Author(s): Yue Peng, H. Mark Kenney, Karen L de Mesy Bentley

Lab PI / Mentor: Edward M. Schwarz

ABSTRACT

Background: Lymphatic dysfunction has been shown to play a critical role in rheumatoid arthritis (RA), contributing to joint inflammation, erosive changes, and disease flares. Recently, a previously unrecognized peri-lymphatic cell population marked by Efhd1 expression was identified through single-cell RNA sequencing (scRNA-seq) of popliteal lymphatic vessels (PLVs). This unique stromal cell population, termed telocytes, are markedly reduced in RA synovium, and their in vivo depletion impairs lymphatic function, suggesting a potential role in disease pathogenesis. Mast cells are also implicated in RA as evidenced by their accumulation in diseased synovial tissue and are potent regulators of lymphatic muscle cell contractility. Transmission electron microscopy and three-dimensional confocal imaging of PLVs demonstrated direct contact between telocytes and mast cells suggesting functional crosstalk between cell types in regulating lymphatic function. We hypothesized that resident telocytes secrete soluble mediators that recruit mast cells to lymphatic vessels.

Methods: Using previous scRNA-seq data of PLVs, established mast cell chemoattractants were queried to identify expression levels within Efhd1+ telocytes. Functional transwell migration assays were conducted using P815 murine mastocytoma cell line and 24-well plates with 8-μm pore polycarbonate inserts. Primary cultures of FACS purified Efhd1-tdT+ cells obtained from a transgenic mouse model were grown to 100% confluency with supernatant being collected to be used the conditioned media. Starved P815 mast cells (1 × 10^5 in 200 μL serum-free media) were seeded into the upper chamber following a 2-hour serum deprivation period. The lower chamber contained 600 μL of serum-free media, complete media with 10% FBS, recombinant murine Ccl11 (10 ng/mL) as a positive control, telocyte-conditioned media, or telocyte-conditioned media and anti-Ccl11 monoclonal antibody. After 8 and 24 hours of incubation at 37 °C, migrated cells were harvested from the lower chamber and counted via automated hemocytometer.

Results: Several candidate chemoattractants, including Ccl11, PGE2, and Kitl, were identified to be expressed by Efhd1+ telocytes. Mast cells exhibited robust chemotaxis toward recombinant Ccl11, confirming assay responsiveness. Importantly, mast cells also migrated toward telocyte-conditioned media, consistent with the presence of secreted chemoattractants. Negligible migration was observed toward serum-free media, indicating minimal basal motility. While statistical significance was not achieved in these preliminary assays, there was a trend towards higher absolute number of mast cells migrated towards telocyte-conditioned media versus other groups. Anti-Ccl11 blockade did not appear to reduce mast cell migration towards telocyte-conditioned media.

Conclusions: These findings provide functional evidence that telocytes contribute to mast cell recruitment by releasing soluble mediators. Future studies will refine experimental parameters, including shorter incubation periods, use of other chemoattractants and their respective blockades, and the use of bone marrow–derived primary mast cells to enhance physiological relevance. Elucidating the molecular mediators governing telocyte–mast cell interactions may reveal novel pathways underlying RA pathogenesis and identify potential therapeutic targets to restore lymphatic function and mitigate disease progression.

15th Annual Center for Musculoskeletal Research Symposium
October 30, 2025

Title: Dissecting TIM-3-Mediated Immunoregulation in Staphylococcus aureus Osteomyelitis

Presenting Author: Chloe Kraft

Co-Author(s):

Lab PI / Mentor: Muthukrishnan

ABSTRACT

Background: Osteomyelitis is a devastating complication of orthopedic surgery, occurring in 1–2% of cases, and is often caused by methicillin-resistant Staphylococcus aureus (MRSA). In chronic osteomyelitis, the immune cell landscape is altered to an immuno-suppressive phenotype. My lab's studies in humanized mice have discovered that bone infections are characterized by an increased bacterial load, bone osteolysis, and compromised T cell function. Notably, we found that the exhaustion-associated immune checkpoint protein TIM-3 was highly predictive of adverse outcomes in patients undergoing revision surgery. While classically linked to T cell exhaustion, TIM-3 expression has recently been associated with exerting immunoregulatory effects on innate immune cells. I am investigating the role of TIM-3-mediated immunoregulation in chronic MRSA osteomyelitis, where I hypothesize that sustained TIM-3 expression drives immunosuppression in both T cells and innate immune cells, thereby facilitating bacterial persistence. In contrast, TIM-3 deficiency may enhance innate immune activation, ultimately leading to improved bacterial clearance.

Methods: I compared male and female control mice (Havcr2fl/fl, n = 19) with global TIM-3 knockout (KO) (Havcr2-/-, n = 14), TIM-3 conditional knockout (cKO) in a broad myeloid cell compartment (Havcr2fl/fl x Cx3Cr1cre, n = 10), and TIM-3 cKO in dendritic cells (Havcr2fl/fl x CD11ccre, n = 14). To model implant associated osteomyelitis, pins inoculated with USA300 LAC:lux (bioluminescent MRSA strain) were inserted transtibially. Mice were sacrificed on day 14 for flow cytometry (bone marrow, spleen), immunohistochemistry for bone pathology, and colony forming unit quantifications for bacterial burden (soft tissue, bone, pin).

Results: TIM-3 global KO showed trending lower bacterial burden in soft tissue and bone, and significantly lower pin CFUs ($p = 0.043$), whereas both TIM-3 cKO strains showed no significant reduction in bacterial burden. Brown-Brenn staining demonstrated high staphylococcal abscess community (SAC) formation in control mice, with variable SAC formation in TIM-3 cKO strains. Notably, flow cytometry analysis of bone marrow cells revealed cellular changes in all TIM-3 knockout strains. In TIM-3 global KO mice, there were significant increases in proliferation (Ki-67+) of multiple immune cell subsets (T cells, macrophages, dendritic cells, natural killer cells), indicative of a lack of cellular exhaustion. Infected control mice exhibited further signs of T cell exhaustion, as evidenced by significantly higher levels of PD-1+TIM-3+ on CD3+ ($p = 0.020$) and CD4+ ($p = 0.042$) T cell subsets compared to sterile control mice. Increases in antigen presentation (MHC-II+) were observed in the myeloid TIM-3 cKO strain, indicative of cell activation and immune cell priming.

Discussion: Genetic disruption of TIM-3 signaling enhanced immune responses during bone infection by boosting immune cell proliferation, diminishing features of T cell exhaustion, and increasing antigen presentation. The observed increase in proliferation and reduction in immune checkpoint protein expression (PD-1+TIM-3+) in the TIM-3 global KO suggest an amelioration of T cell exhaustion, which may improve adaptive immune function and facilitate bacterial clearance. Future studies in a T cell-specific TIM-3 cKO model (Havcr2fl/fl x CD4cre) with detailed characterization of T cell transcriptional programming and functional profiling will be essential to define the precise role of TIM-3 in T cell exhaustion during MRSA bone infection. Additionally, inhibiting TIM-3 with a neutralizing monoclonal antibody during infection could establish its potential as an immunotherapeutic strategy for chronic bone infections.

15th Annual Center for Musculoskeletal Research Symposium
October 30, 2025

Title: Transcriptomic Profiling and Human Tissue-on-Chip Modeling of Synoviocyte-Chondrocyte Crosstalk in Femoroacetabular Impingement and Hip Osteoarthritis

Presenting Author: Gulzada Kulzhanova

Co-Author(s): Gulzada Kulzhanova, Alexis Klee, Mina Botros, Victoria L. Hansen, John Reuter, Eliya Tazreena Tashbib, Eloise Fadial, Benjamin Ricciardi, Brian Giordano, Chia-Lung Wu

Lab PI / Mentor: Dr. Chia-Lung Wu

ABSTRACT

Introduction: Hip osteoarthritis (OA) affects one in four people by the age of 85, and it is linked to abnormal hip morphology, including Cam-type femoroacetabular impingement (FAI), a condition of osseous protrusion from the femoral head-neck junction that impinges on the acetabulum. Thus, FAI patients may exhibit labral tears and cartilage delamination, gradually leading to the development of hip OA (secondary to FAI). Therefore, FAI has been considered a unique early-phase hip OA model for studying regulators implicated in disease progression. Furthermore, while OA is multifactorial, recent evidence suggests that synovial inflammation could be a major driving force of disease onset. Here, we hypothesize that FAI and hip OA synovial cells exhibit distinct transcriptomes and altered synovial cell-cell interactions. We aim to identify the mechanisms underlying hip OA pathogenesis from FAI by integrating innovative single-cell RNA sequencing (scRNA-seq) and spatial transcriptomics (Spatial-seq) approaches.

Methods: Human hip synovium was harvested from patients with Cam FAI or hip OA according to approved IRB protocols. 6 FAI (n=3 per sex) and 6 OA (n=3 per sex) samples were submitted to UR GRC for scRNA-seq and Spatial-seq. Distinct cell populations were annotated based on unbiased clustering and differentially expressed genes. The cells were then mapped to Spatial-seq datasets to visualize their spatial locations and determine potential cell-cell interactions. Cell-cell crosstalk and downstream activated genes were identified by MultiNicheNet R package. Functional analysis of cell subsets was determined by Gene Ontology (GO) enrichment. The bioinformatic results were further validated using immunofluorescent (IF) staining.

Results and Discussion: Fibroblast-like-synoviocytes (FLS), endothelial cells, mural cells, myeloid cells, NK cells, T cells, and mast cells were conserved populations in both FAI and hip OA synovium. Further sub-clustering of CD45+CD14+ myeloid cells yielded 5 distinct cell types: pro-inflammatory macrophages (MΦ), anti-inflammatory MΦ, fibrotic MΦ, monocytes, and dendritic cells. Re-clustering CD45- non-hematopoietic cells resulted in 6 different cell groups: lining, sublining, and transitional FLS as well as endothelial cells, mural cells, and fibrotic chondrocytes. Compared to FAI, epiregulin (EREG)-enriched lining synovial FLS were significantly increased in hip OA. Importantly, our datasets, when compared to publicly available RA and knee OA synovial datasets, have increased expression of EREG, which could serve as a unique biomarker for hip OA synovium. Furthermore, these EREG+ FLS are pro-inflammatory due to elevated expression of CXCL1, IL8, and MMPs. Pseudotime analysis predicts that EREG+ FLS could be derived from DPP4+PI16+ sublining FLS, likely regulated by NIFX and REL, as well as ELK3 and ETV6 transcription factors under FAI or OA conditions, respectively. Importantly, integrative analysis of scRNA-seq and Spatial-seq analyses revealed that COL1A1+IGFBP5+ fibrotic MΦ and EREG+ FLS were mapped adjacent to each other. Furthermore, MultiNicheNet predicted that fibroblast growth factor 2 (FGF2) – syndecan 4 (SDC4) communication is a significant cell-cell interaction between COL1A1+IGFBP5+ fibrotic MΦ and EREG+ FLS. This interaction may induce expression of IL6, IL8, MMP1, and PTGS2 in hip OA synovium. The gene ontology (GO) analysis of activated genes downstream of FGF2-SDC4 signaling revealed that inflammation and angiogenesis could be upregulated in hip OA, while positive gene transcription and skeletal muscle differentiation were dominant in FAI.

Conclusion: In summary, we identified dynamic changes in synovial cell populations and cell-cell crosstalk during disease progression (i.e., FAI vs. hip OA). Most importantly, our results suggest that targeting distinct signaling molecules at different disease stages may be required to prevent hip OA progression from FAI.

15th Annual Center for Musculoskeletal Research Symposium
October 30, 2025

Title:	Antidepressant Use and Risk of Reoperation After Wrist Fracture Fixation
Presenting Author:	Firdavs Kurbanov BS
Co-Author(s):	Christopher Dussik MD, Amy Phan MD, Zion Rouege BS, Constantinos Ketonis MD PhD
Lab PI / Mentor:	Constantinos Ketonis MD PhD

ABSTRACT

Background & Hypothesis:
Distal radius and scaphoid fractures are common, and a minority of patients require reoperation for nonunion or mechanical failure. Selective serotonin reuptake inhibitors (SSRIs) are widely prescribed and have biologic plausibility for impairing bone healing. We examined whether SSRIs and, separately, other antidepressants were associated with unplanned return to the operating room (RTOR) after open reduction and internal fixation (ORIF) of distal-radius or scaphoid fractures.
Experiments & Methods:
We performed a retrospective, multi-institution cohort study using the federated electronic health-record network. Eligible adults had an ICD-10 diagnosis of distal radius or scaphoid fracture and underwent ORIF within 14 days. The ORIF date defined time zero or index event. Patients were assigned to mutually exclusive exposure groups in the 180-day pre-index event window: SSRI users (Arm A), other-antidepressant users (Arm B: SNRIs, bupropion, mirtazapine, or tricyclics), and non-users (Arm C). We grouped SNRIs, bupropion, mirtazapine, and tricyclics into a pragmatic "other-antidepressant" (Arm B) cohort to reflect common non-SSRIs, preserve power for a low-frequency endpoint, and assess whether any association extends beyond SSRI-specific serotonergic effects. For the two prespecified comparisons (Arm A vs Arm C and Arm B vs Arm C), we applied 1:1 greedy nearest-neighbor propensity-score matching (caliper 0.10) to balance baseline characteristics between cohorts. The primary outcome was any unplanned RTOR 30–365 days after index ORIF, which was defined as nonunion repair or repeat fixation. The outcome was identified by procedure codes for scaphoid nonunion repair and forearm non/malunion repair or repeat distal-radius/scaphoid ORIF. We estimated absolute risks, risk differences (ARD), risk ratios (RR), and Cox hazard ratios (HRs) with 95% CIs.
Results:
After matching, SSRI versus non-user analysis included 2,247 per arm and unplanned RTOR occurred in 36 (1.6%) SSRI users versus 12 non-users (0.5%): ARD +1.1% (95% CI 0.5–1.7); RR 3.00 (95% CI 1.57–5.75); adjusted hazard ratio (HR) 2.65 (95% CI 1.38–5.09). Other-antidepressant versus non-user analysis included 3,217 per arm and RTOR occurred in 57 other-antidepressant users (1.8%) versus 14 non-users (0.4%): ARD +1.3% (95% CI 0.8–1.8); RR 4.07 (95% CI 2.27–7.29); HR 3.73 (95% CI 2.08–6.70).
Discussion & Conclusions:
In two separately matched, class-specific analyses, both SSRI and other-antidepressant exposure were associated with higher 1-year unplanned RTOR after distal radius or scaphoid ORIF, with clinically relevant absolute risk increases. These results extend prior biologic and epidemiologic signals by demonstrating a postoperative, healing-related endpoint in a large, real-world network. Practically, antidepressant exposure merits inclusion in preoperative counseling and postoperative surveillance, ideally in coordination with the prescribing clinician rather than routine discontinuation. Prospective work should test whether risk varies by antidepressant class, dose/duration, and modifiable bone-health factors, and evaluate strategies to mitigate failure risk in patients who benefit from ongoing therapy.

15th Annual Center for Musculoskeletal Research Symposium
October 30, 2025

Title:	Range of Motion Outcomes after Primary Flexor Tendon Repair when Evaluating for Patient, Injury, and Surgery Specific Factors
Presenting Author:	Richard Lander
Co-Author(s):	Richard D. Lander, M.D., Andrew Rodenhouse, M.D., Akhil Dondapati, M.D., Thomas Carroll, M.D., Constantinous Ketonis, M.D., Ph.D.
Lab PI / Mentor:	Dr. Ketonis

ABSTRACT

Background

Flexor tendon injuries are serious and potentially debilitating, with an incidence of 33.2 per 100,000 person-years. Despite their frequency, there is a paucity of literature examining patient-, injury-, and surgery-specific variables associated with primary flexor tendon repair across all flexor zones, particularly with regard to range of motion outcomes.

Methods

A retrospective review of patients 18 years of age or older who underwent primary flexor tendon repair between January 1, 2015 and October 1, 2023 was performed. Primary outcomes included total active motion (TAM) defined by the American Society for Surgery of the Hand (ASSH) at the 6 and 12 weeks post-operatively. Descriptive statistics were evaluated along with logistic and linear regression models.

Results

There was 397 patients with 523 injured digits included in our study. Average age of the study population was 39.7 years (SD: 16.1) with 281 (70.8%) patients being male. Laceration-type mechanism was most common (74.8%), followed by sawblade (18.1%) and crush (4.5%) injury. Advanced age, sex, race, body mass index, insurance type, area of deprivation index were patient-specific factors that influenced outcomes (Table 1). Injury-specific factors that significantly influenced postoperative ASSH TAM included the affected digit, zone of injury, and presence of concurrent injuries. At 12 weeks, ring and small finger injuries had impaired functional outcomes when compared to the reference (index fingers) with 19.1 and 23.6 degrees less TAM, respectively. Zone 1 digits had improved functional outcomes when compared to the reference (Zone 2) at both 6 and 12 weeks with 47.0 and 33.2 degrees more TAM, respectively. The presence of a concurrent injury was also predictive of functional outcomes as a concurrent fracture resulted in 36.6 degrees less TAM at 6 weeks whereas a concurrent digital nerve injury resulted in 18.8 degrees less TAM at 12 weeks (Table 2). No patient- or surgery-specific variables were found to be significant predictors of ASSH TAM outcomes in our cohort.

Conclusion

In our study there were injury specific factors which included digit affected, zone of injury, and concurrent injury. that predicted ASSH TAM outcomes after primary flexor tendon repair. This study allows to help manage and counsel patients on risk factors and expectations after primary flexor tendon repair.

15th Annual Center for Musculoskeletal Research Symposium
October 30, 2025

Title:	Patient, Injury, and Surgery-Specific Factors Influence Outcomes Following Flexor Tendon Repair
Presenting Author:	Richard Lander
Co-Author(s):	Richard D. Lander MD, Andrew Rodenhouse MD, Akhil Dondapati MD, Thomas Carroll MD, Gabriel Ramirez MS, Alayna Loiselle PhD, Constantinos Ketonis, MD PhD
Lab PI / Mentor:	Dr. Ketonis

ABSTRACT

Flexor tendon lacerations are significant injuries with unacceptably high complication rates after repair. There is a paucity of literature on factors that predict outcomes as experienced by the patients, namely patient-reported outcome measures (PROMs). The purpose of this study was to elucidate the factors affecting outcomes and complications following flexor tendon repair. We hypothesized that multiple patient-specific, injury-specific, and surgery-specific factors would independently affect PROMIS scores and complication rates.

Methods

This was a retrospective study of patients age 18 years or older who underwent primary flexor tendon repair between January 1, 2015 and October 1, 2023. Outcomes included return to the operating room (RTOR), time until RTOR, time until discharge from hand therapy, time to return to work, and Patient-Reported Outcomes Measurement Information System (PROMIS) scores including Physical Function, Pain Interference, Depression, and Upper Extremity. Appropriate descriptive statistics as well as logistic, negative binomial, and linear regression models were undertaken.

Results

In total, 397 patients with 523 injured digits were identified for analysis. Average age of the study population was 39.7 years (SD: 16.1) with 281 (70.8%) patients being male. Laceration-type mechanism was most common (74.8%), followed by sawblade (18.1%) and crush (4.5%) injury. Advanced age, sex, race, body mass index, insurance type, area of deprivation index were patient-specific factors that influenced outcomes.

The mechanism of injury and involvement of single or multiply injured digits were injury-specific variables that influenced outcomes. Saw blade injuries resulted in significantly increased odds of compliance (Est: 3.22; 95CI: [1.33, 7.79]; p-value: 0.010), time until return to work (Est: 1.83; 95CI: [1.25, 2.68]; p-value: 0.002), and depression scores at 6 weeks (Est: 5.77; 95CI: [0.43, 11.11]; p-value: 0.034). Patients with multiply injured digits required significantly more time until discharge from hand therapy (Est: 1.32; 95CI: [1.20, 1.59]; p-value: 0.003).

Surgeon experience and time to surgery were the surgery-specific factors predictive of outcomes (Table 1). Those whose surgeons had ≥ 15 years of experience had significantly less time until return to work (Est: 0.55; 95CI: [0.33, 0.91]; p-value: 0.020), although surgeon training (orthopaedics versus plastics) and the presence of hand fellowship did not impact outcomes.

Conclusion

In conclusion, multiple patient, injury, and surgery-specific factors were predictive of complications and PROMIS scores, after flexor tendon repair. The findings of this study may allow surgeons and therapists to counsel patients more appropriately on expected outcomes following surgery.

15th Annual Center for Musculoskeletal Research Symposium
October 30, 2025

Title:	Effect of Zinc-Coated Titanium Implants on Neutrophil Swarming and S. aureus Clearance
Presenting Author:	Sashank Lekkala
Co-Author(s):	David Armbruster, Rajendra Kasinath, Edward M. Schwarz, Chao Xie
Lab PI / Mentor:	Edward M. Schwarz, Chao Xie

ABSTRACT

Introduction: Implant-associated osteomyelitis remains a significant challenge in orthopedics. With the rise in antibiotic resistance, there is an increased interest in metal implant coatings as a strategy to prevent and treat infection. Silver coatings are the most studied with a strong antibacterial effect in vitro. However, clinical utility is limited by cytotoxicity, adverse effects, and inconsistent efficacy in infection control. These limitations have shifted interest toward alternative metal ion coatings, such as zinc and copper. We hypothesized that zinc would exhibit antibacterial activity against Staphylococcus aureus with limited toxicity. To test this, we aim to investigate the effect of pure zinc and zinc-coated titanium implants on neutrophil swarming to S. aureus and bacterial clearance using longitudinal confocal imaging and a murine model of implant-associated osteomyelitis.

Methods: For confocal imaging, titanium or zinc wires were contaminated with EGFP+ USA300, a community-acquired methicillin-resistant S. aureus (MRSA). We co-cultured these implants with tdTomato+ neutrophils isolated from the long bones of Catchup mice. Extracellular DNA representing dead cells and neutrophil extracellular traps (NETs) was labeled using POPO dye. Longitudinal 3D imaging was performed at 0-, 1-, 3-, and 6-hours (n=3).
All in vivo studies were approved by the University of Rochester IACUC. To study the dose-dependent effects of zinc, we piloted an in vivo study using titanium, zinc, and zinc-coated titanium implants in C57BL/6 mice (n=5/group). We did not see sexual dimorphism in our infection model; therefore, female mice were used to reduce variability and align with our prior data. Implant-associated osteomyelitis was induced in the right tibia using USA300 LAC::lux contaminated pins. At sacrifice, the implant and the surrounding soft tissue were collected for bacterial enumeration. The bones were either enumerated for CFUs or scanned by μCT and processed for histopathology.

Results: Longitudinal confocal imaging showed that zinc implants significantly reduced bacterial burden vs. titanium. This result was also confirmed by bacterial enumeration from the implant and the media. An efficacy index was measured as the negative slope of the linear regression of S. aureus volume vs. time (Zn=0.20 vs. Ti=0.03). However, zinc also induced neutrophil death, evidenced by decreased tdTomato volume and increased eDNA volume over time. A toxicity index was measured as the positive slope of the linear regression of dead/live neutrophils vs. time (Zn=0.26 vs. Ti=0.04).
To abate the toxicity of zinc, we developed low-dose zinc-coated titanium implants designed to maintain antibacterial efficacy. In vivo studies showed no difference in CFUs across the groups, though the pure zinc group showed increased purulence, consistent with neutrophil toxicity. There were no differences in bioluminescence or the μCT analysis of implant hole area. Interestingly, Brown & Brenn staining showed infected bone fragments in the titanium and the zinc groups, but not in the zinc-coated titanium group, suggesting that controlled zinc release may prevent colonization of the osteocyte lacuno-canalicular network (OLCN), which is a critical reservoir for reinfection.

Discussion: We showed that zinc implants exhibit a strong antibacterial effect in vitro. Elution studies on the implants revealed zinc release at 60 μM, which is far lower than the minimum inhibitory concentration of 2500 μM. These findings indicate that zinc is not directly antimicrobial but instead acts synergistically with neutrophils to enhance antibacterial efficacy. Furthermore, we observed that the zinc-coated titanium implants may prevent bone biofilm formation. Therefore, future studies will evaluate these implants in conjunction with standard-of-care vancomycin therapy to target both planktonic and biofilm bacteria.

15th Annual Center for Musculoskeletal Research Symposium
October 30, 2025

Title:	Anti-S. aureus mAbs Against Autolysin and Pore-Forming Toxins Enhance Vital NETosis and Phagocytosis by Cytoplasts Demonstrated with Real Time Fluorescent Microscopy and Imaging Cytometry
Presenting Author:	Sashank Lekkala
Co-Author(s):	Youliang Ren, Neha Soundar, Hannah Wang, Edward M. Schwarz, Chao Xie
Lab PI / Mentor:	Edward M. Schwarz, Chao Xie

ABSTRACT

Introduction: Patients with osteomyelitis have low protective antibody levels against Staphylococcus aureus and can benefit from passive immunization with anti-S. aureus antibodies. However, all S. aureus vaccine candidates have failed in clinical trials, highlighting the need for novel assays to evaluate these therapies mechanistically. Neutrophils defend against bacterial infections by generating neutrophil extracellular traps (NETs) via lytic NETosis, where neutrophils explode and release DNA, or vital NETosis, where neutrophils extrude DNA but survive as anuclear cytoplasts capable of phagocytosis. As S. aureus remodels NETs into biofilm during chronic osteomyelitis, cytoplasts are critical for combating soft-tissue infection. We hypothesized that monoclonal antibody (mAb) enhancement of vital NETosis reduces nidus formation on implants. To this end, we developed a longitudinal confocal imaging system to visualize neutrophil swarming and phagocytosis on an infected implant, and an imaging cytometry assay to quantify cytoplasts and their phagocytic capacity. We tested two mAbs with known in vivo efficacy: anti-glucosaminidase (Gmd) that enhances S. aureus clustering and opsonophagocytosis; and anti-pore-forming toxins (PFT) that neutralize five toxins (a-hemolysin, Panton-Valentine leucocidin, LukED, HlgAB, HlgCB).

Methods: For the longitudinal confocal imaging model, titanium wires were incubated with EGFP+ USA300, a methicillin-resistant S. aureus (MRSA). The implants were scratched to guide nidus (bacterial aggregation) formation, which served as a defined region of interest for longitudinal imaging. We co-cultured these implants with tdTomato+ neutrophils isolated from the long bones of male and female Catchup mice. The antibodies (50 μg/mL) were added at the beginning of the co-culture. We performed 3D time-lapse imaging at 1-, 3-, and 6-hours using a laser scanning confocal microscope (n = 4/group).
For imaging cytometry, planktonic S. aureus was incubated with bone marrow cells from Catchup mice in a similar co-culture system. At 2 hours, an aliquot was diluted to measure CFUs, and the remaining cells were fixed with 4% PFA and stained with Hoechst to visualize DNA. The samples were analyzed on a Cytek imaging cytometer (n = 3/group). Cytoplasts were identified as tdTomato+ and Hoechst- cells. *$p<0.05$ by ANOVA tests.

Results: Confocal imaging showed that neutrophil volume increased in the antibody-treated groups compared to the untreated control. Extracellular DNA labeled using SYTOX blue was also lower in the antibody-treated groups, indicating reduced lytic NETosis. The co-localization of neutrophils and S. aureus, a surrogate for phagocytosis, was higher in the anti-PFT group. In addition, the diameter of the co-localized clusters was the highest in the anti-Gmd group, supporting the idea that anti-Gmd treatment results in S. aureus megacluster formation.
Imaging cytometry analysis also showed trends toward higher neutrophils in the antibody-treated groups. However, neutrophil phagocytosis was reduced in the antibody-treated groups, potentially due to a mismatch between murine FcR and the humanized Fc on the antibodies. Interestingly, we observed an increase in cytoplasts in the combined anti-Gmd + anti-PFT group concomitant with reduced CFUs at 6 hours. In addition, the number of phagocytic cytoplasts and their phagocytic capacity, measured as the mean fluorescence intensity of GFP, were also increased in the anti-PFT and the combined treatment groups.

Discussion: Confirming the mechanism of action of mAbs in cocktail passive immunizations is critical for their success in clinical trials. Here, we developed two novel imaging tools that can quantify swarming, persistence, and opsonophagocytosis by neutrophils and cytoplasts in vitro. We also utilized these outcomes to demonstrate the synergistic activity of anti-Gmd and anti-PFT mAbs. Future studies will extend these experiments with human neutrophils.

15th Annual Center for Musculoskeletal Research Symposium
October 30, 2025

Title:	Characterizing CD8 T Cell Phenotypes in the Acute Myeloid Leukemia Bone Marrow Microenvironment
Presenting Author:	Zhewen "Kevin" Li
Co-Author(s):	Benjamin Frisch, Azmeer Sharipol, Amanda Streeter, Owen Hodges, Jordyn Waters, Celia Soto
Lab PI / Mentor:	Benjamin Frisch

ABSTRACT

Background and Hypothesis:
Acute myeloid leukemia (AML) is the most common acute leukemia and has an abysmal 5-year survival rate of 30%. Traditional therapies like chemotherapy and targeted therapy lack long-term protection, and the majority of patients will relapse, directly leading to the lack of successful outcomes. Bone marrow microenvironment (BMME) dysfunction leads to bone loss and a lack of normal hematopoiesis, which are critical features of the disease. Furthermore, the mechanisms that give rise to bone loss and hematopoietic marrow dysfunction are poorly understood. CD8 T cells have previously been demonstrated to regulate osteoblastic and osteoclastic differentiation and function. However, the role of CD8 T cells in the AML BMME is poorly understood. To elucidate this phenomenon, we aim to study CD8 T cell phenotypes in the AML BMME and the mechanisms that lead to T cell dysfunction in this disease.

Experiment and Methods:
To study this, we used the MLL-AF9 (MA9), a genetic alteration in HSPCs that induces AML, murine model and blast-crisis myeloid leukemia (bcCML) models. To generate these models, leukemic cells were tail-vein injected into wild-type (WT) C57BL/6 male mice. Mice were sacrificed at the advanced stage of the disease (at least 50% of leukemic burden in the BM), and BM cells were isolated for highly multi-parametric flow cytometry analysis. Our control mice will be WT healthy B6 mice that are age and sex matched. Each group will contains 5 replicates of mice for experimental measurement. Any statistical analysis will be performed with one-way ANOVA test for comparison.

Results:
We discovered that compared to healthy BMME T cells, leukemic BMME CD8 T cells have a significantly higher expression of inhibitory receptors (IRs), including PD-1 (AML=78.50±6.26% vs WT=8.42±4.98%, p=0.0001, n=3 respectively) and Tim-3 (AML=12.00±1.13% vs WT=3.70±1.41%, p=0.0004, n=3 respectively) in both models. Meanwhile, TOX, which is a transcription factor that contributes to CD8 T cell dysfunction, is highly elevated in CD8 T cells (AML=88.13±6.02% vs WT=20.67±6.39%, p=0.0002, n=3 respectively) of MA9 BMME compared to those in healthy BMME. We further classified the exhausted CD8 T cells into progenitor (pro-Tex: Ly108+, CX3CR1-), intermediate (int-Tex: Ly108+/-, CX3CR1+), and terminal (term-Tex: Ly108-, CX3CR1-) exhausted CD8 T cells. In solid tumors, pro-Tex is known to have the highest proliferative potential and differentiate into int- and term-Tex. It has moderate IR expression and effector functions. Int-Tex, however, has moderate stemness that can only differentiate into term-Tex. It has strong effector functions and low IR expression. Lastly, the term-Tex has little stemness, low effector function and high IR expression. We discovered that in bcCML model, pro-Tex (52.20±12.00%) accounts for majority of the population, int-Tex (15.82±7.82%) has the lowest percentage, and term-Tex (27.85±8.13%) accounts for about one third of the population. We then investigated the phenotypes and effector functions within each CD8 Tex subsets. Interestingly, we discovered that pro-Tex expressed the highest level of most IRs such as PD-1 (MFI=18546±1553) and TIM-3 (MFI=2007±145.2) compared to the other two subsets, and term-Tex expressed the lowest IRs (MFI of PD-1=10119±2718; MFI of TIM-3=1082±153.7), failing to match the common phenotypes suggested in solid tumors.

Conclusion and Discussion
Our data suggest that CD8 T cells in the AML BMME are indeed exhausted. However, their exhaustion phenotypes, especially of the exhausted T cell subsets, does not match the model suggested in the solid tumor model clarified in the result session. We aim to further study the phenotypes of AML CD8 T cells by using high dimension data analysis and functional studies.

15th Annual Center for Musculoskeletal Research Symposium
October 30, 2025

Title:	A new mechanistic insight into the pathogenesis of Achilles tendinopathy and heterotopic ossification by study of human patient
Presenting Author:	Haiyin Li
Co-Author(s):	David Ciufo
Lab PI / Mentor:	Chike Cao

ABSTRACT

Introduction: Achilles tendinopathy is one of the most common muskulosketal diseases. A frequent late sequela is tendon heterotopic ossification (HO), which in most cases forms via endochondral ossification. There are currently no disease-modifying therapies for Achilles tendinopathy and HO. The cellular and molecular mechanisms that drive this pathology remain incompletely defined, limiting new therapeutic development. Surgically excised human Achilles tendon provides a direct, clinically relevant tissue source that preserves the disease's chronic remodeling and minearlization patterns. Here, we analyze resected human Achilles tendons to define the cellular and molecular programs underlying tendinopathy and tendon HO, with the goal of identifying human-relevant targets for intervention.

Methods: The use of surgically excised human Achilles tissue was approved by the University's Institutional Review Board. Specimens included Achilles tendon from 9 patients (50~73 years old, both sexes) undergoing surgery and control Achilles tendons from 3 healthy donors (Articular Engineering). Alcian Blue Hematoxylin/Orange G (ABOG) staining was performed on 7-μm paraffin sections and and tartrate-resistant acid phosphatase (TRAP) histochemistry was carried out on serial sections using standard protocol. For immunofluorescence (IF), paraffin sections were incubated with primary antibodies against RUNX2, ALPL, and tenascin-C (TNC), followed by Alexa fluor 647-conjugated secondary antibodies to minimize autofluorescence; nuclei were counterstained with DAPI. Whole-slide images were acquired on Olympus VS120 virtual slide scanner. After IF imaging, the same slides were counterstained with ABOG to map IF-positive cells to corresponding histologic compartments.

Results:

Histological findings: We examined 9 surgical cases from the University of Rochester Medical Center clinic with readiographically comfirmed Achilles tendon mineralization. ABOG staining demonstrated mature lamellar bone in all specimens, with well-formed osteons and vascularized marrow-like spaces but minimal hematopoietic marrow. The ectopic bone was contiguous with adjacent tendon exhibiting proteoglycan enrichment (Alcian blue-positive) and the appearance of chondrocyte-like cells aligned along the native tendon fiber axia, consistent with tenocyte-derived tendon-to-cartilage metaplasia. Alcian blue-positive tendon remnants were frequently trapped within the mature bone in all cases, although the size of the remnants varied among different loci and individuals. Furthermore, TRAP staining identified numerous TRAP-positive multinucleated osteoclasts beneath tendon remnant and along woven-bone surfaces; occasional weak TRAP signal appeared in chondrocyte-like cells within entrapped tendon. Immunofluorescence demonstrated nucelar RUNX2 in a subset of Aclain blue-positive chondrocyte-like cells, in contrast to the negative staining in the spindle-shaped tenocytes of healthy Achilles tendon; ALPL localized to proeteoglycan-rich altered tendon and around entrapped tendon remnants; in contrast, TNC was diminished in these regions. Collectively, these findings indicate ongoing osteocast-mediated remodeling even in late-stage Achilles HO and support an endochondral ossification program in which tendon-derived metaplastic cartilage provided the calcified scaffold for ectopic bone formation.

Discussion and conclusion: Our data support a tendon-origin, endochondral pathway for Achilles tendon HO. Native tendon first undergoes cartilaginous metaplasia, depositing a prtoeoglycan-rich, cartilage-like matrix that then calcifies. This calcified cartilage becomes a substrate for osteoclast-mediated remodeling, thus providing a scaffold for woven bone , subsequently lamellar bone after remodeling. This sequence explains the characteristic mosaic of calcified tendon, woven bone, and lamellar bone observed in late lesions, highlighting stage-specific therapeutic opportunities.

15th Annual Center for Musculoskeletal Research Symposium
October 30, 2025

Title: Synovial Fibroblasts Exacerbate Inflammation and Peritendinous Adhesions in a Human Tendon-on-a-Chip

Presenting Author: Isabelle Linares

Co-Author(s): Sophia Thrall, James McGrath, Hani Awad

Lab PI / Mentor: James McGrath, Hani Awad

ABSTRACT

INTRODUCTION: Biomedical research is prioritizing the development of new approach methodologies (NAMs), with emphasis on tissue chips, to offer alternative human-centric models. By generating predictive human-specific data, these models promise to accelerate drug development while complementing traditional animal models. We previously engineered a human tendon-on-a-chip (hToC) featuring a 3D tendon construct and a vascular flow channel separated by an ultrathin nanomembrane. The hToC recapitulates immune cell–tendon fibroblast interactions and demonstrates hallmarks of fibrosis driven by TGF-β1. However, the model lacks synovial fibroblasts and does not model adhesions. Adhesions are composed of disorganized matrix deposited around the tendon that severely limit joint motion and diminish quality of life. Infiltrating immune cells and extrinsic synovial fibroblasts (FLS) contribute to adhesions by migrating, proliferating, and secreting excess collagen and fibronectin. Our objective here is to model FLS crosstalk in the hToC to determine the role of FLS in promoting fibrotic adhesions. We hypothesize that FLS promote adhesion formation by enhancing inflammatory signaling and matrix deposition, even in the absence of exogenous TGF-β1.
METHODS: We engineered modular microfluidic components, enabling separate maturation of cell types before assembly. Human tendon fibroblasts and peripheral blood monocytes (IRB-approved) were encapsulated in type I collagen and cultured with M-CSF for 6 days in the bottom compartment. On Day -4, membranes were coated with collagen gels with or without primary FLS. HUVECs were cultured in the vascular channel for 24 h. At Day 0, monocytes were added to the channel, and the complete hToC was cultured in serum-free media ±TGF-β1. Tendon hydrogels were imaged daily from Day 0–5, and contraction was quantified in ImageJ. Devices were fixed and labeled for α-SMA, collagen III, and fibronectin, then imaged with confocal or multiphoton microscopy for multiplex IF and SHG. Media from the vascular channel was analyzed by Luminex for TGF-β and cytokines. Circulating monocytes were labeled with CellTracker Orange to quantify infiltration. Data were analyzed by one-way ANOVA with Tukey's post hoc test or unpaired t-tests (n=4).
RESULTS: In the absence of TGF-β1, tendon hydrogel contraction was significantly greater in +FLS vs. -FLS devices as early as Day 3, increasing further by Day 5 (70.3 ± 5.1% vs. 52.5 ± 1.3%). With TGF-β1, +FLS and -FLS devices exhibited comparable contraction. +FLS devices formed fibronectin- and COL3-rich networks connecting the synovial gel and tendon. Adhesion contact points were significantly higher in +FLS devices. COL3 expression was increased in the synovial gel of +FLS devices with TGF-β1, while -FLS devices showed more COL3+ cells in the tendon. α-SMA+ myofibroblasts were higher in +FLS constructs, with synergistic increases with TGF-β1. SHG imaging revealed denser collagen in +FLS cultures. Monocyte infiltration was significantly elevated in +FLS devices, regardless of TGF-β1. Cytokine analysis showed no differences in TGF-β1 in the supernatant; however, IL-6 and IL-8 were significantly elevated in +FLS devices at Day 5.
DISCUSSION: Our findings demonstrate, for the first time, the ability to simulate peritendinous adhesions in a tissue chip platform and support the hypothesis that synovial fibroblasts drive adhesions by enhancing contraction, collagen deposition, and monocyte infiltration precipitated by inflammatory cytokines. Importantly, the fibronectin- and COL3-rich networks connecting tendon and synovial gels resemble adhesion-like pathology, providing a mechanistic model to simulate clinically observed adhesions and test drugs to mitigate them. Increased IL-6 secretion in +FLS devices suggests a potential therapeutic target, which will be pursued in future studies. Limitations include the relatively short culture duration and the use of non-tendon-specific FLS.

15th Annual Center for Musculoskeletal Research Symposium
October 30, 2025

Title: Differentiation and Functional Characterization of Human iPSC-Derived Fibroblast-Like Synoviocytes

Presenting Author: Xinying Lu

Co-Author(s): Victor Zhang, Isabelle Linares, Myla Nover-Estes

Lab PI / Mentor: Hani Awad

ABSTRACT

INTRODUCTION: Fibroblast-like synoviocytes (FLS) drive joint pathology by recruiting leukocytes and driving pannus invasion that erodes cartilage in rheumatoid arthritis (RA) and osteoarthritis (OA). They produce inflammatory mediators and matrix-degrading enzymes, making robust protocols for human iPSC-derived-FLS (iFLS) essential for patient-specific "joint-on-a-chip" models of RA and OA. Building on a murine protocol, we aimed to establish human iFLS differentiation, validate identity by immunostaining, and benchmark functionality against primary FLS using scratch closure assays with TNF-α stimulation. We hypothesized that iFLS would acquire synovial features (PRG4+, CDH11+), express canonical FLS markers (CD90, CD55, PDPN, αSMA), and exhibit proliferative and migratory responses resembling primary FLS.

METHODS: Human iPSCs, reprogrammed from tendon fibroblasts obtained under approved IRB protocols, were plated on Matrigel-coated plates in mTeSR Plus with Y-27632. Mesoderm induction occurred on Day1-4, followed by FLS medium (MesenCult ACF Basal supplemented with 2mM L-glutamine, 10 ng/mL TGF-β1, and 10 ng/mL bFGF) refreshed every 2–3 days until Day 21. Cells were cryopreserved, and recovered in FLS medium for 7 days prior to assays. Primary FLS were cultured in DMEM complete media as control. Immunostaining was performed for PRG4, CDH11, CD90, CD55, PDPN and α-SMA. Scratch wound assays were performed on confluent iFLS and primary FLS ± TNF-α (10 ng/mL). Wounds were imaged at 0, 4, 8, and 24 h, and percent wound closure was quantified in Fiji (ImageJ). Statistics: Data from three independent experiments (n = 3) were analyzed by two-way ANOVA, with Bonferroni correction for multiple comparisons.

RESULTS: Both primary FLS and iFLS expressed characteristic synovial markers, including CD55, CD90, CDH11, and PRG4. iFLS appeared smaller and more compact, with higher cell density across all markers examined. Primary FLS exhibited larger, elongated morphologies with more pronounced spreading. PDPN and α-SMA expression was robust in both cell types upon TNF-α stimulation. However, while primary FLS expressed basal levels of PDPN and α-SMA, iFLS did not express these activation markers in the absence of TNF-α stimulation. Scratch closure assays revealed significant differences in proliferative and migratory rates between iFLS and primary FLS. iFLS exhibited accelerated wound closure, achieving >80% closure within 8 hours under both basal and TNF-α stimulated conditions, while primary FLS showed slower wound closure kinetics regardless of TNF-α treatment. Subtle acceleration in wound closure was observed at 4h under TNF-αstimulation in both cell types, but by 8 and 24h, percent closure converged. Thus, iFLS recapitulate key phenotypic markers of primary FLS but display distinct morphologic characteristics and enhanced migratory activity, particularly in response to TNF-α.

DISCUSSION: iFLS reproduce many primary FLS features, including CD55, CD90, CDH11, PRG4, and TNF-α upregulated PDPN/α-SMA. Enhanced iFLS migratory capacity resembled the aggressive, invasive subset of RA synovial fibroblasts that drive pannus formation and cartilage destruction under inflammatory conditions. Morphologically, primary FLS were noticeably larger than iFLS, underscoring that iFLS are not identical to their primary counterparts. It is possible that the expansion of primary fibroblasts affected their basal expression of activation markers. It is also conceivable that iFLS, which were obtained from pathologic tenolysis fibroblasts, may have retained epigenetic memory of their fibrotic progenitors. Future studies will require additional assays including single-cell RNA sequencing to benchmark these iFLS against published datasets of healthy and diseased primary FLS. Nonetheless, generating a renewable population of FLS-like cells that capture core synovial features offers significant value for disease modeling.

15th Annual Center for Musculoskeletal Research Symposium
October 30, 2025

Title:	Defining profibrotic spatial heterogeneity in the maturing abdominal adhesion
Presenting Author:	Alexander J. Mathewson
Co-Author(s):	Matthew Byrne, MD, Abigail Loszko, MD, Nicole M. Wilson, PhD, MD2, Alayna E. Loiselle, PhD
Lab PI / Mentor:	Alayna E. Loiselle, PhD

ABSTRACT

Introduction: Abdominal adhesions are matrix-dense bands of tissue that form following damage to the peritoneum, resulting in readmission for 20% of abdominal surgery patients and an annual economic burden exceeding $1.3 billion. Adhesiolysis (surgical removal) is the only treatment available for adhesion-related complications, but surgical resection risks patient injury and does not prevent subsequent adhesion formation. Histological evaluation of clinical adhesiolysis samples reveals distinct regions of sparse and dense ECM, suggesting that the fibrotic mechanism that establishes and maintains matrix density is part of a tightly regulated microenvironment. However, the mechanisms that drive spatially heterogeneous fibrosis in the maturing adhesion are unknown. Since matrix-dense adhesions present a greater barrier to surgical resection and are associated with severe adhesive burdens, identifying key components of this fibrotic microenvironment will establish novel therapeutic targets that mitigate adhesive burden and improve patient outcomes.

Methods: Four-month old female C57Bl6/J mice underwent cecal abrasion surgery to generate abdominal adhesions, which were harvested at post-operative days 1, 3, 5, and 7 (n=4 per timepoint). Samples (n=2 per timepoint) were selected for 10X Genomics Visium HD spatial sequencing based on median adhesive burden, submitted to the GRC, and sequenced to obtain a saturation exceeding 50% as recommended by 10X Genomics. Sequencing data was processed via the 10X SpaceRanger pipeline (v3.1.3), capture spots aggregated into pseudocells using Bin2cell, and the resulting dataset analyzed in Seurat. In brief, quality control was performed by timepoint prior to Harmony integration, unbiased clustering, and manual cluster annotation with the assistance of Azimuth.

Results: Analysis of our spatial transcriptomic atlas of mouse post-operative adhesion formation (POD 1-7) identified a fibroblast population marked by Col1a1, Col6a3, and Postn. Subcluster analysis of this general fibroblast population revealed a distinct subset of activated fibroblasts that is localized to the adhesion periphery by POD 7. This population is marked by Tenascin-C (Tnc), a matricellular glycoprotein that mediates cell adhesion, cell signaling, and fibrosis. Differential expression analysis reveals that Tnc+ fibroblasts upregulate Col5a1, Loxl2, Fn1, and Tgfb1/2, indicating a unique role in collagen I fibril formation, crosslinking, and cell fate determination. CellChat analysis predicted Tnc-Sdc4 signaling in these peripherial fibroblasts, suggesting cell adhesion is being modulated.

Conclusion: Based on the analysis of our spatial transcriptomic atlas, we identified the emergence of an activated fibroblast population seven days post-operation. We propose that this fibroblast population, marked by Tnc and expressing several profibrotic factors, is essential for establishing and maintaining the adhesive profibrotic microenvironment that drives heterogeneous matrix deposition. As such, targeted disruption of this population may provide an avenue for the prevention or amelioration of abdominal adhesions. To determine if Tnc+ fibroblasts are required to generate matrix dense adhesive tissue, we are generating Tnc-CreERT2; Rosa26-DTA mice for the inducible ablation of Tnc+ cells, and will follow ablation experiments with the knockout of Tnc to establish its necessity in abdominal adheison maturation.

15th Annual Center for Musculoskeletal Research Symposium
October 30, 2025

Title:	T cell dysfunction during Staphylococcus aureus osteomyelitis in humanized mice
Presenting Author:	Katya McDonald
Co-Author(s):	Motoo Saito, Himanshu Meghwani, Javier Rangel-Moreno, Stephen Kates, Richard Proctor, Edward Schwarz, and Gowrishankar Muthukrishnan
Lab PI / Mentor:	Gowrishankar Muthukrishnan

ABSTRACT

INTRODUCTION: Staphylococcus aureus is the leading cause of implant-associated osteomyelitis. It has a high recurrence rate and a low post-operative cure rate and can lead to sepsis, multiorgan failure, and death. Surgical interventions have high failure rates and reinfection (10-50%), indicating a need for future innovation in therapeutics and vaccines. With our humanized mouse model, we have found enhanced susceptibility to S. aureus infection compared to conventional mice. Therefore, we aimed to investigate the human T cell response during infection, as T cells play a cruical role in controlling bacterial growth during chronic infections. Using single-cell RNA sequencing and immunohistochemistry, we have found preliminary evidence of T cell dysfunction in the bone marrow niche. This has led to our hypothesis that CD4 T cells are becoming exhausted in the bone marrow due to chronic infection. Here, we use high-parameter spectral flow cytometry to characterize the human T cell response to S. aureus and show the occurrence of CD4 T cell dysfunction locally (the bone marrow).

METHODS: Female humanized NSG-SGM3 BLT mice (20-24 weeks old) underwent transtibial implant-associated osteomyelitis using bioluminescent MRSA (USA300 LAC::lux) or sham surgery. At fourteen days post-infection, bone marrow cells were isolated and subjected to flow cytometry (n=4-12/group) and single-cell RNA sequencing (n=3/group). For flow cytometry, two panels were used to evaluate changes in CD4 T cell phenotypes and their functional capacity, and data analysis was completed using the OMIQ platform.

RESULTS: In the bone's local infection environment, we observed an influx of Th1/Th17 cells through single-cell RNA sequencing. To quantify CD4 T cells more precisely, we used spectral flow cytometry and observed increases in immune checkpoint proteins LAG-3 ($p<0.05$), PD-1($p<0.05$), and TIM-3($p<0.05$). Interestingly, we also discovered that TIM-3-positive CD4 T cells exhibited reduced Ki67 staining ($p<0.001$), a marker of proliferation, suggesting potentially impaired functional capacity. To explore this further, we examined the effector profile (IFN-γ ($p<0.05$), IL-17A ($p<0.01$), and TNF-α ($p<0.01$)) of these cells and observed diminished cytokine production in TIM-3-positive cells. Finally, to validate the clinical relevance, we analyzed human serum from arthroplasty patients and found TIM-3 levels to be highly predictive of adverse outcomes ($p<0.001$).

DISCUSSION: At the bone marrow site, we have observed an increase in LAG-3+ and TIM-3+ cells during infection, indicating that these cells have diminished proliferation capacity and cytokine production. This suggests they may be dysfunctional and contribute to the chronicity of infection. In future experiments, adding timepoints during infection will allow us to observe a phenotypic switch of the CD4 T cells during the transition from acute to chronic infection. Ultimately, this work will provide novel mechanistic insights into bacteria-T cell interactions during S. aureus bone infections, hoping to inform better diagnostics and therapeutics.

15th Annual Center for Musculoskeletal Research Symposium
October 30, 2025

Title:	Mesenchymal Stem Cell-derived Size Separated Extracellular Vesicles for Treatment of Inflammation in a Macrophage Model
Presenting Author:	Lucia Morales
Co-Author(s):	Varun Purvanesarajah, M.D. (University of Rochester)
Lab PI / Mentor:	Karin Wuertz-Kozak

ABSTRACT

Intervertebral disc (IVD) degeneration is a leading cause of disability, affecting an estimated 80% of the global population over their lifetime. Painful IVD degeneration is characterized by neoinnervation of the disc space and increased inflammation. Current treatment strategies are largely invasive and do not address these underlying mechanisms. Extracellular vesicles (EVs) derived from mesenchymal stem cells (MSCs) have demonstrated anti-inflammatory effects and have gained clinical relevance due to their immunologically inert properties. To date, most research has focused on small EVs. Consistent with this emphasis, previous work in our lab has shown that small EVs significantly reduce inflammation in both primary human IVD cells and human macrophages. The goal of this current research project is to examine whether EVs of different sizes (small vs. large) vary significantly in their anti-inflammatory properties.

EVs were isolated from MSCs and separated into small (50–250 nm) and large (200–1000 nm) populations using differential centrifugation. Specifically, the EVs were first centrifuged at low speed (16,000 ×g, 30 minutes) to isolate the large EV population. The supernatant was then collected, filtered (0.22 μm), and ultracentrifuged at high speed (118,000 ×g, 2.5 hours) to isolate the small EV population. Size separation was confirmed using nanoparticle tracking analysis (NTA). THP-1 monocytes were differentiated into macrophages using PMA and polarized into a pro-inflammatory phenotype via LPS treatment. Small and large EVs were then applied at varying concentrations. Real-time qPCR was used to measure the expression of pro-inflammatory cytokines, including IL-1β, IL-8, and COX2.

NTA confirmed that the stepwise isolation protocol yielded large EVs with a mean size of 230 nm and small EVs with a mean size of 177.8 nm, consistent with values reported in the literature. Preliminary results indicate that both large and small EVs from MSCs possess anti-inflammatory properties in the macrophage model. While further experiments are needed to validate these findings, large EVs appeared to more strongly suppress COX2 expression compared to small EVs, while IL-1β and IL-8 expression were similarly reduced by both populations.

As a next step, we will verify these size-dependent effects using a larger sample size and additional target genes, and expand our analysis to include IVD cells. If confirmed, this would represent the first demonstration of the (potentially superior) effectiveness of large EVs in treating painful IVD degeneration and would warrant omics-based analysis to compare the cargo contents of small vs. large EVs. Importantly, since macrophages play a role in numerous chronic inflammatory-degenerative conditions, our findings may have broad implications for regenerative medicine.

15th Annual Center for Musculoskeletal Research Symposium
October 30, 2025

Title: Use of nonsteroidal anti-inflammatory drugs is associated with increased rates of subsequent rotator cuff repair following arthroscopic rotator cuff repair: a database study of 97,792 patients

Presenting Author: Nicholas Morriss, MD

Co-Author(s): Sameer Jain BS, Omkar Prabhavalkar BA, Michaela Malin BA, Christopher Dussik MD, Patrick Castle MD, Brett P. Salazar MD, Hashim JF. Shaikh MD, Sandeep Mannava, MD, PhD

Lab PI / Mentor: Sandeep Mannava, MD, PhD

ABSTRACT

Introduction: Arthroscopic rotator cuff repair (aRCR) is one of the most commonly performed orthopedic surgeries performed in the United States with historically high rates of anatomic healing and patient satisfaction. However the rate of failure of aRCR continues to present a challenge for many patients and surgeons, usually through failure of healing of the bone-tendon interface. Nonsteroidal anti-inflammatory drugs (NSAIDS) have previously come under scrutiny as potential inhibitors of bone-tendon interface healing. The present database study aimed to compare failure rate of aRCR in patients who were prescribed NSAIDs acutely following surgery with that of patients who were not prescribed NSAIDs. We hypothesize that NSAIDs will increase the rates of both subsequent RCR in the short term as well as rates of total shoulder arthroplasty (TSA) in the long term.

Methods: A retrospective cohort study was conducted using the TriNetX Research Network, a federated, de-identified electronic health record database representing multiple healthcare organizations. Adult patients who underwent arthroscopic rotator cuff repair between October 1, 2015, and August 1, 2020, were identified using CPT code 29827. Two cohorts were defined: those prescribed oral nonsteroidal anti-inflammatory drugs (NSAIDs) within 1 month postoperatively and those without an NSAID prescription during this period. Baseline demographics and comorbidities were extracted, and 1:1 propensity score matching was performed using logistic regression with a caliper of 0.1 standard deviations of the logit to balance measured covariates between groups. Prior to matching, 121,952 patients were identified. After matching, 97,792 patients were included (48,896 per cohort). The primary outcome was subsequent rotator cuff repair surgery at 6 months, 1 year, 3 years, and 5 years postoperatively. The secondary outcome was undergoing subsequent shoulder arthroplasty. Risk ratios with 95% confidence intervals were calculated for each time point, and Kaplan–Meier survival analyses with log-rank testing were performed to compare time-to-event outcomes. Hazard ratios were estimated using Cox proportional hazards models. Statistical significance was defined as $p < 0.05$.

Results: After propensity score matching, cohorts were well balanced (all standardized differences < 0.02). Repeat arthroscopic rotator cuff repair (RCR) occurred at similar rates between NSAID and non-NSAID patients at 6 months ($p = 0.088$). However, at later follow-up, NSAID patients demonstrated consistently higher rates of subsequent rotator cuff repair surgeries: 3.3% vs. 2.9% at 1 year ($p < 0.001$; HR 1.138), 6.6% vs. 5.8% at 3 years ($p < 0.001$; HR 1.164), and 7.9% vs. 7.0% at 5 years ($p < 0.001$; HR 1.185). Across all time points, conversion to shoulder arthroplasty remained low (<2% at 5 years) and did not significantly differ between groups.

Discussion: These findings suggest that acute postoperative NSAID use is associated with a progressively higher likelihood of subsequent rotator cuff repair surgeries beyond 1 year, persisting through 5 years. This may support prior findings suggesting that NSAIDs inhibit tendon to bone healing, leading to higher rates of clinical failure in the long term. This is the first study of this size to evaluate the association of acute peri-operative NSAID use with long term outcomes following RCR. Further research with access to granular patient data and long-term follow-up is needed to elucidate the role of NSAIDs in clinical failure following arthroscopic rotator cuff repair.

15th Annual Center for Musculoskeletal Research Symposium
October 30, 2025

Title:	Association Between NSAID Use and Postoperative Outcomes Following ACL Reconstruction: A Retrospective Cohort Analysis
Presenting Author:	Nicholas Morriss, MD
Co-Author(s):	Sameer Jain BS, Omkar Prabhavalkar BA, Michaela Malin BA, Patrick Castle MD, Brett P. Salazar MD, Christopher Dussik MD, Sandeep Mannava MD, PhD
Lab PI / Mentor:	Sandeep Mannava MD, PhD

ABSTRACT

Introduction: Nonsteroidal anti-inflammatory drugs (NSAIDs) are commonly prescribed for postoperative pain management following anterior cruciate ligament (ACL) reconstruction. However, concerns have emerged regarding their potential effects on soft tissue healing and the development of complications requiring further surgical intervention. The present study aimed to evaluate whether postoperative NSAID use was associated with an increased risk of subsequent ACL reconstruction or other knee surgeries. We hypothesized that there would be no significant difference in rates of subsequent ACL repairs or other knee surgeries between patients who received NSAIDs postoperatively and those who did not.

Methods: A retrospective cohort analysis was conducted using the TriNetX Research Network, a real-time database aggregating de-identified electronic health records from over 100 healthcare organizations. Patients who underwent primary ACL reconstruction were identified via CPT codes and stratified based on whether they received a prescription for NSAIDs within 1 month postoperatively. Propensity score matching (1:1) was performed based on age, sex, and medical comorbidities to reduce confounding. While NSAID use without prescriptions could not be controlled for, they were unlikely to be taken at comparable doses to prescription NSAIDs. Outcomes included repeat ACL reconstruction, any subsequent knee arthroscopy, manipulation under anesthesia (MUA), arthroscopic lysis of adhesions (LOA), or arthroscopic synovectomy. Outcomes were evaluated at 6 months, 1 year, 2 years, and 5 years postoperatively using odds ratios and Chi-square analysis.

Results: The study included 52,124 patients total, 26,062 patients who recieved NSAIDS postoperatively and 26,062 who did not. At 6 months, NSAID use was not significantly associated with increased odds of subsequent ACL repair or knee surgery. By 1 year, NSAID users demonstrated significantly higher rates of repeat ACL reconstruction (1.92% vs. 1.45%; OR 1.323, $p<0.001$), a pattern that persisted at 2 years (3.49% vs. 2.54%; OR 1.388, $p<0.001$) and 5 years (4.98% vs. 3.63%; OR 1.392, $p<0.001$). Similarly, rates of subsequent knee arthroscopy were greater in the NSAID cohort at 1 year (4.59% vs. 3.81%; OR 1.214, $p<0.001$), 2 years (7.20% vs. 6.10%; OR 1.194, $p<0.001$), and 5 years (9.38% vs. 8.07%; OR 1.180, $p<0.001$). NSAID use was also associated with increased likelihood of undergoing lysis of adhesions at 1 year (1.53% vs. 1.19%; OR 1.291, $p=0.001$), 2 years (1.75% vs. 1.44%; OR 1.217, $p=0.005$), and 5 years (1.91% vs. 1.53%; OR 1.250, $p=0.001$). Rates of manipulation under anesthesia (MUA) trended higher in the NSAID group across timepoints (1 year: 0.65% vs. 0.53%, $p=0.076$; 2 years: 0.68% vs. 0.55%, $p=0.057$; 5 years: 0.71% vs. 0.58%, $p=0.070$), but did not reach statistical significance. No significant association was found between NSAID use and synovectomy at any time point.

Discussion: Postoperative NSAID use following ACL reconstruction was associated with increased likelihood of subsequent ACL reconstruction, additional knee arthroscopy, and lysis of adhesions beginning at 1 year postoperatively and persisting through 5 years. Although rates of MUA trended higher in NSAID users, statistical significance was not reached. No association was observed between NSAID use and arthroscopic synovectomy. These findings indicate a potential association between NSAID exposure and impaired graft healing leading to graft failure or potential increased risk for subsequent injury following ACL reconstruction. Given the widespread use of NSAIDs in postoperative protocols, even modest increases in risk may have significant implications at the population level. Clinicians should weigh the benefits of NSAID-based analgesia against the potential for long-term complications, especially in patients with additional risk factors. Further research is warranted to determine causality and optimal pain management regimens.

15th Annual Center for Musculoskeletal Research Symposium
October 30, 2025

Title:	Achilles Tendons Maintain Homeostasis in Response to Physiological Load via Spatially-Distinct Celluar Processes
Presenting Author:	Samantha Muscat
Co-Author(s):	Elsa Lecaj, Nolan Sparks and Mark Buckley
Lab PI / Mentor:	Anne Nichols

ABSTRACT

Background and hypothesis: Tendons are composed of collagen fibrils and other critical extracellular matrix (ECM) components that allow them to withstand extreme loads. Previous work has shown that in response to physiological loading, tendon cells produce collagen and other important matrix proteins to maintain the tendon's structure and functional properties (homeostasis). However, the precise cellular processes that allow tendon cells to perform this critical function remain unknown. Wild mice can run long distances which suggest that normal cage activity in a laboratory setting limits their natural activity levels resulting in an underloaded tendon. Other models of loading like forced treadmill running (FTR) induce a stress response and can cause tendon degeneration, which suggests that FTR does not model physiological load, but overuse. In the present study, we evaluated voluntary wheel running (VWR) in the mouse Achilles tendon to investigate how tendon cells maintain homeostasis in response to physiological load. Methods: Male (10 weeks) C57BL/6J mice (n=25) were chosen as male mice do not exhibit significant levels of stress when singly housed. Mice were allowed to run on a saucer shaped wheel for 8 weeks. Underloaded controls had wheels locked to prevent running. Biomechanical properties were assessed by preloading with 10 cycles at 6% strain and single ramp-to-failure (n=10/group). Paraffin sections were stained for Collagen Hybridizing peptide (CHP)-Cy3 and DAPI (n=3/group). Total RNA was isolated from individual tendons for bulk-RNA sequencing and differential expression analysis (n=7/group). Spatial RNA sequencing was performed using the Visium HD platform (n=5/group). Differences in biomechanics and CHP staining were assessed by unpaired t-tests.Results: Mice ran a total of 854 ± 83.52 km during the 8 weeks. No significant differences were observed in cross sectional area or stiffness between VWR and underloaded controls, suggesting that there are no large structural changes with physiological loading. 8 weeks of VWR led to an increase in peak load ($p=0.0178$), peak stress ($p=0.0009$) and elastic modulus ($p=0.0058$), suggesting that VWR tendons are stronger compared to underloaded controls. Bulk-RNA sequencing revealed that VWR tendons upregulate genes with known roles in collagen remodeling Lum [$p=0.0028$], P4ha3 [$p=0.0003$]), compared to underloaded controls. CHP-Cy3, which binds to unfolded collagen chains, was used to validate the observed upregulation of collagen remodeling-related genes. Significant collagen remodeling was observed in VWR calcaneal insertion compared to underloaded controls ($p=0.0057$). No collagen remodeling was present at the midsubstance of VWR tendons where mechanical properties are increased. Initial clustering of spatial transcriptomics data revealed clusters that are specific to the midsubstance and calcaneal insertion. Differential expression analysis indicates that cells in the midsubstance upregulate different ECM-related genes compared to cells in the calcaneal insertion. Taken together, our data suggests that in response to physiological load, tendons maintain homeostasis via spatially-distinct cellular processes. Discussion: The results of our study show that after 8 weeks of physiological loading, tendons are mechanically superior with upregulation of collagen remodeling compared to underloaded controls. Interestingly, this appears to occur in a spatially-dependent manner as we observed increases in mechanical properties at the midsubstance, with significant collagen remodeling restricted to the calcaneal insertion. Indeed, our spatial transcriptomics data shows that cells in the midsubstance and calcaneal insertion of VWR tendons produce distinct ECM components. Ultimately, understanding how tendons maintain homeostasis in response to physiological load can help identify targets to preserve tendon health.

15th Annual Center for Musculoskeletal Research Symposium
October 30, 2025

Title:	Assessing the Accuracy of XSENSOR Intelligent Insoles for Motion Analysis
Presenting Author:	Dennis Nimoh
Co-Author(s):	Chelsea Maynard
Lab PI / Mentor:	Dr. Cherice Hill

ABSTRACT

Introduction:
Biomechanical data is essential in understanding human movement and musculoskeletal health, and is increasingly applied to diagnosis, injury prevention, and performance optimization. Movement kinetics, such as ground reaction forces (GRFs), are central to this analysis, yet their measurement is typically restricted to force plates— highly accurate but costly devices that require precise foot placement and restrict testing to laboratory settings. As the demand for accessible and field-based assessment grows, wearable in-shoe systems have emerged to help capture kinetics in real-world environments. The XSENSOR Intelligent Insole is one such system for kinetic analysis, designed with high-resolution pressure sensors and an integrated IMU, but its accuracy in dynamic tasks has not been fully validated. The purpose of this study was to assess the accuracy of XSENSOR insoles in capturing vertical GRFs, with the hypothesis that the insoles will underestimate vGRFs forces while demonstrating high consistency.

Method:
Thirty participants (22 female, 8 male) completed five walking, jogging, and drop vertical jump (DVJ) trials on a force-plate walkway while wearing shoes lined with XSENSOR Intelligent Insoles. Force plate data were sampled at 1200 Hz and insole data at 120 Hz, synchronized via Qualisys software. Valid steps were identified and temporally aligned for pairwise comparison. Peak vertical ground reaction force (vGRF), impulse, stance time, and weight-acceptance and push-off ground reaction force peaks (walking only), were computed for each task. Agreement between systems was assessed using intraclass correlation coefficients [ICC(3,1)] and MANOVA with paired t-test/Wilcoxon post hoc comparisons. Time-normalized vertical load waveforms were further compared using 1D statistical parametric mapping (SPM) paired t-tests to assess methodological consistency throughout the stance phase.

Results:
Discrete measures across walking, jogging, and DVJ showed good to excellent consistency (ICC = 0.76–0.96) between force plates and XSENSOR insoles. The omnibus MANOVA revealed significant system effects ($p < 0.001$), and post hoc paired t-tests/Wilcoxon tests confirmed lower peak vGRF and impulse with longer stance times in insoles across all tasks ($p < 0.01$). Despite these systematic differences, the waveform shapes were largely preserved between systems. SPM showed significant stance-phase differences ($p < 0.001$), as the insoles underestimated vGRF across most of stance with brief overestimations at initial contact and terminal stance.

Discussion and Conlusion:
As hypothesized, XSENSOR insoles systematically underestimated vGRFs compared to force plates but demonstrated strong reliability across tasks. The preserved waveform shape, timing, and high ICCs indicate that XSENSOR insoles can reliably track relative changes in loading, making them suitable for rehabilitation follow-up, and field-based performance monitoring where trends over time are more important than absolute peak magnitudes. SPM analysis further highlights the need to interpret insole loads relative to stance phase timing, as XSENSOR insoles underestimated loads throughout most of stance but overestimated loads at heel strike and toe-off. The consistent underestimation and systematic bias are due to limitations, including alignment errors during step matching, lower sampling rate of the insoles relative to force plates (120 Hz vs 1200 Hz), and shoe-insole deformation, which dampens the transmitted vertical forces. Future work will explore calibration models or correction algorithms to adjust insole kinetic measures toward force-plate equivalence and extend validation to clinical populations. While not a direct substitute for force plates, XSENSOR insoles provide a portable and reliable alternative that enables field-based kinetic assessment in sports medicine, injury rehabilitation, and gait analysis.

15th Annual Center for Musculoskeletal Research Symposium
October 30, 2025

Title: Differential effect of exercise on chondrocyte viability and mechanical susceptibility in young and aged mouse knee joints

Presenting Author: Cortney Pang

Co-Author(s): Seonjoo Lim

Lab PI / Mentor: Whasil Lee, Ph.D.

ABSTRACT

Introduction: Chondrocytes are the primary cells responsible for cartilage homeostasis in load-bearing joints through mechanotransduction mechanisms. Because adult cartilage has limited regenerative capacity and chondrocytes in adult cartilage are post-mitotic with limited proliferation, chondrocyte survival is crucial for cartilage remodeling and maintenance. While exercise and physical therapy have been shown to benefit joint health for patients with osteoarthritis, the most common disease of load-bearing joints, the effect of exercise on chondrocyte viability and mechanical susceptibility is unknown. Here, we hypothesize that exercise modulates articular cartilage chondrocyte density and its mechanical susceptibility in a region-dependent and age-dependent manner. By using a voluntary exercise mouse model and ex vivo mechano-death assay, we monitored the lateral condyle of left hind limb murine knees and quantified chondrocyte density and its mechanical susceptibility against impact post-4 weeks of exercise.

Materials and Methods: To measure the effect of physiologic loading on chondrocytes, C57BL6/J female mice were housed in a voluntary wheel running (VWR) cages with wheels that were locked or unlocked based on sedentary (sed) or exercise (ex) designations for 4 weeks. Mice were sacrificed at the age of 3 months (3M), 4 months (4M), and 17 months (17M) (UCAR:2018-019). The average running revolution was 27k for the 3M and 4M ex mice, and 20k for 17M ex mice. Post-exercise, we harvested knee joints and measured chondrocyte density and mechanical vulnerability on the lateral femoral condyle explant ex vivo. Briefly, distal femurs with intact cartilage were stained with calcein-AM and Propidium Iodide (PI), then subjected to 1 mJ kinetic energy on the patellar-femoral groove using our custom-built impact device. Chondrocytes on the lateral femoral condyles were z-stack imaged by a confocal microscope before and after the impact. Chondrocyte density and damaged area were quantified using ImageJ and QuPath software.

Results and Discussion: We observed the significant chondrocyte loss in the posterior cartilage in 4M and 17M-old joints, revealing the region-dependent cartilage damage over natural aging. Interestingly, the chondrocyte density on the lateral femoral condyle was significantly increased in the 4M ex group than the control 4M sed group (28% increase, $p=0.01$), whereas no significant change was observed in chondrocyte density between the 17M sed and 17M ex group. These data suggest exercise-induced chondrocyte proliferation in young adult mice (4M) but not in the aged mice. Next, we observed age-dependent and exercise-dependent chondrocyte susceptibility against injurious loading. The 3M ex group exhibited a significantly reduced area of injury (chondrocyte death zone) compared to 3M sed group. This trend indicates the chondroprotective effect of exercise at 3M of age. However, both the 4M sed and 4M ex groups exhibit a significantly increased area of injury (5-fold) compared to 3M sed without exercise-driven chondroprotection ($p=0.17$). Strikingly, 17M ex group exhibits significantly increased area of injury ($p=0.01$) compared to 17M sed, revealing the adverse effects of exercise on cartilage. Collectively, these results indicate region-dependent cartilage integrity and the age-dependent exercise effect on chondrocyte viability and mechanosusceptibility.

Conclusion: Chondrocyte survival is crucial for cartilage remodeling. Our confocal 3D microscopy data revealed chondrocyte-empty zones in the ACL-PCL region of the posterior cartilage, especially in the sedentary and aged groups. Strikingly, while exercise provided chondroprotective benefits against impact loading in young mice (3- months-old), it had the inverse effect in aged mice (17-months-old), indicating reduced chondroprotection. Together, our results strongly support the age-dependent exercise effect on chondrocyte viability and susceptibility.

Increased Nonunion Rates for Scaphoid Fractures Treated Nonoperatively with Recent NSAID Prescription

Background & Hypothesis:

Acute scaphoid fractures constitute up to 80% of all carpal bone fractures with reported union rates of nondisplaced scaphoid fractures between 90-95% after casting and immobilization. The purpose of our study was to evaluate the relationship of usage of prescription non-steroidal anti-inflammatory drugs (NSAIDs) and nonunion rates in nonoperatively and operatively managed scaphoid fractures. We hypothesized that operatively and nonoperatively treated scaphoid fractures would have higher nonunion rates if they had a recent NSAID prescription within one month of diagnosis or surgery.

Experiments & Methods:

We queried the TriNetX database to identify all patients diagnosed with scaphoid fractures using a combination of International Classification of Diseases (ICD) and Current Procedural Terminology (CPT) codes. Patients were stratified by operative versus nonoperative management, as well as by receipt of a prescription for NSAIDs within one month of scaphoid fracture diagnosis. We then assessed the incidence of scaphoid nonunion and the rate of salvage procedures for nonunion within two years of the initial diagnosis or scaphoid ORIF. Analyses were matched for comorbidities, smoking status, and alcohol use. Chi-squared testing and odds ratio analysis were used to determine statistical significance.

Results:

After matching, there were 17,241 patients in the nonoperative group and 1,410 patients in the operative group (Table 1). Within the matched nonoperative treatment cohort, patients with prescription NSAIDs had a significantly increased incidence of scaphoid nonunion (3.6% vs. 1.7%, odds ratio (CI): 2.17 (1.88-2.51)) and significantly increased incidence of salvage procedures (1.2% vs. 0.6%; odds ratio (CI): 1.98 (1.56-2.52)) (Table 2). In contrast, within the matched operative fracture group with and without perioperative NSAID prescriptions, there were no significant differences between the incidence of scaphoid nonunion (7.0% vs. 8.1%; OR (CI): 1.18 (0.89-1.56)), or of salvage procedures (2.5 vs. 2.8%, OR (CI): 0.90 (0.56-1.42)) (Table 2).

Discussion and Conclusions:

Among patients with nonoperatively managed scaphoid fractures, those prescribed NSAIDs within one month of diagnosis demonstrated an approximate two-fold increase in the risk of nonunion and subsequent salvage procedures. This association was not observed in operatively managed patients with peri-operative prescribed NSAIDs, suggesting that mechanical fixation may offset the potential adverse effects of NSAIDs on bone healing. These findings highlight the importance of advising patients to avoid NSAID use in the early post-injury period after scaphoid fractures, especially when nonoperative management is planned.

Psychiatric Outcomes after Digital Replantation Versus Primary Digital Amputation

Background & Hypothesis:

The loss of a limb is a physical and psychological trauma that can result in conflicts of loss and dependency. The purpose of this study was to compare the psychological outcomes following digital amputations, successful digital replantation surgeries, and failed digital replantation surgeries. We hypothesized that there would be no statistical difference in the psychiatric outcomes between the primary amputation and replantation surgery cohorts.

Materials & Methods:

This was a retrospective cohort study performed using the TriNetX database, which is a large, multicenter database which we used to study patients who had undergone digital amputation or digital replantation. The TrinetX database was queried using the appropriate Current Procedural Terminology (CPT) or International Classification of Diseases (ICD) codes. We found 19,146 patients who had undergone primary digital amputations, 570 patients who had successful digital replantation surgeries, and 264 patients with failed digital replantation surgery that required revision amputation. We then queried the database for new diagnoses of depression, generalized anxiety disorder, substance abuse, and PTSD or adjustment disorders using the appropriate ICD-10 codes for new psychiatric diagnoses within 3 years after the index surgery.

Results:

Within the primary digital amputation group, the incidence of depression, generalized anxiety disorder, substance abuse, and adjustment disorder or PTSD was 11.9%, 10.8%, 8.3%, and 4.9% respectively. The incidence of depression, generalized anxiety disorder, substance abuse, and adjustment disorder or PTSD for all replantation surgery patients was 7.3%, 6.4%, 4.9%, and 6.6% respectively. The incidence of depression, generalized anxiety disorder, and substance abuse were found to be significantly lower in all patients who underwent replantation surgeries compared to the primary amputation group ($p < 0.05$). Meanwhile, the incidence of depression, generalized anxiety disorder, substance abuse, and adjustment disorder or PTSD for the successful replantation group was 7.5%, 6.0%, 3.5%, and 4.2%, and was 6.1%, 5.3%, 5.3%, and 9.8% respectively for the failed digital replantation surgery cohort.

Discussion and Conclusions:

With the exception of adjustment disorder/PTSD, the incidence of all the psychiatric outcomes listed were found to be significantly lower in all patients who undergone replantation surgeries compared to the primary amputation group, regardless if the replantation was successful. Interestingly, patients who had undergone digital replantation surgeries that ultimately failed had a statistically higher incidence of adjustment disorder/PTSD compared to those who received a digital amputation as the initial treatment at three years postoperatively. These results are especially pertinent as replantation attempts trend downward in hand surgery.

15th Annual Center for Musculoskeletal Research Symposium
October 30, 2025

Title:	Hyperlipidemia Increases the Risk of Secondary Procedures in Patients Undergoing Arthroscopic Rotator Cuff Repair: A Database Study of 144,555 Patients
Presenting Author:	Omkar N. Prabhavalkar, BA
Co-Author(s):	Nicholas Morriss, MD; Michaela Malin, BA; Sameer Jain, BA; Brett Salazar, MD; Patrick Castle, MD; Christopher M. Dussik, Sandeep Mannava, MD, PhD
Lab PI / Mentor:	Sandeep Mannava, MD, PhD

ABSTRACT

Introduction

Hyperlipidemia (HLD) has been implicated as a potential risk factor for impaired tendon-to-bone healing after arthroscopic rotator cuff repair (RCR). Statin therapy may attenuate this risk, but findings remain inconsistent. Large-scale population data also suggest an increased incidence of rotator cuff disease in hyperlipidemic patients, with possible protective effects of statins. Given this conflicting evidence and the multifactorial nature of cuff healing, further investigation in large, diverse patient populations is warranted. It was hypothesized that HLD will be associated with higher rates of both repeat RCR and total shoulder arthroplasty.

Methods

We conducted a retrospective cohort study using the TriNetX Research Network, a federated, de-identified electronic health record database comprising over 120 million patients from multiple healthcare organizations. Adults undergoing primary arthroscopic rotator cuff repair between October 1, 2015, and August 1, 2020, were identified using CPT code 29827. Patients were categorized into three cohorts: (1) no diagnosis of hyperlipidemia, (2) hyperlipidemia without perioperative statin use, and (3) hyperlipidemia with perioperative statin use. Hyperlipidemia was defined by ICD-10 codes E78. * within 12 months prior to surgery. Perioperative statin use was defined as an active prescription from 90 days before to 90 days after surgery. A separate analysis was run comparing groups based on total cholesterol and LDL levels. The primary outcome was subsequent rotator cuff repair identified by CPT 29827. Secondary outcomes included arthroscopic debridement for cuff pathology, conversion to total shoulder arthroplasty, repeat rotator cuff repair, removal of foreign body, lysis of adhesions, and manipulation under anesthesia. Outcomes were assessed at 6 months, 1 year, 2 years, and 5 years postoperatively. Propensity score matching (1:1 nearest neighbor, caliper 0.1) was performed between cohorts on demographics, comorbidities, and surgical factors. Risk ratios (RR) with 95% confidence intervals (CI) were calculated, and Kaplan–Meier survival analysis with log-rank testing was used for time-to-event comparisons. Significance was set at $p < 0.05$.

Results

Following propensity matching, there were 40,430 patients in the HLD and control groups. Across 6-month to 5-year follow-up, patients with HLD had higher risks of repeat rotator cuff repair (RCR) and shoulder debridement at all time points ($p < 0.05$), with additional increased risks for lysis of adhesions (LOA) at 1 ($p = 0.049$), 3 ($p = 0.030$), and 5 ($p = 0.008$) years, arthroplasty at 3 ($p = 0.024$) and 5 ($p < 0.001$) years, and removal of foreign implant/body at 5 ($p = 0.012$) years. Cholesterol category comparisons (<200 vs. 200-239 or >240 mg/dl) showed no significant differences in complications, except for higher manipulation under anesthesia (MUA) risk in the 200-239 mg/dl group ($p = 0.016$). Among patients with low cholesterol, statin use was associated with increased 3-year risks of repeat RCR ($p = 0.014$) and arthroplasty ($p = 0.008$). LDL category comparisons revealed no differences for <100 vs. ≥160 mg/dl, while <100 mg/dl vs. 100-160 mg/dl showed mixed findings, including lower repeat RCR risk at 3 years ($p = 0.027$) but higher arthroplasty risk at 5 years in the low LDL group ($p = 0.015$).

Conclusion

Hyperlipidemia was consistently associated with higher rates of revision RCR, conversion to total shoulder arthroplasty, and select secondary procedures up to 5 years after surgery. Cholesterol and LDL levels alone were not reliable predictors, and even patients with low cholesterol on statins showed elevated risks, highlighting the complexity of lipid metabolism in

tendon healing. These findings suggest that lipid status and statin use may significantly influence postoperative outcomes after RCR and should be considered in perioperative risk management and patient counseling.

15th Annual Center for Musculoskeletal Research Symposium
October 30, 2025

Title: Application of Machine Learning Techniques to Identify Predictors of PROMIS Outcomes After ACL Reconstruction

Presenting Author: Omkar N. Prabhavalkar, BA

Co-Author(s): Patrick Castle, MD, Melissa Holloway, MD, Sandeep Mannava, MD, PhD

Lab PI / Mentor: Sandeep Mannava, MD, PhD

ABSTRACT

Background: There is a paucity of literature employing regression and predictive modeling techniques to identify preoperative factors that influence outcomes after anterior cruciate ligament (ACL) reconstruction. The purpose of this study was to understand which preoperative variables most strongly predict postoperative outcomes can help clinicians better counsel patients regarding their expected recovery. It was hypothesized that factors such as age, body mass index (BMI), and socioeconomic status indicators – specifically the Area Deprivation Index (ADI) and Social Vulnerability Index (SVI) – would emerge as important predictors of postoperative physical function, pain interference, and depression.

Methods: A retrospective cohort study of patients undergoing ACL reconstruction at our institution between 1/1/2015 and 1/31/2023 was conducted. Inclusion criteria included patients aged 13 years or older with a diagnosis of complete or partial ACL tear who completed both preoperative and six-month postoperative Patient-Reported Outcomes Measurement Information System (PROMIS) questionnaires. Eighteen preoperative demographic and patient-specific variables were evaluated as predictors of three postoperative outcomes: physical function (PF), pain interference (PI), and depression. Four modeling approaches – multivariate linear regression, LASSO regression, Random Forest, and XGBoost – were employed to assess predictive performance and identify significant variables. Predictors were identified as significant at $p < 0.05$ in linear regression, retained at the optimal penalty in LASSO, and ranked by importance using %IncMSE in Random Forest and gain in XGBoost. Model fit and predictive accuracy were compared using root mean squared error (RMSE), mean absolute error (MAE), and R-squared (R2) values.

Results: A total of 568 patients met inclusion criteria with minimum 6-month follow-up (mean 17.0 months). Model performance varied by outcome. For postoperative PF, LASSO regression performed best (RMSE = 9.1, MAE = 6.7, R2 = 0.10). For PI, LASSO again performed best (RMSE = 7.94, MAE = 6.51, R2 = 0.18). For Depression LASSO yielded the strongest fit (RMSE = 7.47, MAE = 6.01, R2 = 0.32). Across all four models, common significant predictors included baseline PROMIS scores (preop PF/PI/depression), insurance status, smoking status, BMI, age, time to surgery, and concomitant ligament/meniscus procedures, with ADI/SVI and sport/cause of injury appearing in specific models. Predictive performance was modest for PF and PI but moderate for depression.

Conclusion: Preoperative clinical and social factors—including baseline PROMIS measures, insurance, BMI, age, smoking, and time to surgery—are associated with postoperative PROMIS outcomes after ACL reconstruction. Depression proved moderately predictable, while PF and PI showed limited predictability, suggesting additional unmeasured clinical and psychosocial determinants. Importantly, across four distinct modeling approaches, LASSO regression consistently demonstrated the strongest predictive performance. These models could support personalized preoperative counseling by estimating expected PROMIS outcomes and highlight the need for future work integrating broader contextual variables (e.g., rehab adherence, psychosocial stressors, access to care). To our knowledge, this is the first study to apply multiple modeling approaches to PROMIS outcomes after ACL reconstruction, highlighting the potential of these methods to advance individualized patient care.

15th Annual Center for Musculoskeletal Research Symposium
October 30, 2025

Title: ACL Reconstruction in Skiers vs Pivoting Sports Athletes: A Comparative Analysis of PROMIS Outcomes

Presenting Author: Omkar N. Prabhavalkar, BA

Co-Author(s): Patrick Castle, MD; Melissa Holloway, MD; Hashim Shaikh, MD; Sandeep Mannava, MD, PhD

Lab PI / Mentor: Sandeep Mannava, MD, PhD

ABSTRACT

Background: Anterior cruciate ligament (ACL) reconstruction is a common procedure to restore knee stability and function following rupture. Extreme sport athletes, such as skiers, may face unique postoperative challenges due to the high-impact landings, rotational forces, and non-linear movements inherent to their sport, potentially necessitating different rehabilitation strategies compared with athletes in traditional pivoting sports like soccer, football, and basketball. This study aimed to compare outcomes after ACL reconstruction between skiers and pivoting sport athletes, with the hypothesis that skiers would demonstrate worse PROMIS outcomes given the greater impact demands of their injuries.

Methods: Patients who underwent arthroscopic ACL reconstruction at our institution between January 1, 2015, and December 31, 2023, were retrospectively reviewed. Inclusion criteria were age ≥13 years, diagnosis of partial or complete ACL tear, and completion of both preoperative and ≥6-month postoperative PROMIS questionnaires. MCID was defined as one-half the standard deviation of preoperative PROMIS scores. Athletes who were injured skiing were matched to a group of athletes injured while playing soccer, football, or basketball in a 1:2 ratio on the basis of age, gender, insurance status, race, and BMI. The mean and standard deviation for continuous demographic and outcome measures were calculated and compared between groups using 2-tailed t-tests while categorical variables were compared using Chi-square analysis.

Results: A total of 53 skiers were matched to 86 pivoting sport athletes. All athletes had recreational or higher levels of participation in their sport. Baseline demographics, including age ($p = 0.052$) and BMI ($p = 0.52$), were similar between groups. Preoperatively, skiers had lower PROMIS Physical Function (PF) scores compared with pivoting sport athletes (36.4 ± 7.7 vs 41.0 ± 7.5, $p < 0.001$), while Pain Interference (PI) and Depression scores were comparable ($p > 0.05$). At latest follow-up, both groups demonstrated significant improvements in PF, PI, and Depression (all $p < 0.001$ within-group), with no between-group differences in absolute postoperative scores. However, skiers achieved greater improvement in PF compared with pivoting athletes (10.9 ± 12.0 vs 7.8 ± 10.5, $p = 0.041$). Rates of achieving MCID were not statistically different between groups.

Conclusions: Both skiers and pivoting sport athletes experienced significant improvements in PROMIS outcomes after ACL reconstruction. Despite worse preoperative function, skiers achieved greater gains in physical function. These findings suggest ACL reconstruction is effective in skiers, with outcomes comparable to or exceeding those of athletes in traditional pivoting sports. Future work should evaluate return-to-sport timelines and the role of tailored rehabilitation strategies in optimizing outcomes for athletes in sports with different physical demands.

15th Annual Center for Musculoskeletal Research Symposium
October 30, 2025

Title: Biomechanical Predictors of Injury Risk in Athletes: Translating Motion Analysis into Clinically Relevant Prevention Strategies

Presenting Author: Emily Schillinger, MS

Co-Author(s): Brett P. Salazar, MD; Ye Shu, BS; Zachary Ferrara M EdS; Conner Lorenzo, MS; Jillian Santer, PT DPT; Eward M. Schwarz, PhD; Michael D. Maloney, MD; Katherine H. Rizzone, MD MPH

Lab PI / Mentor: Ram Haddas, PhD

ABSTRACT

Introduction: Running-related injuries (RRIs) are common overuse injuries, affecting 15% to 62% of recreational and competitive runners. Their etiology is multifactorial, involving intrinsic and extrinsic factors such as alignment, range of motion, neuromuscular control, and training load. Traditional 2D gait evaluations often lack the sensitivity to detect subtle asymmetries and compensations that predispose runners to injury. To address this limitation, we developed a clinically feasible, multimodal running assessment protocol utilizing 3D markerless motion capture, ground reaction force (GRF) analysis, and surface electromyography (sEMG). We hypothesized that this integrated approach would identify biomechanical and neuromuscular asymmetries associated with RRIs and could inform more targeted prevention and treatment protocols for athletes.

Methods: We retrospectively reviewed 20 runners presenting to an outpatient rehabilitation clinic with musculoskeletal RRIs. Subgroups included low back pain (n=5), hip pain (n=5), knee pain (n=5), and foot/ankle pain (n=5). Fifteen asymptomatic, age- and sex-matched runners served as controls. All participants completed a standardized 10-minute treadmill running trial. Data was simultaneously captured using an eight-camera markerless motion analysis system (100 Hz), an instrumented dual-belt treadmill with integrated force plates (2000 Hz), and wireless sEMG sensors applied bilaterally to the tibialis anterior, gastrocnemius medialis, rectus femoris, and semitendinosus. Data processing included kinematic reconstruction, gait event detection (heel strike, mid-stance, and toe-off), GRF normalization, and EMG root mean square (RMS) analysis with submaximal voluntary contraction (sMVC) normalization. Key outcomes included joint angles, moments, power, vertical and anterior-posterior GRF metrics, and muscle activation timing.

Results: The knee group exhibited a lower mean running speed (2.76 ± 0.38 m/s) compared with controls (3.28 ± 0.62 m/s, $p<0.05$). Kinematic differences included reduced sagittal trunk angle at heel strike in the knee group (3.2 ± 1.8° vs 6.4 ± 3.4°, $p<0.01$), decreased sagittal knee angle in the spine group (16.2 ± 2.2° vs 19.6 ± 4.7°, $p<0.05$), and lower sagittal pelvic angle at toe-off in the spine group (9.3 ± 6.0° vs 12.6 ± 3.4°, $p<0.05$) compared with controls. EMG analysis revealed elevated anterior tibialis activation in the spine cohort (79.9 ± 5.7% vs 60.0 ± 22.7%, $p<0.01$), reduced gastrocnemius, rectus femoris, and semitendinosus activity in the hip cohort (all $p<0.05$), and decreased semitendinosus activation with corresponding reduction in peak hip extension moment in the knee cohort (0.91 ± 0.35 vs 1.35 ± 0.23 Nm/kg, $p<0.05$). The foot/ankle group showed reduced rectus femoris activation duration (27.0 ± 3.6% vs 34.7 ± 10.3% of gait cycle, $p<0.05$), suggesting impaired neuromuscular control.

Discussion: This study establishes a reproducible and clinically relevant protocol integrating 3D motion analysis, kinetic data, and sEMG to assess biomechanical and neuromuscular risk factors for RRIs. Compared to traditional 2D gait evaluations, this approach enables more precise detection of gait asymmetries and compensatory loading patterns that often precede overuse injuries. Findings support the potential of advanced, technology-driven biomechanical assessment to optimize athlete performance, reduce injury risk, and inform precision-based rehabilitation strategies. For athletes, early identification of modifiable risk factors may enable proactive interventions that reduce injury risk and promote long-term musculoskeletal health. By embedding this multimodal assessment into preseason screenings, return-to-sport evaluations, and longitudinal monitoring, clinicians and trainers can implement individualized, evidence-based strategies that minimize injury incidence and recurrence, preserve functional capacity, and support sustained athletic performance.

Bone Marrow on Chip for Advancing In Vitro Models in Preclinical Acute Myeloid Leukemia Studies

Azmeer Sharipol, Maggie L. Lesch, Amal Khan, Celia A. Soto, Amanda Streeter, Danielle S.W. Benoit, Benjamin J. Frisch

Keywords:

Bone marrow niche, cancer and metastasis, preclinical model, organ culture and other in vitro models

Our goal is to develop a clinically relevant 3D model of the leukemic microenvironment (AML BMME-chip) that can recapitulate the phenotypes of acute myeloid leukemia (AML). AML results in a dismal 30% 5-year survival rate. Leukemic cells hijack the BMME to create a favorable niche for expansion and protection from chemotherapy. This dysregulates the function of hematopoietic stem and progenitor cell (HSPC) niche components including osteoblasts, bone marrow stem/stromal cells (BMSCs), and endothelial cells. Thus, recent research has focused on the BMME to develop therapies that will be more effective and better tolerated than traditional chemotherapy. However, *in vitro* models of the AML-BMME to study microenvironmental interactions are severely lacking. We previously developed a multicompartment BMME-chip using Emulate Chip-S1™ containing an apical channel with a mineralized osteoblastic layer and a fibrin-gel encapsulating whole bone marrow cells (WBMCs) and BMSCs, and a basal channel with a flow-induced endothelium layer mimicking blood vessels using murine cells[1]. To generate the AML-BMME-chip, murine leukemic cells were incorporated into the apical, bone marrow compartment of the BMME-chip. By D7, osteoblast activity was lost in the AML chip, shown by reduced mineralized calcium and lower osteocalcin expression (0.421 ± 0.20 vs. 1.14 ± 0.70 in non-leukemic, N=12). CCL3, a chemokine linked to osteoblast inhibition in AML, is upregulated >2-fold in D0-D4 effluent and >4-fold in D5-D7 effluent of AML-chip compared to non-leukemic-chip. Studies are underway using CCL3 receptor (CCR1/CCR5) knockout BMSCs to validate mechanistic studies in vitro. To model later stages of disease we increased the number of WBMCs to 5.6 x 10^5 and extended the culture period to 14 days. Flow cytometry results closely mimic *in vivo* phenotypes. HSPC frequency was increased 8-fold compared to the WT group (2.52 ± 0.95% vs 0.29% ± 0.13%, N=4). Multipotent hematopoietic progenitor populations, MPP3 (myeloid) and MMP4 (lymphoid), were also significantly increased by 7-fold and 11-fold. These findings validate that the AML chip is capable of recapitulating complex interactions with the HSPC niche that have previously been demonstrated in vivo, including a loss of osteoblastic function, expansion of HSPC populations, and accumulation of the chemokine CCL3.

1. Sharipol, A., et al., *Bone Marrow Microenvironment-On-Chip for Culture of Functional Hematopoietic Stem Cells.* Frontiers in Bioengineering and Biotechnology, 2022. **10**.

15th Annual Center for Musculoskeletal Research Symposium
October 30, 2025

Title:	Restoring Gait Efficiency After Lumbar Decompression: Quantitative Biomarkers in Patients with Radiculopathy and Neurogenic Claudication
Presenting Author:	Ye Shu, BS
Co-Author(s):	Prasanth Romiyo, MD; Paul Rubery, MD; Ashely Rogerson, MD; Varun Puvanesarajah, MD; Ram Haddas, PhD, MBA
Lab PI / Mentor:	Ram Haddas, PhD, MBA

ABSTRACT

Background: Degenerative lumbar spine disorders (LD) are common conditions that cause pain, impaired mobility, and reduced quality of life (QoL), often presenting as unilateral radiculopathy or neurogenic claudication. The surgical treatment usually involves decompression to relieve the pressure on nerves. Patients often have reduced walking speed and stride length, with greater variability between steps and a forward-leaning posture. While the literature suggests that surgical treatment of LD improves gait function, there is currently a lack of decompression surgery specifically on LD patients' gait parameters using full-body biomechanics analysis. This study aims to evaluate the effects of lumbar decompression surgery on gait in LD patients using comprehensive 3D motion analysis.

Method: Thirty-two patients with LD who underwent decompression surgery with radiculopathy or neurogenic claudication preoperatively were included in the study. Prior to each visit, the patients filled out the Patient-reported outcome measurement information system(PROMIS), Oswestry Disability Index (ODI), and Tampa Scale of Kinesiophobia (TSK). Patients were fitted with 41 reflective markers for 3D gait analysis. Patients walked for 10m at their comfortable walking speed and repeated this five times. Spatial-temporal and joint angles were measured and compared before and 3-month after surgery using mixed-effect linear regression in R.

Results: Patients who underwent lumbar decompression demonstrated significant improvements in spatiotemporal gait parameters, including cadence (95.2 vs 99.4, $p<0.001$), walking speed (0.9m/s vs 1.0 m/s, $p<0.001$), and stride length (1.1m vs 1.2m, $p<0.001$). During both stance (T) and swing phase (W), there is a significant increase in range of motion of ankle dorsiflexion (T: L: 23.6 vs 25.7, $p<0.001$, R: 24.4 vs 26.5, $p<0.001$; W: L: 14.4 vs 15.8, $p=0.002$; R: 13.6 vs 16.1, $p<0.001$), knee flexion (T: L: 35.1 vs 36.4, $p=0.008$; R: 35.4 vs 36.3, $p=0.038$; W: L: 51.1 vs 53.4, $p=0.002$; R: 51.8 vs 53.9, $p<0.001$), hip flexion (T: L: 33.5 vs 36.7, $p<0.001$; R 34.8 vs 36.2, $p<0.001$; W: L: 27.0 vs 29.3, $p<0.001$; R: 28.4 vs 29.7, $p<0.001$), pelvis rotation (T: 8.3 vs 9.7, $p<0.001$; W:5.9 vs 7.2 $p<0.001$). Moreover, there is an increase in lumbar spine flexion (T: 3.1 vs 3.5, $p<0.001$) during the stance phase. On average, there is an improvement in PROMIS function (34.9 vs 42.0), pain interference (66.5 vs 57.5), ODI (44.9 vs 25.9), and TSK (43.4 vs 36.2).

Discussion: Lumbar decompression surgery yields significant improvements in spatiotemporal gait parameters, spine and lower extremity range of motion, and overall walking efficiency in LD patients. These improvements likely reflect the alleviation of neural compression, enabling patients to adopt a more upright posture, reduce compensatory forward stooping, and normalize lower extremity mechanics. Such changes not only improve walking tolerance and performance but may also mitigate secondary musculoskeletal strain associated with prolonged compensatory gait patterns. Patients who undergo lumbar decompression demonstrate increased lumbar extension, hip flexion/extension, and knee mobility during gait, leading to smoother and more coordinated movement patterns. This restoration of functional mobility underscores the multifactorial benefits of decompression surgery: while pain relief is often the primary clinical target, improvements in biomechanical efficiency and joint kinematics contribute to enhanced physical function and improved QoL. Objective gait analysis provides a robust, clinically actionable framework for evaluating recovery, complementing traditional outcome measures and informing individualized postoperative care. Incorporating dynamic gait assessment into routine spine practice has the potential to optimize surgical decision-making, personalize rehabilitation, and enhance long-term outcomes for patients with lumbar degenerative pathology.

Background & Hypothesis: Immunosenescence, an age-related decline in immune function commonly occurs together with osteoporosis. However, the biological features, mechanisms and relationship of immunosenescence to osteoporosis remain poorly understood. TRAF3 acts as a multifaceted regulator influencing T cell immunity. Absence of TRAF3 impairs early TCR signal transduction. Besides, TRAF3 maintains bone formation by preventing beta-catenin degradation in mesenchymal progenitor cells (MPCs) and limits bone destruction directly by non-canonical NF-κB signaling. In aging, increased TGF-β results in TRAF3 lysosomal degradation in MPCs, contributing to osteoporosis by reducing bone formation. However, the mechanisms underlying the restoration of T cell function by stabilizing TRAF3 remain unclear. Here, we hypothesize that TGF-β causes TRAF3 degradation by upregulation of Cbl-b, an E3 ubiquitin ligase, and TGF-β induced SMAD7 interferes with NF-κB activation. These could lead to impaired T cell function, but dysfunctional T cells could be repaired by hydroxychloroquine (HCQ) lysosome inhibitor.

Experiments & Methods: Young (3-mon-old) and old (22-mon-old) C57BL/6 mice were used. Bone marrow cells (BM) were flushed out for BM cells and BM fluid. BM cells were stained with antibodies to detect the % of cytokine producing T cells by flow cytometry. Cytokine and chemokines in BM fluid were detected by cytokine array and ELISA. To detect $CD4^+$ T cell functions, $CD4^+$ T cells were sorted out from BM using CD4 microbeads followed by treatment with either TGF-β, HCQ, or Cbl-b inhibitor before staining with antibodies to be detected by flow cytometry. Sorted $CD4^+$ T cells from BM were treated with indicated treatments or overexpressed with TRAF3 by retroviral transduction and detected protein expressions by Western blot. The immunoprecipitation was performed by incubating ubiquitin antibody with treated $CD4^+$ T cell lysate before detection by Western blot. For *in vivo* experiments, old mice were intraperitoneal immunized with 20 mM/kg of bone-targeted hydroxychloroquine (BTHCQ) or vehicle for five weeks and bone structural parameters were detected by Micro-CT.

Results: We found that old mice have a significantly lower % of total, and naïve T cells, and higher % of memory T cells in the peripheral blood than young mice. In contrast, in the BM of old mice, the % of total, and memory T cells were increased. However, $CD4^+$ T cells from the BM of old mice had reduced production of certain cytokines, including TNF-α, IL-4, and IL-17. Notably, old mice had a higher % of T cells expressing PD-1 and lower levels of numerous cytokines and chemokines in BM. Interestingly, protein levels of TRAF3 were reduced in $CD4^+$ T cells from BM of old mice. Overexpression of TRAF3 increased protein levels of IKKα/IKKβ and decreased phosphorylated I-κBα, key activators and inhibitors, respectively, of canonical NF-κB activation in $CD4^+$ T cells. TGF-β, levels of which are increased in the BM of old mice, reduced TRAF3 protein levels in $CD4^+$ T cells, associated with increased Cbl-b, and a Cbl-b inhibitor mitigated this reduction. Notably, the lysosome inhibitor HCQ increased ubiquitinated TRAF3 levels in $CD4^+$ T cells and blocked TRAF3 degradation by TGF-β. Importantly, a BTHCQ not only increased trabecular bone mass but also prevented the accumulation of $CD4^+$ T cells in the BM of old mice, while promoting their expression of TNF-α and IL-4 and inhibiting the expression of PD-1. In addition, BTHCQ also reduced bone resorption in *S. aureus*-induced osteomyelitis by partially rejuvenating aged T cells.

Discussion & Conclusions: Lysosomal degradation of TRAF3 is a common mechanism underlying functional impairment of T cells, contributing to immunosenescence, and reduced osteoblast differentiation. We conclude that targeted delivery of a lysosome inhibitor to bone has the potential to treat both age-related osteoporosis and immunosenescence.

15th Annual Center for Musculoskeletal Research Symposium
October 30, 2025

Title:	Elucidating the role of S. aureus proteases in fibrin ring degradation during sitafloxacin eradication of Staphylococcal abscess communities
Presenting Author:	Levy A. Sominsky
Co-Author(s):	Karen L. de Mesy Bentley, Gowrishankar Muthukrishnan, Chao Xie, and Edward M. Schwarz
Lab PI / Mentor:	Edward M. Schwarz

ABSTRACT

Introduction: Staphylococcus aureus is the primary pathogen in bone infections, where it evades antibiotic therapy and the immune system by forming Staphylococcal abscess communities (SACs). These structures are encased in a self-produced fibrin pseudocapsule, which shields bacteria from immune attack and antibiotic penetration, rendering standard therapies such as vancomycin ineffective. In contrast, sitafloxacin not only kills bacteria within SACs but also degrades the protective fibrin ring in vivo and in vitro. However, the mechanism of fibrin ring degradation remains undefined, and elucidating this pathway could reveal a novel dispersal program that enhances antimicrobial efficacy and informs new therapeutic strategies for osteomyelitis. Since S. aureus proteases are well-established mediators of biofilm dispersal, we tested the hypothesis that they contribute to sitafloxacin's disruption of SAC fibrin ring architecture. Here, we leveraged our in vitro SAC model to perform longitudinal bulk RNA sequencing of treated SACs to identify mediators of sitafloxacin-induced fibrin ring degradation, and to directly assess proteolytic activity of targets against fibrinogen.

Methods: RNA was extracted from SACs treated with sitafloxacin, vancomycin, and PBS for 5, 15, and 30 minutes, sequenced with Illumina NovaSeq X , and analyzed with the limma-voom pipeline with Benjamini-Hochberg correction (FDR<0.05). Recombinant staphopain A (ScpA) was expressed in E. coli BL21, solubilized, purified by Ni-affinity chromatography, and refolded to yield active protease. For the semi-quantitative fibrinogen cleavage assay, human fibrinogen was incubated with recombinant proteases, and cleavage products were resolved with Coomassie-stained SDS-PAGE. Human plasmin served as a positive control. For quantitative activity and ScpA refolding confirmation, azocasein was incubated with increasing ScpA concentrations. Undigested substrate was then precipitated with trichloroacetic acid, and soluble cleavage product absorbance was measured at 440 nm. Data were fitted with a logistic regression model.

Results: Bulk RNA sequencing showed that sitafloxacin upregulated multiple protease-encoding genes within SACs when compared to vancomycin and PBS controls. Two proteases, scpA and V8 protease (sspA), showed significant time-dependent increases in expression when compared to both controls, demonstrating induction is sitafloxacin-specific. In our fibrinogen cleavage assay, both ScpA and SspA cleaved all three chains of fibrinogen, with strong activity against the alpha chain (0.1% and 1.3%, respectively). SspA cleaved the beta (2.2%) and gamma chains (4.9%) more efficiently than ScpA (68.0% and 31.5%, respectively) and displayed greater activity against the gamma chain (48.1%) than plasmin. The azocasein cleavage assay of refolded ScpA demonstrated a dose-dependent increase in absorbance at 440 nm ($R^2=0.9825$, $p=0.00879$), consistent with a characteristic logarithmic enzyme response curve.

Discussion: These findings suggest that sitafloxacin promotes fibrin ring degradation in SACs by inducing scpA and sspA, which encode proteases with potent activity against human fibrinogen. Thus, we posit that sitafloxacin's unique efficacy against SACs stems from its ability to cleave the fibrin ring through ScpA and SspA, and therefore, enhance antibiotic penetration. In future studies, we will inject in vitro SACs with recombinant ScpA and SspA to determine their sufficiency for fibrin ring cleavage and characterize their influence on the antimicrobial susceptibility of SACs. We will supplement this with scpA and sspA deletion mutants, which will illustrate whether these proteases are necessary for sitafloxacin to destabilize the fibrin ring. Defining this mechanism highlights protease induction as a strategy to disperse SACs, thereby increasing bacterial susceptibility to antimicrobials and host immunity, and ultimately improving therapeutic outcomes in osteomyelitis.

15th Annual Center for Musculoskeletal Research Symposium
October 30, 2025

Title:	Continuous monitoring of cytokine secretion in human tendon-on-a-chip using an optical biosensor
Presenting Author:	Deepak Sonker
Co-Author(s):	Joesph Bucukovski, James McGrath, Hani Awad, Benjamin L. Miller
Lab PI / Mentor:	Benjamin L. Miller

ABSTRACT

INTRODUCTION: Tendinopathies place a heavy burden on healthcare systems and reduce quality of life. Current treatments are limited: NSAIDs only relieve symptoms, and surgery often leads to recurrent adhesions. Mouse studies identified TGF-β1 as a key driver of fibrosis in tendon healing, promoting tenocyte-to-myofibroblast differentiation, tissue contraction, matrix deposition, and secretion of senescence-associated secretory proteins (SASP). To this end, a university-wide collaboration has led to the development of a human tendon-on-a-chip (hToC) model to study tendon fibrovascular injury. A previous student (Joseph Bucukovski) and I have integrated an optical biosensor into the hToC for continuous monitoring of SASP molecules (hToC-SE). The biosensor quantifies refractive index changes when analytes bind to surface-immobilized antibodies, enabling kinetic measurements with high temporal resolution. We hypothesize this will advance our understanding of inflammatory and fibrotic kinetics in ways not accessible through endpoint assays.

METHODS: To test the hypothesis, the SASP and control antibodies were covalently immobilized on epoxy-silane (GPTMS) functionalized integrated sensor. The dose-dependent response of four SASP molecules, IL-6, CCL2, CCL3, and IL-17A, was used to calibrate the sensor. The stability of the sensor was tested in nano-pure water and X-Vivo10 serum-free media for 72 hours. The hToC-SE was then incorporated with tendon tissue construct (5E5 cell/mL) basally and endothelial barrier (5E5 cell/mL) simulating the vascular barrier apically. Both layers are physically separated by the nanoporous membrane of 50 nm pore size. The experiment was performed for 72 hours, and 3-4 replicates of hToC devices were made for each experiment. The tendon-hydrogel construct was stimulated by TGF-β1 (10 ng/mL) by placing the hToC-SE device inside the mini-incubator at 37 °C and 5% CO2. Also, a replicate hToC-SE device was kept inside the cell culture incubator. After each experiment, immunofluorescence nucleus and actin filament staining were done for the bottom hToC component.

RESULTS: The results show that the sensor remained stable in water for 72 hours, but in serum-free media, it showed a continuous decrease in refractive index, causing a blue shift in the sensor response, possibly due to sensor fouling caused by dissolved gases or changes in pH and temperature. Furthermore, through control experiments we found out that the blue shift (or bulk refractive index shift) has the same temporal rate in serum free media. By subtracting the control from the capture ring responses, kinetic signals of SASPs molecules were isolated from the background shift. Using this approach, unstimulated TGF-β1 hToC devices exhibited kinetic responses for all four SASPs, though with considerable variability observed between replicate experiments (n=3). Similar variability was also observed in stimulated hToC experiments. Confocal staining showed a lower cell density inside the mini incubator hToC device compared to the cell culture incubator device, likely, due to cellular stress caused by variable pH and temperature. In future studies, we plan to place the hToC device and optical setup inside the cell culture incubator to minimize stress in continuous monitoring experiments.

DISCUSSION: While there remains significant variability in observed responses, this preliminary study will serve as a basis for future work to test the therapeutic efficacy of drugs by continuously monitoring microphysiological systems.

SIGNIFICANCE: To our knowledge, this is the first biosensor-integrated human tendon tissue-chip model. This platform will enable the identification of donor-specific pathobiological differences through real-time biomarker analysis, which will be used for future patient-specific therapeutic interventions. Furthermore, as a research tool, it will advance fundamental understanding of tendon inflammation and fibrosis.

15th Annual Center for Musculoskeletal Research Symposium
October 30, 2025

Title:	Microscope Mountable Compression Bioreactor for Real-Time Mechanosensing Studies in IVD Cells
Presenting Author:	Gabriella Wagner
Co-Author(s):	Alex McMahon
Lab PI / Mentor:	Karin Wuertz-Kozak

ABSTRACT

Intervertebral disc (IVD) degeneration is a leading contributor to low back pain, a condition estimated to affect nearly 80% of the global population over their lifetime and a leading cause of disability worldwide. Despite its prevalence, current treatment strategies remain largely invasive and fail to address the cellular and mechanobiological underpinnings of disease progression. IVD cells are inherently mechanosensitive, with activation of mechanosensitive ion channels driving their response to physiologically relevant cues , which – depending on the loading characteristics – can support tissue homeostasis or induce pathological processes. In vivo, IVDs are subjected to dynamic compressive forces during routine movement, yet most in vitro systems fail to replicate these conditions. As a result, the mechanistic understanding of disc degeneration and associated mechanosensors and signaling pathways remains elusive. To address this gap, a microscope-mountable compression bioreactor that enables live fluorescent calcium imaging under physiologically relevant compressive forces was designed and manufactured, bridging the gap between classical unloaded in vitro culture models and in vivo conditions.

The bioreactor incorporates a modular design with optically clear viewing ports, allowing high-resolution live fluorescent calcium imaging of cultured cells, a key read-out for mechanosensor activation, including TRP channel–mediated calcium influx. A resin-printed cell chamber, fabricated from BioMed Clear Resin (Formlabs) that incorporates a PDMS substrate as a means to adjust cell substrate stiffness to tissue-relevant values, fits securely within the bioreactor, allowing controlled deformation under applied compression. Cyclic loading is generated using an air-driven syringe system in which a linear actuator advances and retracts the plunger, modulating air pressure to compress the chamber. The position of the plunger dictates both the magnitude and frequency of applied stress, enabling precise mechanical stimulation. In its current configuration, the system achieves compressive loads of 0.2–2.4 MPa at 2.2 cycles per minute, with ongoing optimization targeting 0.1–10 Hz to cover the physiological range of spinal loading. The device mounts directly to a Leica DMI6000 B inverted microscope, providing a platform for live-cell imaging under physiologically relevant mechanical conditions. Biological testing with the device is ongoing. Our laboratory has extensive prior experience monitoring calcium flux in IVD cells subjected to tensile loading, providing established protocols that will be applied within this platform.

This work introduces a novel, microscope-mountable compression bioreactor that enables direct, real-time observation of mechanosensing events in IVD cells. By combining physiologically relevant cyclic loading with live fluorescent calcium imaging, the system uniquely supports investigation of calcium flux and can easily identify involved mechanosensors through pharmacological inhibition or knockdown studies. The resin-printed design reusability, biocompatibility, and optical clarity, in combination with the employed modular engineering approach, allows adaptation to additional microscope platforms and experimental applications. Future studies will apply this platform to investigate how compression influences calcium dynamics, mechanosensitive channel activity, and early cellular responses associated with disc degeneration. Beyond disc biology, this technology may be extended to other load-bearing tissues such as cartilage and bone, positioning the device as a broadly applicable tool for advancing mechanobiology.

15th Annual Center for Musculoskeletal Research Symposium
October 30, 2025

Title: Macrophages Expressing Membrane-bound TGFβ1 in Bone Marrow Contribute to Low Bone Turnover Associated with Immunosenescence and Age-Related Osteoporosis

Presenting Author: Cheng Xiang

Co-Author(s): Chutamath Sittplangkoon, Rong Duan, Philip Milton, Leah Tang, Nida Pellett, Andrea Baran, Juilee Thakar, Jennifer Anolik, Brendan F. Boyce

Lab PI / Mentor: Zhenqiang Yao

ABSTRACT

Background & Hypothesis: Age-related osteoporosis (AROP) and immunosenescence are associated with aging. AROP is characterized by low bone turnover, with both bone formation and resorption being reduced. Immunosenescence is an acquired dysfunction of adaptive and innate immunity during aging. However, the mechanisms underlying the low bone turnover in AROP and its relationship to immunosenescence remain unclear. Transforming Growth Factor Beta 1 (TGFβ1) is a key cytokine contributing to bone loss in AROP and plays a crucial role in maintaining T cell tolerance and immunosuppression. However, activation of TGFβ1 from its latent form may be limited during aging due to reduced bone resorption. We identified a novel subset of F4/80^{+} macrophages expressing membrane-bound TGFβ1 (mbTβ1), which we call MbTβ1Macs that are increased in number in bone marrow (BM) in aged mice. Our hypothesis is that MbTβ1Macs cause low bone turnover in AROP and contribute to immunosenescence.

Experiments & Methods: Serum bone turnover markers and BM cytokine levels measured by ELISA in young and aging mice. Immunostaining to localize MbTβ1Macs within BM, and single-cell RNA-seq and flow cytometry to define their phenotypic and functional characteristics. Osteoclastogenic potential of MbTβ1Macs was assessed. Effects of MbTβ1Macs on osteoblast (OB) differentiation from mesenchymal progenitor cells (MPCs) from young, aging, or conditional knockout (cKO) mice, were tested in a co-culture system. In vivo, we generated mice with cKO of TGFβ1 in macrophages (TGFβ1f/fLysMcre), Integrin Beta-8 (ITGB8) in macrophages (ITGB8f/fLysMcre), or TGFβ receptor II in OBs (TbRIIf/fCol1cre-ERT2, tamoxifen-inducible) and examined trabecular bone mass. Western blotting and flow cytometry to investigate how Th1-derived IFN-γ regulates mbTβ1 expression by macrophages and how MbTβ1Macs influence immunosenescence.

Results: We confirmed low bone turnover in AROP, with significantly lower serum bone formation and resorption markers in 22-mon-old aged mice. MbTβ1Macs were enriched along trabecular surfaces in bone sections from aged mice. Single-cell RNA-seq analysis revealed that MbTβ1Macs from BM highly express TRAF3, NF-κB2, RelB, IRF3, IRF5, IRF8, and STAT5, factors known to inhibit osteoclast (OC) differentiation. MbTβ1Macs from aged mice have reduced OC-forming potential in response to RANKL, but they do not express M1 or M2 polarization marker genes, including iNos, arginase 1, IL-10, HIF2A and IL-1β. TGFβ1 is typically secreted as a nonfunctional latent form. However, MbTβ1Macs highly express ITGB8, which recognizes TGFβ1 latency-associated protein and thus activates mbTβ1. Interestingly, MbTβ1Macs inhibited MPC differentiation into OBs, and this inhibitory effect was blocked by a TGFβ neutralizing antibody. Importantly, cKO of TGFβ1 in macrophages (TGFβ1f/fLysMcre) resulted in increased trabecular bone mass in both male and female adult mice. Similarly, tomaxifen-inducible cKO of TGFβ receptor II in OBs (TbRIIf/fCol1cre-ERT2) also increased trabecular bone mass in mice. BrdU labeling showed that MbTβ1Macs did not proliferate in the BM of young or aged mice. In addition, IFN-γ, the major cytokine produced by Th1 and cytotoxic T cells, promoted MbTβ1Macs expression.

Discussion & Conclusions: Macrophages expressing membrane-bound TGFβ1 (MbTβ1Macs) accumulate in the BM during aging, have reduced OC-forming potential by expressing multiple OC inhibitors, and directly inhibit OB differentiation through membrane-bound TGFβ1 on these macrophages by activating ITGB8, thereby causing low bone turnover in AROP. In addition, MbTβ1Macs are polarized by the Th1 cytokine, IFN-γ, and in turn suppress T cell function, contributing to immunosenescence. We conclude that strategies that abolish accumulation of MbTβ1Macs in BM could be a novel way to treat both AROP and immunosenscence.

Keywords: Age-related osteoporosis, immunosenescence, Macrophage, TGFβ1, bone turnover

15th Annual Center for Musculoskeletal Research Symposium
October 30, 2025

Title: $CD11c^+CD21^-$ Autoimmune-Associated B Cells Derived from Double-Negative IgD^-CD27^- Subsets Exhibit Enhanced IFNLR1 Expression in Systemic Lupus Erythematosus

Presenting Author: Roukaya Yaakoubi

Co-Author(s): Diana Alzamareh, Alexander Bae William

Lab PI / Mentor: Jennifer Barnas
Division of Allergy, Immunology and Rheumatology, University of Rochester Medical Center, Rochester, NY

ABSTRACT

-Background & Hypothesis:
Autoimmune-associated B cells (ABCs) are increasingly recognized for their role in the pathogenesis of systemic lupus erythematosus (SLE), yet their developmental origins and specific functions remain unclear. Interferon-lambda (IFN-λ), a type III interferon implicated in SLE, may have distinct effects from the well-established pathogenic role of interferon-alpha (IFN-α), still its contribution remains incompletely understood. Prior studies suggest that ABCs—characterized by a $CD11c^+CD21^-$ phenotype—are most prevalent within the double-negative (DN) B-cell subset, which also shows heightened responsiveness to IFN-λ. We hypothesize that $CD11c^+CD21^-$ ABCs, predominantly arising from the DN IgD^-CD27^- B-cell subset, exhibit enhanced responsiveness to IFN-λ, contributing to their pathogenic role SLE through upregulated IFNLR1 expression.

-Experiments & Methods: To investigate the development and function of ABCs, peripheral blood mononuclear cells (PBMCs) were isolated from patients with SLE (n = 18). Flow cytometry was employed to quantify $CD11c^+CD21^-$ ABCs across four B-cell subsets: naïve, switched memory (SM), unswitched memory (USM), and DN. IFNLR1 expression was later assessed within these subsets (n = 3).
To explore the intrinsic differentiation potential of ABCs, in vitro stimulation assays were performed using sorted-purified naïve, SM, USM, and DN B cells from healthy donors (HDs) (n = 3). Cells were cultured under ABC-inducing conditions, including B-cell receptor stimulation, R848 (TLR7/8 agonist), IFN-γ, IL-21, and BAFF. Following culture, the induction of $CD11c^+CD21^-$ ABCs and IFNLR1 expression were analyzed by flow cytometry.

-Results
Flow cytometric analysis of PBMCs from SLE patients (n = 18) revealed that $CD11c^+CD21^-$ ABCs were most enriched within DN B-cell subset. Their frequency was significantly higher relative to total $CD19^+$ B cells compared to other subsets. The mean frequencies of ABCs were 6.46% in DN, 2.59% in USM, 1.37% in naïve, and 0.29% in SM B cells ($p < 0.02$).
In vitro differentiation assays using sorted B-cell subsets from HDs (n = 3) demonstrated that DN and SM B cells exhibited the highest propensity to differentiate into ABCs under stimulatory conditions. The mean frequencies of induced ABCs were 46.2% for DN, 32.4% for SM, 13.4 for naïve and 4.3 for USM B cells.
Assessment of IFNLR1 expression showed significantly elevated levels on $CD11c^+CD21^-$ ABCs within the DN subset in SLE patients ($p < 0.02$). In vitro, ABCs derived from DN B cells exhibited a 6.3-fold increase in IFNLR1 expression under ABC-inducing conditions, compared to 2.5-fold, 1.6-fold, and 1.6-fold increases in ABCs derived from SM, naïve, and USM B cells, respectively.

-Discussion & Conclusions:These findings identify the DN B-cell subset as a key origin of $CD11c^+CD21^-$ autoimmune-associated B cells in SLE and highlight their enhanced capacity for IFNLR1 expression. The preferential differentiation of DN B cells into ABCs, coupled with their heightened responsiveness to IFN-λ, driven by increased IFNLR1 expression, suggests a distinct IFN-λ–mediated pathway in B-cell–driven autoimmunity. This IFN-λ–IFNLR1 axis may represent a novel therapeutic target for modulating B-cell–driven autoimmunity in SLE.

15th Annual Center for Musculoskeletal Research Symposium
October 30, 2025

Title:	Metacarpal Cortical Index: An Accessible Alternative for Assessing Wrist Bone Health and Fracture Risk
Presenting Author:	Anthony Yosick
Co-Author(s):	Sophia Turbide MD, Hani Awad PhD
Lab PI / Mentor:	Hani Awad PhD

ABSTRACT

Background & Hypothesis: Osteoporosis (OP) is a silent bone disease. Without effective screening, diagnosis, and treatment, bone mineral density (BMD) loss often goes unnoticed leading to a fragility fracture. Dual-energy X-ray absorptiometry (DXA) is the clinical standard for measurement of BMD and diagnostic classification using T-score. T-score has limitations in accurately capturing overall fracture risk alone. It is further undermined by low screening rates leaving many at-risk individuals undiagnosed and untreated. The Fracture Risk Assessment Tool (FRAX) has attempted to address these limitations by incorporating clinical risk factors, but remains reliant on BMD, limiting its accessibility. Alternative methods have been proposed to investigate bone size and geometry, microarchitecture, and composition. One method, metacarpal cortical index (MCI), offers a practical and accessible option by using a standard hand radiograph to quantify normalized cortical thickness of the second metacarpal. This study aims to evaluate whether MCI can reliably diagnose OP and to assess the performance of MCI in estimating fracture risk compared to DXA T-score and FRAX.

Experiments & Methods: Human cadaveric specimens (n=39 females, mean age 68.7±13.5 years, mean BMI 28.2±8.6 kg/m^2) were obtained through Anatomy Gifts Registry. Given the higher risk factor for OP in females, this cohort comprised of female only non-paired cadaver arms. DXA scans of the 1/3 radius (Hologic Horizon Ci) classified donors as normal (N; n=14), osteopenic (OPE; n=10), and OP (n=15). Biomechanical testing simulated a fall on an outstretched hand (FOOSH) using established protocols with forearms in pronation with 15° radial abduction and loaded at 3.3 mm/s on an Instron ElectroPuls E10000. Force-displacement data was used to determine work to fracture force to estimate fracture risk. Posterior–anterior hand radiographs were acquired using a Hologic UltraFocus Faxitron to assess fracture locations and measure MCI. Donors were classified as N (T-score > -1), OPE (-2.5 < T-score ≤ -1), OP (T-score ≤ -2.5) and as low (≥19 J) versus high (<19 J) wrist fracture risk using an average threshold from a simulated FOOSH model.

Results: FRAX measurements were only available for 37 donors, as two exceeded the FRAX upper age limit of 90 years. Comparison of wrist work to fracture across WHO classifications were significant between N and OP (P= 0.0110). Power analysis between N and OP yielded a power of 0.8 with an effect size of 1.08. Comparisons involving the OPE group (N vs. OPE or OPE vs. OP) showed the expected trends but were not statistically significant and did not reach a power of 0.8. MCI differentiated between N and OP (AUC= 0.986, cutoff = 0.395), N and OPE (AUC=0.779, cutoff = 0.462), and OPE and OP (AUC=0.940, cutoff = 0.409). Work to fracture force was significant between low and high wrist fracture risk (p=0.0002). For distinguishing low from high wrist fracture risk, performance was highest for MCI (AUC = 0.855, cutoff = 0.524), followed by T-score (AUC = 0.796, cutoff = –1.6) and FRAX (AUC = 0.713, cutoff = 21.5%).

Discussion & Conclusions: Our findings demonstrate that MCI is an accessible and effective tool for diagnosing OP, outperforming DXA T-scores and FRAX in this cohort. Of all modalities, MCI showed the highest predictive performance. Both MCI and T-scores surpassed FRAX in distinguishing wrist fracture risk defined by FOOSH biomechanical testing. These results suggest MCI may serve as a practical alternative to DXA T-scores, particularly in rural settings lacking DXA access. Limitations include some medical history discrepancies: hospice-related rather than long-term medication data, absent familial fracture history, and inconsistent smoking and alcohol records. FRAX calculations were based on 1/3 radius BMD, which may not align with femoral neck BMD. Future studies will incorporate femoral assessments, another major site of osteoporotic fracture.

15th Annual Center for Musculoskeletal Research Symposium
October 30, 2025

Title:	Development of a vascularized tendon fibrotic organoid in a microfluidic device
Presenting Author:	Victor Zhang
Co-Author(s):	Mariana Rodriguez, William H. Torp
Lab PI / Mentor:	Hani Awad and James McGrath

ABSTRACT

INTRODUCTION: Tendon microphysiological systems (MPS), or tendon-on-chips, are rapidly developing as human-relevant tools for research and anti-fibrotic drug development. Our lab models the myofibroblast microenvironment using tendon MPS to better understand the mechanisms driving fibrosis including the role of immune cells, extracellular matrix, and hypervascularization in the overactivation of myofibroblasts. These platforms will accelerate the development of strategies for scarless repair of tendon through high-throughput drug testing and discovery. In this study, we created tendon fibrotic organoids to model a focus of peritendinous adhesion. We then began incorporating these organoids in microfluidic devices with ultrathin silicon nitride membranes to create a vascularized organoid model.

METHODS: Fibrotic organoids were created by culturing tendon-derived fibroblasts and human umbilical vein endothelial cells (HUVECs) together at a 1:1 ratio in Matrigel droplets at 6 million cells per mL. Organoids were either cultured floating or embedded in type I collagen hydrogels with 20% type III collagen in EGM-2 media (Lonza). Floating organoids were cultured with or without 10 ng/mL TGF-Beta1 to simulate fibrotic conditions. After culture for 7 to 14 days, organoids were fixed and stained to visualize cell morphology and organization via confocal microscopy. Cell positions were extracted from images to examine spatial clustering. The clustering of HUVEC around fibroblasts was compared to alpha-SMA signal intensity. To test vascularization, we used 2-compartment microfluidic devices with ultrathin (1 micrometer thin) membranes with 20 micrometer diameter pores separating the two compartments. Matrigel droplets with cells were added to one compartment, and high type III collagen hydrogels with 2 million HUVEC per mL and 500,000 fibroblast per mL were added to the other side. Then, the devices were cultured for 7 days while using a syringe pump to pull media through the device at a slow interstitial flowrate of 5 micrometers per second.

RESULTS: Fibrotic organoids demonstrated three-dimensional (3D) organization of fibroblasts and HUVECs in floating culture with small vascular tubes supported by fibroblasts. When treated with 10 ng/mL TGF-Beta1, organoids lost their organized cell structure and demonstrated increased spatial clustering of HUVEC around fibrotic myofibroblasts. Fibroblasts with high alpha-SMA signal intensity were more likely to have closer HUVEC neighbors. Fibrotic organoids embedded in collagen hydrogels demonstrated robust angiogenic sprouting with large, open-lumen vascular tubes growing in 3D to form branching networks around the organoids. When combined in microfluidic devices, we saw that vascular structures were able to cross the membrane and connect the two compartments of the device. HUVECs tubes weaved in and out of membrane pores and formed anastomoses in the pores.

DISCUSSION: These experiments show the capability of our tendon-on-chip system to capture key features of tendon scar tissue such as fibrotic signaling, disorganization, and hypervascularization. Under fibrotic conditions, the spatial organization of cells found in organoids is dramatically altered, mimicking the disorganization of scar tissue. Tendon derived fibroblasts were also able to support both vasculogenic network formation, and robust angiogenic sprouting. Future work aims to perfuse the network for introducing circulating immune cells or drugs for testing. This would facilitate the modeling of progressive inflammatory phases in tendon repair and the delivery of systemically circulating signals or drugs. In this study, we demonstrate the potential of in vitro tendon models to recapitulate key features of fibrosis for drug testing. We also highlight the role of diseased vasculature in the myofibroblast microenvironment as it contributes to poor healing.


MELIORA
University
of Rochester